

SMALL AROMATIC MOLECULES STUDIED BY SPECTROSCOPY

-WHAT FUNDAMENTAL RESEARCH TELLS US-

Small aromatic molecules studied by spectroscopy

-What fundamental research tells us-

Catharina Maria Remmers

Thesis Katholieke Universiteit Nijmegen - Illustrated

With references - With summary in Dutch

ISBN 90-9013762-9

Subject headings: molecular spectroscopy / laser spectroscopy

Cover: Design by the author.

SMALL AROMATIC MOLECULES STUDIED BY SPECTROSCOPY

-WHAT FUNDAMENTAL RESEARCH TELLS US-

EEN WETENSCHAPPELIJKE PROEVE OP HET GEBIED VAN DE
NATUURWETENSCHAPPEN, WISKUNDE EN INFORMATICA

PROEFSCHRIFT

TER VERKRIJGING VAN DE GRAAD VAN DOCTOR
AAN DE KATHOLIEKE UNIVERSITEIT NIJMEGEN,
VOLGENS BESLUIT VAN HET COLLEGE VAN DECANEN
IN HET OPENBAAR TE VERDEDIGEN
OP DINSDAG 6 JUNI 2000,
DES NAMIDDAGS OM 1.30 UUR PRECIES

DOOR

CATHARINA MARIA REMMERS

GEBOREN OP 18 AUGUSTUS 1970
TE TILBURG

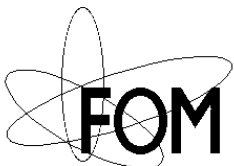
PROMOTOR : PROF. DR. G.J.M. MEIJER

CO-PROMOTOR DR. W.L. MEERTS

MANUSCRIPTCOMMISSIE : PROF. DR. H.J. NEUSSER
TECHNISCHE UNIVERSITÄT MÜNCHEN

PROF. DR. F. LAHMANI
UNIVERSITÉ DE PARIS-SUD

DR. W.C.M. BERDEN



This work is part of the research program of the Stichting voor Fundamenteel Onderzoek der Materie (FOM) and has been made possible by financial support from the Nederlandse Organisatie voor Wetenschappelijk Onderzoek (NWO).

aan Marit

Voorwoord

Ik was precies één dag volwassen (lees 18) toen ik richting Nijmegen vertrok om aan een studie Natuurkunde te beginnen. Na eerst nog een weekend onder meiden te hebben doorgebracht (meisjes introductie voor beta studentes), belandde ik dan eindelijk in de mannenwereld die Natuurkunde heet. En geen seconde heb ik daar spijt van gehad. Toen ik, na mijn afstudeeronderzoek op de afdeling "Molecuul- & Laserfysica", hier onder leiding van Leo Meerts als AIO kon beginnen, was het Annette, toenmalig secretaresse van de afdeling, die de mogelijkheid ter sprake bracht om part-time, voor 4 dagen in de week, te gaan werken. Hiervoor ben ik haar, alsmede ook Leo, die zeer positief stond tegenover dit plan, nog steeds dankbaar. Ik kwam in januari 1995 als AIO in dienst van de Katholieke Universiteit. Dit was echter maar voor korte duur, omdat ik na twee maanden Giel's onderzoek "Spectroscopie aan aromatische moleculen" mocht overnemen en hierdoor in dienst kwam van de stichting voor Fundamenteel Onderzoek der Materie (FOM). -Lang leve het kinderopvangbeleid van de KUN!-

Het werk, waarvan de resultaten in dit proefschrift beschreven staan, heb ik natuurlijk niet alleen gedaan. Ik heb tijdens mijn promotietijd met een heleboel mensen mogen samenwerken. Stuk voor stuk hebben zij hun bijdrage geleverd aan de realisering van dit boekje, waarvoor ik hen van harte wil bedanken.

Allereerst was daar Jack, toen als student bij "mijn" opstelling, die mij een opfriscursus kon geven. Want, hoewel ik mijn afstudeeronderzoek met behulp van dezelfde opstelling had verricht, was dat toch al weer zo'n anderhalf jaar geleden en moest ik er toch weer even inkomen. Ook was Giel nog in de buurt (en nog steeds) om mij toen, maar ook in alle jaren daarna, in raad en daad bij te staan. Zijn inbreng bij de totstandkoming van het eerste artikel was dan ook onmisbaar.

It was very instructive for me to do my first measurements in collaboration with Mike Schmitt and Karl Kleinermanns. Although we did succeed in measuring the phenol-dimer, the spectrum turned out to be so dense and complex that we never came to analysing it. Mike, however, was so impressed by the setup that he built one himself.

Erko Jalviste, regular visitor of the lab, was interested in measuring 3- and 5-methylindole. He modified the simulation and fitting programs so we could fully analyse the spectra. Everyone who was at the department at that time, will remember (the smell of) those measurements.

The first time Anne Zehnacker came to Nijmegen, was not very fruitful. Fortunately, the second time she came was not in vain and we were able to measure spectra of fluorophenol, which, in combination with the measurements she did in Orsay, yielded some very nice results.

The last day of Irving Ozier's visit to Nijmegen I was finally able to show him a (still very

small) benzoic acid dimer signal. So we decided to continue our collaboration, and used the powerful medium of e-mail.

Voor de totstandkoming van het laatste hoofdstuk heb ik mogen samenwerken met het zeer efficiënte team van Gerard Meijer. Ik moet hier natuurlijk bekennen dat mijn bijdrage aan de eigenlijke metingen bij FELIX minimaal is geweest en dat Rob, Hans, Gert en Gerard zich hiervoor hebben uitgesloofd. Rob heeft er daarnaast zorg voor gedragen dat er in de beschrijving van de FELIX opstelling geen onwaarheden geslopen zijn.

Two students were entrusted to me; Ivan, who made the recorder in the lab superfluous, and Izabela, who, I know, will do a good job showing Grzegorz how to operate the laser.

Ik mag natuurlijk op dit punt Leo niet vergeten, allereerst voor zijn bijdrage aan het onderzoek als mijn directe begeleider, maar ook voor zijn hulp bij allerlei problemen van computer-technische aard.

Een opstelling blijft niet draaien zonder technische ondersteuning. Ik ben blij dat ik kon terugvallen op de expertise van Frans, John en Chris voor elektronische ondersteuning en die van Eugène, Cor en André bij alle andere problemen die zich voordeden. Magda was er natuurlijk altijd voor de secretariële ondersteuning.

Naast bovengenoemde mensen bedank ik ook alle andere medewerkers en studenten, die, nu en in het verleden, voor de prettige sfeer op de afdelingen Molecuul- & Laserfysica I en II en Toegepaste Fysica hebben gezorgd. Ik heb al die tijd met veel plezier hier gewerkt. Zonder iemand voor het hoofd te willen stoten, wil ik hier alleen de namen noemen van Genie en Martina, die naast collega's ook *friends for life* zijn geworden en zonder wie dit hele traject niet half zo leuk was geweest; Genie, die er was sinds het begin van onze studie en Martina, die het gat dat Genie liet toen ze naar de Graalburcht vertrok, moeiteloos wist te vullen.

Buiten de afdeling was daar de ondersteuning van de medewerkers van de Instrumentmakerij, de Zelf-service werkplaats, Electronica, de Glasinstrumentmakerij en Grafische vormgeving.

Ik wil ook studievrienden Paul, Peter, Erno en natuurlijk Johan bedanken. Van Johan's aanbod om op te passen wanneer dat ook maar nodig was (behalve dan wanneer we met z'n allen gingen stappen) heb ik zeker de eerste jaren van mijn promotietijd dankbaar gebruik gemaakt. Ook wil ik mijn broer Twan en zijn vriendin Hèlen bedanken voor hun steun en belangstelling.

Bijna aan het eind gekomen van deze lijst mensen, moet ik ruimte maken om mijn ouders te bedanken. Zonder de wetenschap dat ik altijd op hen kan rekenen en terug vallen, had ik dit niet kunnen volbrengen. Altijd stonden zij klaar wanneer Marit ziek was, of ik naar een conferentie moest. Hoewel deze taak nu is overgenomen door Eric, weet ik dat ze er altijd zullen zijn, wanneer ik ze nodig mocht hebben. Pap, mam, bedankt!

De twee belangrijkste mensen in mijn leven heb ik tot het laatst bewaard. Eric, jouw vriendschap is voor mij altijd een enorme steun geweest. Alles wat er daarna bijgekomen is, zou ik voor geen goud meer willen missen. En Marit, jij maakt van mij een hele trotse moeder!

Contents

1	Introduction	1
1.1	The techniques	2
1.2	The molecules	4
1.3	The spectrometers	6
1.3.1	The LIF spectrometer	6
1.3.2	The REMPI spectrometer	9
	References	10
2	Internal rotation effects in the rotationally resolved $S_1(^1L_b) \leftarrow S_0$ origin bands of 3-methylindole and 5-methylindole	13
2.1	Introduction	14
2.2	Theory	15
2.2.1	Model and Calculations	15
2.2.2	Effects on rotational spectra	18
2.2.3	Computational Approach	21
2.3	Experiment	22
2.4	Frequency analysis	22
2.4.1	3-methylindole	22
2.4.2	5-methylindole	25
2.5	Intensity analysis	26
2.6	Discussion	29
2.7	Summary	30
	Acknowledgments	30
	References	30
3	Structural information on the S_0 and S_1 state of <i>o</i>-fluorophenol by hole burning and high resolution ultraviolet spectroscopy	35
3.1	Introduction	36
3.2	Experiment	37
3.3	Results	39
3.3.1	Low resolution measurements	39
3.3.2	High resolution measurements	40
3.4	Discussion	43
3.4.1	Structural information deduced from the high resolution measurements	43
3.4.2	Out-of-plane deformation	44

3.5	Summary	49
	Acknowledgments	50
	References	50
4	Proton tunneling in the benzoic acid dimer studied by high resolution ultraviolet spectroscopy	53
4.1	Introduction	54
4.2	Experiment	57
4.3	Results	57
4.4	Conclusion	61
	Acknowledgments	62
	References	62
5	Rotational contour and gas-phase infrared spectroscopy on the lowest triplet state of pyrazine, the pyrazine-argon complex and its deuterated substituents	67
5.1	Introduction	68
5.2	Experiment	70
5.3	Results and discussion	73
	5.3.1 Rotational contour spectra	73
	5.3.2 Vibrational spectra	75
5.4	Conclusion	78
	Acknowledgments	80
	References	80
	Samenvatting	85
	Curriculum Vitae	89
	Publications	91

Chapter 1

Introduction

Aromatic molecules have a very distinctive smell, which validates their name, since aromatic means "heaving a strong smell". However, in chemistry the definition of an aromatic molecule is given by Hückel's rule. In order to be considered aromatic, a molecule (1) must be cyclic, (2) it must be planar, (3) each atom of the ring must have a p orbital, which is perpendicular to the plane of the ring, and (4) it must contain $(4n + 2)\pi$ electrons (where $n = 0, 1, 2, \dots$). In short, this describes a group of molecules characterized by an increased chemical stability. This stability results from the electronic arrangement in these molecules, which is most stable when all bonding molecular orbitals are filled.

Aromatic molecules form an extensively studied group of molecules. This is not at all surprising since these molecules can be found (mostly as subunits) in a large number of everyday materials. Aromatic molecules are the building blocks for several fuels, pharmaceuticals, pesticides, and fertilizers, as well as modern textiles and dyes. Fundamental knowledge of these aromatic molecules can therefore help to understand the way these molecules behave or react in these materials. This knowledge can then be used to influence materials to produce stronger textiles or new pharmaceuticals. New applications can be found, like the use of polyaromatics in light-emitting diodes, which allows the fabrication of lightweight, flexible displays, with extreme brightness. Conducting polymers can also be used in the fabrication of rechargeable batteries, that have a very high energy density.

Polyaromatic hydrocarbons (PAH) are widely accepted candidates for the origin of the unidentified infrared (UIR) bands seen in the IR emission spectra of many celestial objects. It is speculated, that they might also explain the diffuse interstellar bands (DIB's). Determination of the spectral properties of different polyaromatic hydrocarbons might help in the identification of these bands. Vast quantities of aromatic molecules have indeed been found in interstellar space. And, since aromatic molecules unquestionably are part of organic material, some scientists even speculate that aromatic molecules may have led to life on earth.

This thesis discusses fundamental research on a few small aromatic molecules. The largest system studied is the benzoic acid dimer, consisting of a total of 30 atoms. Although these are relatively simple systems, the description of their spectra can turn out to be quite complicated. A perfect example of this, is the benzene molecule. Consisting of a 6-membered carbon ring with 6 hydrogen atoms attached to it, it is the most symmetric molecule among the aromatics. It has been extensively studied throughout decades, but unraveling its spectra still remains a challenge to many scientists. So a lot can still be learnt from the study of these "simple" systems.

1.1 The techniques

Five different molecules are studied in this thesis. Spectroscopic techniques are used to get information on the structure and behavior of these molecules. Besides knowledge of the properties of the ground state, also information on the electronically excited states of a molecule can be very useful, since a lot of chemical reactions involve molecules in electronically excited states, where the internal energy can be used to overcome the reaction barrier. By studying electronic transitions, properties of both the ground and the electronically excited state can be uncovered from the measured spectra.

All experiments described here, involve a molecular beam set up. The molecular beam is formed by a supersonic expansion of the molecules of interest, seeded in a carrier gas. The expansion cools the internal degrees of freedom of the molecules, leaving only the lowest vibrational and rotational levels populated in the molecular beam. This greatly simplifies the measured spectra. Furthermore, weakly bound clusters, formed during the expansion, can be stabilized at low internal temperatures, allowing them to be studied by spectroscopic techniques.

The molecules described in Chapters 2 to 4 are studied by rotationally resolved laser induced fluorescence (LIF) spectroscopy, for which the scheme is given in Figure 1.1(a). A continuously tunable, narrow band UV source excites the molecules to an electronically excited state. As the frequency of the UV source is scanned, the fluorescence from the excited state is detected by a photomultiplier. In this way an excitation spectrum is recorded, which contains information on both the ground and the electronically excited state [1, 2]. The resolution, that is necessary to resolve rotational transitions of the smallest aromatic molecules, is achieved by combining the

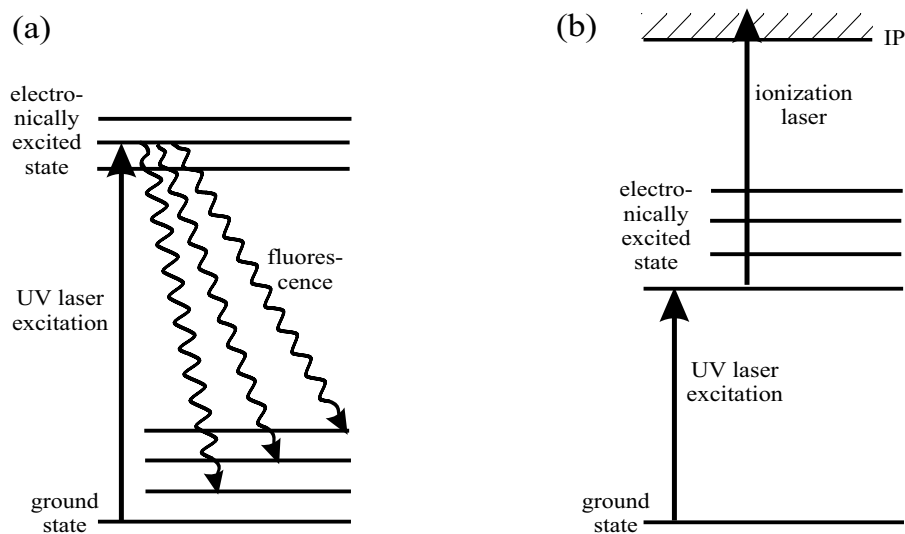


Figure 1.1: *Excitation scheme for laser induced fluorescence (LIF) (a) and resonance enhanced multiphoton ionization (REMPI) (b) spectroscopy. Using LIF the levels of the excited state are probed by monitoring the fluorescence, while with REMPI the ion signal is monitored.*

narrow band UV source with a molecular beam machine [3].

The spectra, that are obtained using this technique are governed by the rotational constants, A , B , and C , of the molecule studied. If the relative positions of the atoms are fixed during rotation, the rotational energy levels can be described by a rigid rotor Hamiltonian, in which the rotational constants are the only parameters:

$$H_r = AJ_a^2 + BJ_b^2 + CJ_c^2. \quad (1.1)$$

J_a , J_b , and J_c are the projections of the total angular momentum on the principle inertial axes a , b , and c of the molecule (see *e.g.* Ref. [4]). The rotational constants are determined by the structure of the molecule. Knowing the complete structure of a molecule in a given state, the rotational constants of this state can be calculated. Unfortunately, the reverse is not true; it is impossible to determine the relative position of more than three atoms from only three parameters. However, if the structure of the molecule is already partially known, it is at times possible to determine the full structure of the molecule. This for example, was the case for triphenylamine [5], which consists of three phenyl groups attached to a nitrogen atom. Since the structure of the phenyl groups was already known, the unknown parameters, describing the relative orientations of the phenyl groups, could be determined from the rotational constants. In other cases, it is often possible to compare the rotational constants to those of related molecules with a well known structure, or with *ab initio* calculations of the molecule, in order to get more information on the structure. One aspect of the structure of a molecule can always be determined once the rotational constants are known. For a planar molecule, the rotational constants satisfy $\frac{1}{C} - \frac{1}{B} - \frac{1}{A} = 0$, so it is readily seen whether a molecule is planar or not.

If a molecule is not rigid, *i.e.* if the relative positions of the atoms are not fixed while the molecule rotates, this will show up in the rotationally resolved spectrum of the molecule. The spectrum cannot be described by a rigid rotor Hamiltonian and more parameters will be needed. This is the case for phenol, where the hydroxyl group rotates with respect to the benzene frame [6]. This internal rotation is described by a two-fold potential barrier and causes all the rotational lines in the spectrum to be split. A deviation from a normal rigid rotor spectrum has also been seen for pyrazine [7]. In this case the perturbation is caused by an interaction between the excited singlet state and a near by triplet state [8]. Every rotational energy level couples to a number of *quasi*-isoenergetic levels of the triplet state, resulting in the creation of eigenstates, that have both singlet and triplet character. Thus, instead of a single transition to each of the individual rovibronic singlet levels, many more lines were found in the spectrum, corresponding to transitions ending in one of the eigenstates.

The linewidth of the individual rotational transitions is a convolution of the spectral linewidth and the natural linewidth due to the lifetime of a state. Thus, if the spectral linewidth is known, the lifetime of a state can be determined from a deconvolution of the linewidth of individual transitions. A parameter that can be extracted from the relative intensities in the measured spectra is the direction of the transition dipole moment. It indicates the direction in which the electronic charge is displaced upon electronic excitation. Since this is naturally very dependent on the electronic state that is excited, in some molecules it might be used to distinguish different electronic transitions. In indole derivatives for example, the transition dipole moment directions of the ${}^1L_a \leftarrow S_0$ and ${}^1L_b \leftarrow S_0$ transitions are found to be almost perpendicular [9]. Since the rotational intensities depend on the square of the electronic transition dipole moment, normally only the absolute value of the angle between the transition dipole moment and the inertial axes

can be determined. However, in special cases it is also possible to determine the sign of this angle (see Chapter 2).

The last chapter describes experiments using resonance enhanced multiphoton ionization (REMPI). Several different excitation schemes are possible. Figure 1.1(b) shows the excitation scheme for 2-color (1+1') REMPI, where two pulsed dye laser systems are used. One (frequency doubled) dye laser excites an electronically excited state, while the second UV source subsequently ionizes the molecules. The ions that are formed are detected by a microchannel plate. Since the second step does not strongly depend on the laser frequency, the structure in the ion signal, that is seen while scanning the excitation laser, is mainly due to the first excitation step. An advantage of this technique is that, in combination with a mass spectrometer, different masses can selectively be detected. The high power of pulsed laser systems makes it possible to study singlet-triplet transitions. By scanning the excitation laser, a rotational contour spectrum can be measured. This contour can then be compared to calculated spectra, to validate the theory of rotational singlet-triplet transitions. The use of an infrared laser as a third laser source, makes it possible to study vibrational transitions. In the experiments described here, a free electron laser was used to induce vibrational transitions in the electronically excited state. The exact excitation scheme is discussed in more detail in Chapter 5. The infrared absorption spectra, that are obtained, can be compared to *ab initio* calculations, to get more information about the electronic state and the distortions that might be involved.

1.2 The molecules

In Chapter 2 the spectra of 3- and 5-methylindole are discussed. These molecules are chromophores of the aminoacid tryptophan and consist of an indole frame, with a methyl group attached at third and fifth position, respectively. 3-Methylindole (skatole), the molecule that causes the bad smell of meat and feces, is a breakdown product of tryptophan, which, instead of a methyl group, has a $\text{CH}_2\text{—CH—COOH—NH}_2$ group attached at third position. This aminoacid is responsible for the bulk of UV absorption in proteins. Two close-lying excited singlet electronic states, labeled 1L_a and 1L_b , form the basis for this UV absorption. These states can be found in any indole chromophore. Since the 1L_a state is much more sensitive to solvent and substitution effects than the 1L_b state is, the frequency spacing between the two states is different for different indole derivatives. In 5-methylindole, the excited electronic states are widely separated, but they approach each other in 3-methylindole.

The addition of a methyl group to a rigid indole frame can provide information about the electronic structure of this frame, since the barrier height for internal rotation of the methyl group is sensitive to the electronic distribution near the substitution site. The effect of the internal rotation of the methyl group on the overall rotation is studied by rotationally resolved UV spectroscopy on the $S_1(^1L_b) \leftarrow S_0$ origin bands. The internal rotation is described by a threefold potential, resulting in overlapping $0a_1 \leftarrow 0a_1$ and $0e \leftarrow 0e$ transitions. From the analysis of the spectra in combination with torsional data, the barrier heights in the ground and electronically excited state of the two molecules could be determined. Furthermore, intensity analysis of the spectra yielded information on the direction of the transition dipole moment of the studied transitions.

Structural information about *o*-fluorophenol is obtained in Chapter 3. For long a controversy

existed, whether or not the two major transitions seen in the excitation spectrum of this molecule [10, 11] belong to different isomers. The difference between the two isomers is the direction of the hydroxyl group with respect to the fluorine atom. In the *trans* isomer the hydroxyl group is directed away from the fluorine atom, whereas in the *cis* isomer it is directed towards the fluorine atom and an intramolecular hydrogen bond is formed. By measuring the OH stretching vibration in the ground state via the two transitions of interest, it was found that both transitions can be attributed to the *cis* isomer [12]. However, the nature of the transitions, denoted A and B, was still not clear. Hole burning measurements were performed to verify that both transitions originate in the same ground state. Rotationally resolved UV spectra of the two transitions were measured to gain insight in the structure of *o*-fluorophenol in the ground and both electronically excited states. From the analysis of these spectra it was found that the ground state of the *cis* isomer of *o*-fluorophenol is planar. However, the electronically excited state was found to be nonplanar, with an increased nonplanarity in the excited B state. This implies the enhancement of an out-of-plane vibrational mode. It was thus concluded that the A band transition corresponds to the origin transition, whereas the B band transition corresponds to an overtone transition belonging to an out-of-plane vibration.

Chapter 4 discusses the benzoic acid dimer. Benzoic acid can be found in many substances. It occurs naturally in, amongst others, yoghurt and cinnamon and is used as a preservative in many other foods. Dimers are abundant at low temperatures, since two intermolecular hydrogen bonds between the two monomer units stabilize the dimer by about 6000 cm^{-1} . Many chemical and biological processes involve hydrogen bonded systems, and are governed by proton transfer. The two hydrogen bonds in the benzoic acid dimer make it a well suited object to study the process of proton transfer and in particular proton tunneling. The concerted proton exchange in the benzoic acid dimer is described by a double minimum potential, in which all levels are split. This leads to the existence of two overlapping components in the high resolution UV spectrum of the $S_1 \leftarrow S_0$ transition, resulting from transitions originating in different ground state tunneling levels. The frequency shift between these two transitions can accurately be determined by calculating the autocorrelation of the measured spectrum. Due to the large size of the dimer the individual rotational transitions in the spectrum are not resolved, but an estimation of the rotational constants can nevertheless be given.

The last chapter discusses measurements done on pyrazine. Since pyrazine is the prototype for so-called intermediate type molecules, it has been extensively studied throughout the last decades. In contrast to the other chapters that deal with singlet-singlet transitions, in the last chapter the lowest singlet-triplet transition of pyrazine is discussed. This chapter presents rotational contour spectra of pyrazine, pyrazine-argon, and its deuterated constituents, pyrazine-*d*4 and the pyrazine-*d*4-argon complex. These spectra are measured using 2-color resonance enhanced multiphoton ionization (1+1' REMPI). The resolution of these spectra is not high enough to allow a detailed analysis of the spectra, but a comparison with calculated spectra is made.

In the same chapter, vibrational spectra of the pyrazine-argon complex are discussed. This experiment is performed in order to get more information on the vibrational levels in the triplet state of pyrazine, since this state is involved in interactions with the lowest excited singlet state, leading to intersystem crossing (ISC). From previous experiments, it was concluded that the vibrational spectrum of an argon cluster does not differ much from that of the bare molecule. Using a free electron laser as a third laser source, it was possible to measure the infrared ab-

sorption spectrum of the triplet state of the pyrazine-argon complex. This spectrum was then compared to *ab initio* calculations performed on the triplet state of the bare pyrazine. No good correspondence between measured and calculated spectra was found, indicating a distortion of this state. Only one of the vibrational lines could be assigned. The same experiment was performed for the pyrazine-*d*4-argon complex, yielding similar results. The measured spectra, however, might be a guide to incorporate different coupling mechanisms, that cause the distortions, in order to improve the *ab initio* calculations. .

1.3 The spectrometers

1.3.1 The LIF spectrometer

The LIF spectrometer is schematically shown in Figure 1.2. The main parts are the molecular beam apparatus and the UV laser system. Ultraviolet laser light is generated by frequency doubling the radiation of a continuous ring dye laser, pumped by an argon ion laser. The laser cavity is formed by four mirrors and has two foci. Fluorescence from the dye jet, that is positioned in the first focus, will be reflected between the four mirrors and laser action will occur if the

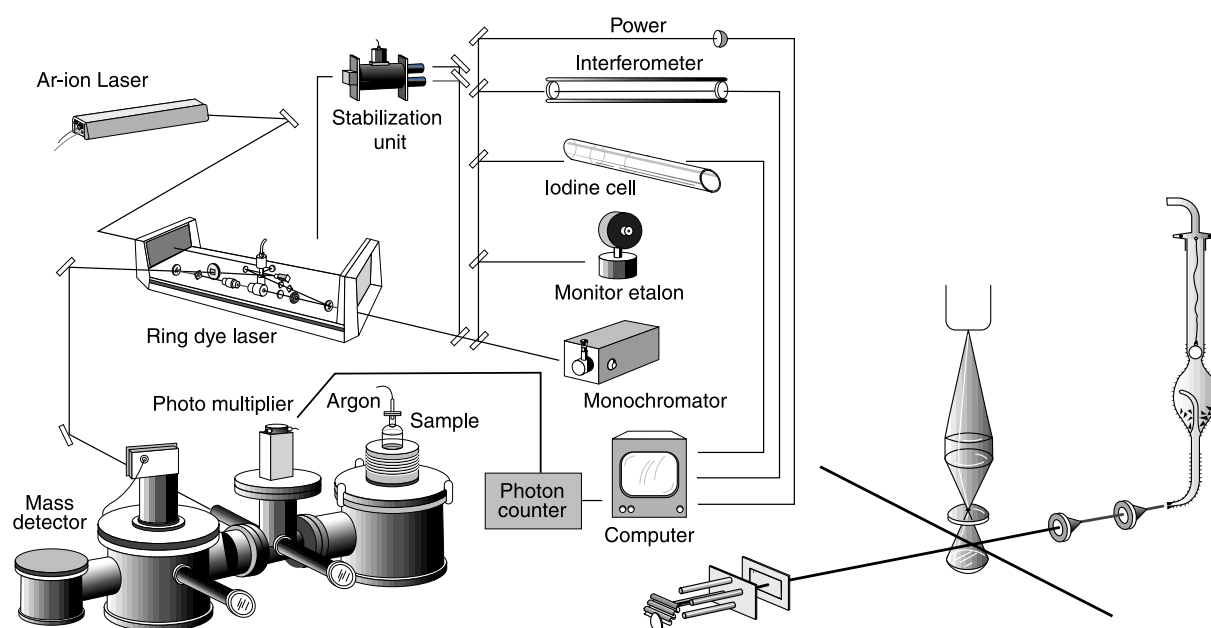


Figure 1.2: The experimental setup used for the high resolution UV measurements. It shows the laser system, the molecular beam apparatus, and several components that are used for laser calibration. The scheme of the molecular beam apparatus is given on the right, showing the quartz nozzle, two skimmers through which the molecular beam is formed, the fluorescence collection optics, and the mass spectrometer.

cavity is well aligned. A birefringent filter, a thin plate etalon, and a piezo-scanned thick etalon are inserted in the cavity to allow the selection of a single laser mode. To inhibit laser radiation in two directions, a unidirectional device rotates the polarization of the wave travelling in one direction, without influencing the polarization of the counterpropagating wave. Since most elements in the cavity are positioned at Brewster angle, the wave with the rotated polarization will be attenuated and will never reach lasing threshold. The frequency of the laser can be scanned by counterrotating two galvo plates. Finally, a Brewster cut frequency doubling crystal is positioned at the second focus of the laser cavity to generate UV radiation.

UV laser radiation between 265 and 342 nm can be generated using different dyes and doubling crystals. For frequencies above 300 nm LiIO_3 crystals can be used and output powers of a few milliwatts can be obtained. Below 300 nm LiIO_3 crystals start absorbing the UV radiation, so that different crystals have to be used. With the use of $\beta\text{-BaB}_2\text{O}_4$ (BBO) crystals, output powers between 50 and 500 μW can be achieved. A small fraction of the fundamental laser radiation is coupled out of the cavity and is used for stabilization and calibration purposes. A 30 GHz monitor etalon is used to check the mode structure of the laser, while the frequency is monitored by a monochromator for a crude wavelength estimation. The absolute frequency is calibrated by measuring the iodine absorption spectrum, that can be compared to the well documented reference spectrum [13]. A high-finesse, temperature-stabilized Fabry–Perot interferometer, with a free spectral range of 74.195 MHz, is used for relative frequency calibration. The laser is stabilized by a modified Coherent CR 599 stabilization system, that locks the frequency to the transmission curve of a low-finesse interferometer. The bandwidth of the laser is determined by the frequency jitter and is about 3 MHz.

The molecular beam apparatus consists of 5 differentially pumped vacuum chambers. The first chamber contains a quartz nozzle and sample compartment, where the molecules of interest are kept. The sample compartment can be heated by a heating wire in order to increase the vapor pressure of the molecules. The nozzle has an opening diameter of 150 μm and can be heated separately. Keeping the nozzle at a slightly higher temperature than the sample compartment, prevents condensation of the molecules in the orifice. The system is constructed in such a way, that the sample compartment can be filled without influencing the vacuum conditions. By flowing a carrier gas over the molecules in the sample compartment, a mixture is formed and expanded through the nozzle. This expansion is skimmed twice to form the molecular beam. The first skimmer separates the source chamber from a buffer chamber, while after passing the second skimmer the molecular beam enters the first interaction chamber. Here it is crossed perpendicularly by the excitation laser, which enters the set up through a window at Brewster angle. After the first interaction chamber, the molecular beam can enter a second interaction chamber, where it again can be crossed by a laser beam. The last chamber holds a quadrupole mass spectrometer, that can be used to check the alignment of the molecular beam through the skimmers.

In the first interaction region the total undispersed fluorescence from the excited molecules is collected by two spherical mirrors and focused onto a photomultiplier through a hole in the upper mirror. This photomultiplier is connected to a photoncounter PC card, and the data are stored in a computer. At the same time also the output of the calibration interferometer, the iodine absorption spectrum and the fundamental laser output can be fed into the computer via a KDAC575 A/D converter (Keitley Instruments). Similar detection optics as used in the first interaction chamber, can also be used in the second interaction chamber, so that, e.g. when a

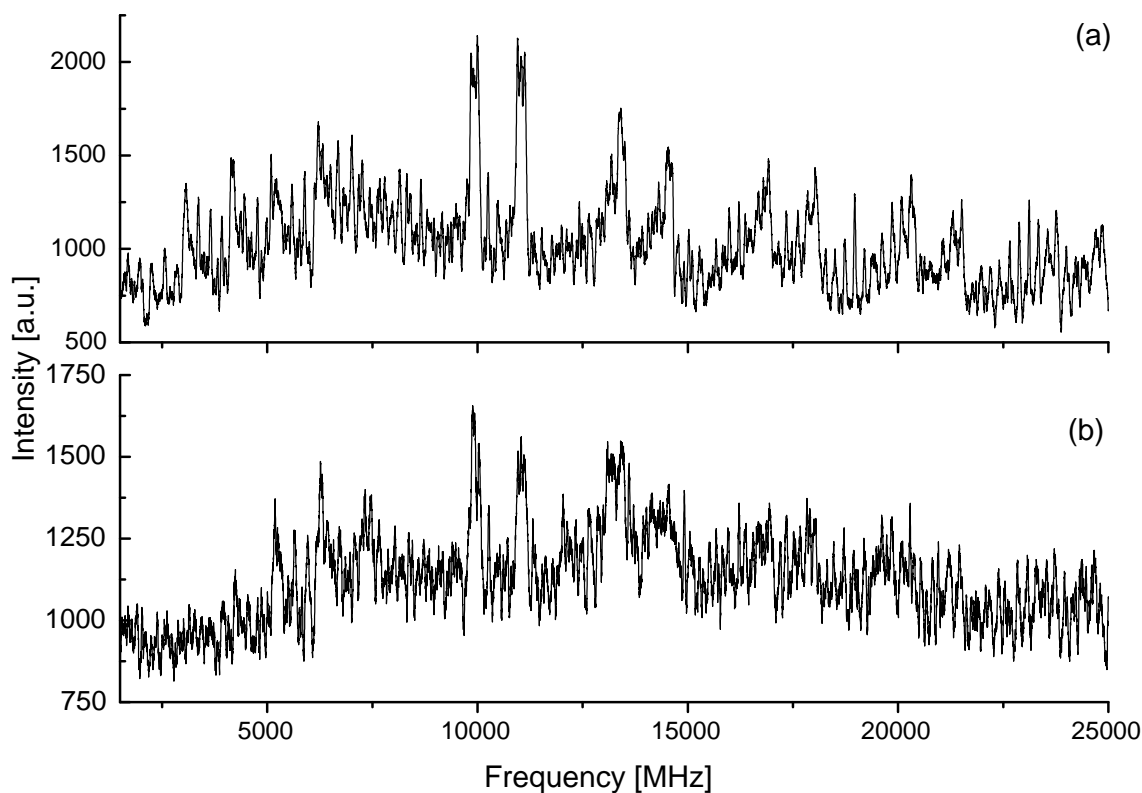


Figure 1.3: Fluorescence excitation spectra of the $S_1 \leftarrow S_0$ transition in the benzoic acid dimer, illustrating the effect of the use of different carrier gases on the rotational temperature in the beam. The rotational cooling is more efficient using neon as a carrier gas (estimated rotational temperature 5 K) (a), than when helium is used as a carrier gas the (estimated rotational temperature 15-20 K) (b).

monochromator is positioned before the photomultiplier, it can be used to monitor the dispersed fluorescence from an electronically excited state. The collection optics, that are used to collect the fluorescence, also serve as a spatial filter, selecting only the center part of the molecular beam. The linewidth due to the distribution in velocities perpendicular to the molecular beam will thus be reduced.

The spectral linewidth strongly depends on the carrier gas used, as the Doppler broadening in a molecular beam is proportional to $\frac{1}{\sqrt{M}}$, where M is the mass of the molecules of the carrier gas [14]. The carrier gas also influences the rotational cooling during the jet expansion, since the decrease in internal energy is proportional to M [14]. This is illustrated in Figure 1.3, showing spectra of the benzoic acid dimer taken with different carrier gases. It is seen that the rotational spectrum is less dense when neon (mass 20.2 amu) is used as a carrier gas (Figure 1.3(a)), than when helium (mass 4.0 amu) is used (Figure 1.3(b)), illustrating that the rotational cooling is more efficient for heavier carrier gases. Unfortunately, using argon as a carrier gas (mass 39.9 amu), clusters between argon atoms and the benzoic acid were formed, thereby decreasing the

benzoic acid dimer signal. Therefore, for the benzoic acid measurements, neon was used as a carrier gas, whereas for the other molecules described in this thesis, argon was used.

A full report on the data acquisition, processing, and analysis of the measured spectra is given in Ref. [2].

1.3.2 The REMPI spectrometer

The REMPI spectrometer, schematically shown in Figure 1.4, is currently installed at the "Free-Electron Laser for Infrared eXperiments" (FELIX) user facility in Nieuwegein, the Netherlands [15, 16], and consists of a molecular beam apparatus, several tunable pulsed laser systems and a differentially pumped Wiley-McLaren-type linear time-of-flight mass spectrometer. A full description of the setup is given in Ref. [17].

A tunable dye laser system (Spectra Physics, PDL-2) is pumped by the second harmonic of a Nd:YAG laser (Spectra Physics, DCR-11). The output of this laser is frequency doubled using a KDP crystal, to generate UV laser radiation, with a bandwidth of 0.15 cm^{-1} . This laser is used to electronically excite the molecules of interest. A second Nd:YAG laser (Spectra Physics, GCR-150) pumps a second dye laser system (Spectra Physics, PDL-3). The output of this laser is frequency doubled in a KDP crystal (Spectra Physics, WEX-2B) and mixed with the fundamental dye laser frequency in a BBO crystal to generate UV laser radiation, that is used to ionize the molecules after they are electronically excited. Besides the two dye laser systems,

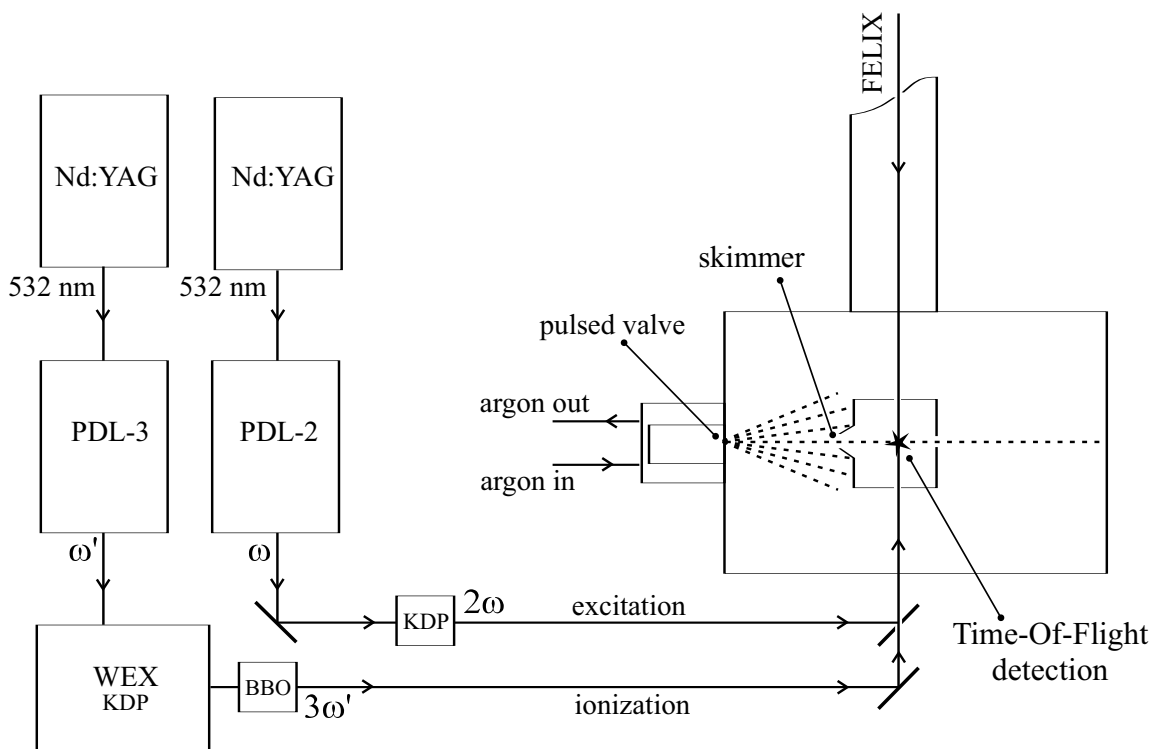


Figure 1.4: Schematic overview of the REMPI spectrometer.

also an infrared laser source is available. This is the free electron laser, FELIX. Electrons from an accelerated electron beam perform a wiggling motion inside an undulator, during which they produce synchrotron radiation. This radiation is stored and amplified in an optical cavity. The frequency of the radiation depends on the magnetic field strength of the undulator and the energy of the electrons. Using two different undulators, the whole frequency range between 40 and 2000 cm^{-1} is covered. The radiation appears in the form of macropulses of about 4 μs duration, containing up to 100 mJ of energy. Each of these pulses is made up of a train of micropulses that are 0.3-5 ps long and 1 ns apart. The laser is continuously tunable over the whole frequency range of the undulator, with a laser bandwidth that is typically 0.5-1.0% of the central frequency. In the experiments described in this thesis, only one undulator is used, covering the frequency range between 300 and 2000 cm^{-1} , a perfect range to study heavy-atom vibrations [18–21].

The molecular beam apparatus consists of two differentially pumped vacuum chambers. The molecules of interest are put in the sample compartment of a pulsed valve (R. M. Jordan Co.), which can be heated, and has a 0.5 mm diameter orifice. Seeded in argon, the molecules are expanded into vacuum of 10^{-6} Torr and skimmed upon entering the interaction chamber. Here the molecular beam is crossed perpendicularly by the laser beams. The delay time between the valve and the lasers is set for maximum signal by a delay generator (Stanford Research DG-535). To ensure field-free conditions during excitation, the ions generated in the interaction region are extracted 1 μs after ionization. They are accelerated into a time-of-flight tube, which is positioned perpendicular to the plane formed by the molecular beam and the laser beams, and detected by a microchannel plate detector. The time-of-flight tube enables the selective detection of a particular ion mass, since ions that have the same kinetic energy, but a different mass, have different velocities. Thus, by setting a time gate at the detector, only ions of a particular mass are detected. The signal of the microchannel plate detector is amplified and fed into a digital oscilloscope (LeCroy 9430), connected to a PC. The whole system runs at a 10 Hz repetition rate.

If the excitation laser is scanned and the ionization laser is fixed above the ionization potential, a rotational contour spectrum can be measured by monitoring the ion signal as a function of the excitation laser frequency. If the excitation laser, on the other hand, is fixed to the origin transition, the vibrational structure of the excited state can be probed by subsequent IR laser excitation. Vibrational excitation of Van der Waals complexes will lead to dissociation, if the IR photon energy is higher than the binding energy of the complex. So, after IR laser excitation, the complex will dissociate and can no longer be ionized. The vibrational structure of the electronically excited state of the Van der Waals complex can thus be monitored via a depletion of the ion signal at the mass of the complex. This technique has been used to measure the vibrational spectra of the pyrazine-argon and pyrazine-*d*4-argon Van der Waals complexes (see Chapter 5).

References

- [1] P. Uijt de Haag. *Energy Redistribution in Photoexcited Molecules*. PhD thesis, Katholieke Universiteit Nijmegen, 1990.

- [2] G. Berden. *High Resolution UV Spectroscopy of Aromatic Molecules*. PhD thesis, Katholieke Universiteit Nijmegen, 1995.
- [3] W. A. Majewski and W. L. Meerts. *Near-UV spectra with fully resolved rotational structure of naphthalene and perdeuterated naphthalene*. *Journal of Molecular Spectroscopy* **104**:271–281, 1984.
- [4] E.W. Gordy and R. L. Cook. *Microwave Molecular Spectra*. John Wiley & Sons, New York, 3rd edition, 1984.
- [5] G. Meijer, G. Berden, W. L. Meerts, H. E. Hunziker, M. S. de Vries, and H. R. Wendt. *Spectroscopy on triphenylamine and its Van der Waals complexes*. *Chemical Physics* **163**:209–222, 1992.
- [6] G. Berden, W. L. Meerts, M. Schmitt, and K. Kleinermanns. *High resolution UV spectroscopy of phenol and the hydrogen bonded phenol-water cluster*. *Journal of Chemical Physics* **104**:972–982, 1996.
- [7] B. J. Van der Meer, H. Th. Jonkman, J. Kommandeur, W. L. Meerts, and W. A. Majewski. *Spectrum of the molecular eigenstates of pyrazine*. *Chemical Physics Letters* **92**:565–569, 1982.
- [8] J. Kommandeur, W. A. Majewski, W. L. Meerts, and D. W. Pratt. *Pyrazine: An "exact" solution to the problem of radiationless transitions*. *Annual Review of Physical Chemistry* **38**:433–462, 1987.
- [9] B. Albinsson, M. Kubista, B. Nordén, and E. W. Thulstrup. *Near-ultraviolet electronic transitions of the tryptophan chromophore: Linear dichroism, fluorescence anisotropy, and magnetic circular dichroism spectra of some indole derivatives*. *Journal of Physical Chemistry* **93**:6646–6654, 1989.
- [10] A. Oikawa, H. Abe, N. Mikami, and M. Ito. *Electronic spectra and ionization potentials of rotational isomers of several disubstituted benzenes*. *Chemical Physics Letters* **116**:50–54, 1985.
- [11] G. N. R. Tripathi. *Electronic absorption spectrum of ortho-fluorophenol in vapor state*. *Journal of Molecular Spectroscopy* **37**:486–493, 1971.
- [12] T. Omi, H. Shitomi, N. Sekiya, K. Takazawa, and M. Fujii. *Nonresonant ionization detected IR spectroscopy for the vibrational study in a supersonic jet*. *Chemical Physics Letters* **252**:287–293, 1996.
- [13] S. Gerstenkorn and P. Luc. *Atlas du Spectroscopie d’Absorption de la Molecule d’Iode*. (CNRS, Paris, 1978).
S. Gerstenkorn and P. Luc. *Absolute iodine (I_2) standards measured by means of Fourier-transform spectroscopy*. *Reviews of Physical Applications* **14**:791–794, 1979.
- [14] W. Demtröder. *Laserspektroskopie Grundlagen und Techniken*. Springer-Verlag, Berlin Heidelberg New York, 2nd edition, 1991.

- [15] D. Oepts, A. F. G. Van der Meer, and P. W. Van Amersfoort. *The free-electron-laser user facility FELIX*. *Infrared Physics & Technology* **36**:297–308, 1995.
- [16] G. M. H. Knippels, R. F. X. A. M. Mols, A. F. G. Van der Meer, D. Oepts, and P. W. Van Amersfoort. *Intense far-infrared free-electron laser pulses with a length of six optical cycles*. *Physical Review Letters* **75**:1755–1758, 1995.
- [17] M. Boogaarts. *Laser Desorption Jet Cooling Mass Spectrometry and Optical Spectroscopy of Involatile Molecules*. PhD thesis, Katholieke Universiteit Nijmegen, 1996.
- [18] M. Putter, G. Von Helden, and G. Meijer. *Mass selective infrared spectroscopy using a free electron laser*. *Chemical Physics Letters* **258**:118–122, 1996.
- [19] J. A. Piest, G. Von Helden, and G. Meijer. *Infrared spectroscopy of jet-cooled neutral and ionized aniline-Ar*. *Journal of Chemical Physics* **110**:2010–2015, 1999.
- [20] J. A. Piest, G. Von Helden, and G. Meijer. *Infrared spectroscopy of jet-cooled cationic polyatomic hydrocarbons: Naphthalene⁺*. *The Astrophysical Journal* **520**:L75–L78, 1999.
- [21] R. G. Satink, J. A. Piest, G. von Helden, and G. Meijer. *The infrared spectrum of the benzene-Ar cation*. *Journal of Chemical Physics* **111**:10750–10753, 2000.

Chapter 2

Internal rotation effects in the rotationally resolved $S_1(^1L_b) \leftarrow S_0$ origin bands of 3-methylindole and 5-methylindole

Abstract

The rotationally resolved UV excitation spectra of the $S_1(^1L_b) \leftarrow S_0$ origin bands of 3-methylindole and 5-methylindole have been measured and analyzed. As a result of an internal rotation of the methyl group, each spectrum consists of rotational lines of overlapping $0a_1 \leftarrow 0a_1$ and $0e \leftarrow 0e$ torsional transitions. Like indole, 3-methylindole and 5-methylindole undergo axis reorientation upon electronic excitation. The Hamiltonian used to describe all observed spectral features includes a pure rotational part, a pure torsional part, and terms describing the interaction between the internal rotation and the overall rotation. It also accounts for the axis reorientation effect. Values for the barrier heights of the methyl torsion, the angle of the methyl top axis with the inertial axes, and the rotational constants are obtained for both the S_0 and the S_1 state. From an analysis of the intensities of the rotational transitions, the direction of the transition moment and the axis reorientation angle are obtained. Due to quantum interference effects in the 5-methylindole spectrum the sign of these angles could be determined.

2.1 Introduction

Indole, its derivatives and complexes have attracted significant attention because indole is a chromophore of the amino acid tryptophan. In these molecules the π -conjugated electrons give rise to two close lying electronically excited states, labeled 1L_a and 1L_b . Excitation to the 1L_a state causes a significantly larger amount of charge transfer than does excitation to the 1L_b state [1, 2]. This larger charge transfer is responsible for the much larger solvent and substitution shifts for $^1L_a \leftarrow S_0$ transitions in comparison with $^1L_b \leftarrow S_0$ transitions [1, 3].

Methyl substitution into different sites can provide a spectroscopic probe of the electronic structure of the parent molecule since the methyl torsional barrier height is sensitive to the π electron density of the bonds adjacent to the methyl group [4–6]. Following this line of thought Bickel *et al.* [7] analyzed the torsional excitation and dispersed fluorescence spectra of the $S_0 - S_1$ transitions of seven monomethyl indoles. For 5-methylindole and 6-methylindole a long torsional progression was observed, which was explained by a phase shift between the S_0 and S_1 torsional potentials owing to the 60° rotation of the methyl group upon excitation. No phase shift was found for the other methylindoles. For 2-methylindole and 3-methylindole (skatole) only the origin band was observed due to the lack of Franck–Condon activity; it was not possible to determine the barrier heights. Later, Sammeth *et al.* [8] presented a vibrational and rotational band contour analysis of 3-methylindole (3-MI) and 5-methylindole (5-MI) by using one- and two-photon laser induced fluorescence spectroscopy. For 3-MI it was possible to assign two of the weak bands near the origin to the transitions terminating in the $2a_1$ and $2e$ torsional levels of S_1 .¹

Another point of interest is the possibility of ‘tuning’ the frequency spacing between 1L_a and 1L_b states, which depends on the site to which the methyl group is attached and on the solvent that is used [9, 10]. The $^1L_a - ^1L_b$ spacing will influence the frequencies and intensities of the whole excitation spectrum due to the vibronic interactions between the two states. It has been shown that in solutions the electronically excited states are widely separated for 5-MI but approach each other for 3-MI [11]. Several studies were performed in order to distinguish between the two different electronic states and determine the position of the 1L_a origin of different indole derivatives [9, 12–16]. Polarized two-photon excitation spectroscopy enabled Sammeth *et al.* [14] to discriminate between 1L_a and 1L_b type bands of jet-cooled 3-MI and 3-trideuteromethylindole. A number of intense 1L_a type vibronic bands were identified in this way. Albinsson *et al.* [17] determined the transition moment directions for both 1L_a and 1L_b states of indole, 3-MI, 5-MI, and 5-methoxyindole oriented in stretched polyethylene films, and showed that the transition moments of 1L_a and 1L_b were almost perpendicular to each other.

Rotationally resolved spectra of molecules with an internal rotation degree of freedom can provide several important molecular properties (the rotational constants for the ground and excited state, the direction of the methyl top axis and the transition moment angle) that cannot be determined precisely by other techniques [18–20]. Besides this, a joint analysis of rotational and torsional data can yield more accurate values for torsional barrier heights. In both 3-MI and 5-MI the interaction between torsion and overall rotation of the molecule perturbs the rotational spectra. For these molecules a vibration-torsion analysis is already performed [8, 14], a prerequisite for the high resolution measurements. In this paper, we present the full (frequency and

¹The levels are labeled by their ν value, whereas in Ref. [8] the free rotor label m is used.

intensity) analysis of rotationally resolved fluorescence excitation spectra of the origin bands of the $S_1(^1L_b) \leftarrow S_0$ transitions of 3-MI and 5-MI.

2.2 Theory

2.2.1 Model and Calculations

The choice of an appropriate model for analyzing the measured spectra is important for the extraction of a maximum amount of information (molecular constants and their error limits) within a reasonable computing time. Both 3-MI and 5-MI are assumed to consist of a methyl top attached to a planar frame (indole). The methyl top axis and the transition dipole moment are assumed to lie in the plane of the indole frame in both the ground and excited state. Molecules of this type belong to the molecular symmetry group G_6 , which has three symmetry species, a_1 , a_2 , and e [21, 22]. We consider only one large amplitude motion, which is the methyl top torsion (internal rotation) around its symmetry axis. In our calculations the reference coordinate system is formed by the principal inertial axes (the principal axis method, PAM). In this method the rotational constants are directly related to the geometry of the entire molecule and do not include contributions from internal rotation.

In general, the solution of the torsion-rotation problem can be described by the Hamiltonian [23, 24]:

$$H_{tr} = F(p - \vec{\rho} \cdot \vec{J})^2 + V(\alpha) + AJ_a^2 + BJ_b^2 + CJ_c^2 \quad (2.1)$$

in a torsion-rotation basis $|e^{im\alpha}\rangle|J, K\rangle$. Here, F is the internal rotation constant:

$$F = \hbar^2/2rI_\alpha = F_\alpha/r, \quad (2.2)$$

where

$$r = 1 - I_\alpha \sum_g \cos^2 \eta_g / I_g, \quad (2.3)$$

$p = -i\hbar \frac{\partial}{\partial \alpha}$ is the angular momentum operator conjugate to the torsional angle α , $V(\alpha)$ is the torsional potential function, A , B , C are the rotational constants, and J_a , J_b , J_c are the projections of the total angular momentum on the principal inertial axes a , b , and c of the molecule. The components of the vector $\vec{\rho}$ are given by the direction cosines $\cos \eta_g$ of the methyl top axis in the principal axis system, the moments of inertia of the entire molecule I_g ($g = a, b, c$), and the moment of inertia of the methyl group I_α :

$$\rho_g = \cos \eta_g I_\alpha / I_g. \quad (2.4)$$

For the methylindoles $\rho_c = 0$, since the methyl top axis lies in the ab plane; we write $\cos \eta_a = \cos \eta$ and $\cos \eta_b = \sin \eta$, where η is the methyl top angle with respect to the a axis (left part of Figure 2.1).

An exact solution of Eq. (2.1) is impractical for spectra containing lines starting from high J levels, because of the long computational time needed. We therefore applied a perturbation

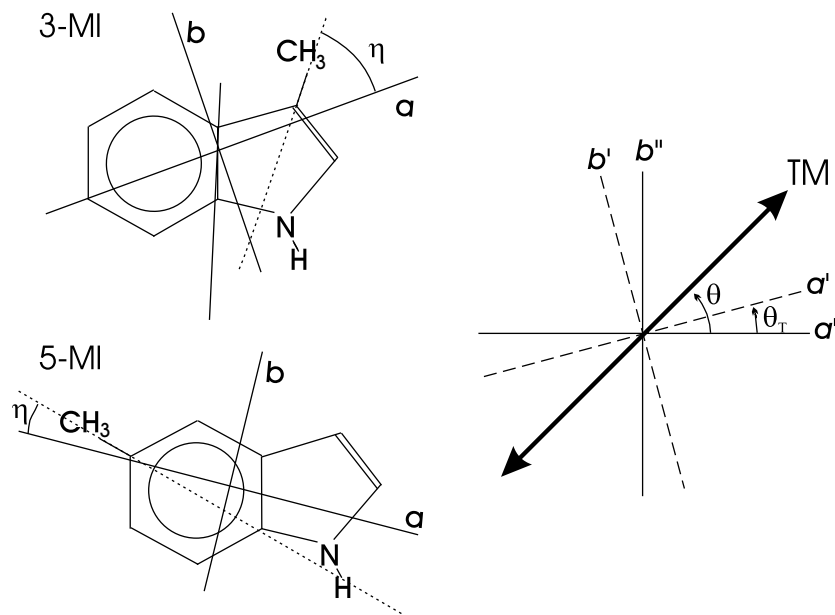


Figure 2.1: Definition of η , the angle between the internal rotation axis and the principal a axis, for 3-methylindole and 5-methylindole (left panel). In the right panel the transition moment angle θ and the axis reorientation angle θ_T are defined. Angles measured in counterclockwise sense are taken to be positive. a'' and b'' are the principal axes in the ground state, a' and b' are the principal axes in the excited state. The c axes are perpendicular to the indole frame.

approach [18, 23, 24], which permits us to solve the torsion and rotation problems separately. First, the pure torsional Hamiltonian is solved. The torsional Hamiltonian is expressed as [21, 23]:

$$H_t = Fp^2 + V_3(1 - \cos 3\alpha)/2 + V_6(1 - \cos 6\alpha)/2. \quad (2.5)$$

Eigenfunctions of this Hamiltonian are given by:

$$|\nu\sigma\rangle = \sum_{k=-\infty}^{\infty} A_k^{(\nu)} e^{i(3k+\sigma)\alpha}, \quad (2.6)$$

where ν is the torsional level label and σ can take on the values $-1, 0$, and $+1$ [21, 23]. This label indicates the symmetry of the torsional functions; levels with $\sigma = 0$ are of a symmetry and levels with $\sigma = \pm 1$ (two-fold degenerate levels) are of e symmetry.

Treating the interaction of the torsion with the overall rotation as a perturbation in the rotational Hamiltonian, an effective rotational Hamiltonian can be constructed for each $\nu\sigma$ torsional level [23, 24]:

$$H_{\nu\sigma} = AJ_a^2 + BJ_b^2 + CJ_c^2 + F \sum_{n=1}^{\infty} W_{\nu\sigma}^{(n)} (J_a\rho_a + J_b\rho_b)^n, \quad (2.7)$$

where $W_{\nu\sigma}^{(n)}$ is the n -th order perturbation coefficient for the $\nu\sigma$ level. The dimensionless perturbation coefficients $W_{\nu\sigma}^{(1)}$ and $W_{\nu\sigma}^{(2)}$ can be expressed in terms of matrix elements of the internal rotation angular momentum operator p in the basis of the torsional wave functions given in Eq. (2.6) [23]:

$$\begin{aligned} W_{\nu\sigma}^{(1)} &= -2\langle\nu\sigma|p|\nu\sigma\rangle \\ W_{\nu\sigma}^{(2)} &= 1 + 4F \sum_{(\nu\sigma)'} \frac{|\langle\nu\sigma|p|(\nu\sigma)'\rangle|^2}{E_{\nu\sigma} - E_{(\nu\sigma)'}} \end{aligned} \quad (2.8)$$

where $E_{\nu\sigma}$ and $E_{(\nu\sigma)'}$ are the torsional energies of the $\nu\sigma$ and $(\nu\sigma)'$ levels. Higher order coefficients $W_{\nu\sigma}^{(n)}$ can be expressed in terms of $W_{\nu\sigma}^{(1)}$ and $W_{\nu\sigma}^{(2)}$ via the relationship [23, 24]:

$$\frac{W_{\nu\sigma}^{(n+2)}}{W_{\nu\sigma}^{(n)}} \approx \frac{-(2\pi/3)^2}{(n+1)(n+2)} \quad \text{for } n > 0. \quad (2.9)$$

For the non-degenerate states (a levels), all odd-order perturbation terms are zero [23, 24]. This implies that for these states the rotational Hamiltonian in first approximation is given by a rigid rotor Hamiltonian with effective rotational constants [23]:

$$\begin{aligned} A_{\nu\sigma} &= A + F W_{\nu\sigma}^{(2)} \rho_a^2 \\ B_{\nu\sigma} &= B + F W_{\nu\sigma}^{(2)} \rho_b^2 \\ C_{\nu\sigma} &= C + F W_{\nu\sigma}^{(2)} \rho_c^2. \end{aligned} \quad (2.10)$$

For e levels also the odd-order perturbation terms should be taken into account. In both cases rotational basis functions up to $\Delta K = 4$ are mixed by the matrix elements for the effective rotational Hamiltonian [Eq. (2.7)] up to 4th order, which are given in Appendix B of Ref. [24].² The matrix of size $(2J+1) \times (2J+1)$ was diagonalized for every J for the two lowest torsional states, $0a_1$ and $0e$. K_a and K_c labels were assigned to the calculated rotational levels of a given J by their energy ordering, despite of the absence of a clear physical meaning of K_a (and especially K_c) labels in the presence of the torsion-rotation interaction [22]. The intensities of the rotational lines are calculated from the eigenvectors of the effective rotational Hamiltonian and the known direction cosine matrix elements [23]. The only selection rule used is $\Delta J = 0, \pm 1$ which distinguishes P , Q , and R branches. If the transition dipole moment (TM) vector lies in the ab plane the line strength is proportional to:

$$A_{r''r'} \propto |\mu_a \langle r' | \Phi_{Za} | r'' \rangle|^2 + |\mu_b \langle r' | \Phi_{Zb} | r'' \rangle|^2 + 2\mu_a \mu_b \langle r' | \Phi_{Za} | r'' \rangle \langle r' | \Phi_{Zb} | r'' \rangle, \quad (2.11)$$

where the Z axis is the space-fixed axis along the direction of the laser polarization, $|r\rangle \equiv |J, K_a, K_c\rangle$, $\mu_a = \mu \cos \theta$, and $\mu_b = \mu \sin \theta$. The double and single prime denote the ground

²The use of a different basis set, in which the symmetric top basis functions are related to the a axis (the I representation) and the matrix elements of both J_a and J_b are real, (a convention also used by Hougen *et al.* in Ref. [22]), will slightly alter the coefficients of the matrix elements. The methyl top axis is in the ab plane ($\rho_c = 0$). Two matrix elements were found to differ from those given in Ref. [24]: $\langle K | (\rho_a J_a + \rho_b J_b)^4 | K \rangle = \rho_a^4 K^4 + \frac{1}{2} \rho_a^2 \rho_b^2 [(P^2 - K^2)(6K^2 + 1) - 4K^2] + \frac{1}{8} \rho_b^4 [3(P^2 - K^2)^2 - 2(P^2 - K^2) + 3K^2]$ and $\langle K | (\rho_a J_a + \rho_b J_b)^4 | K \pm 1 \rangle = \rho_a^3 (2K \pm 1) [K^2 + (K \pm 1)^2] + \frac{1}{2} \rho_a \rho_b^2 (2K \pm 1) \{3[P^2 - K(K \pm 1)] - 4\}$.

and excited state, respectively, μ is the absolute value of the transition dipole moment (TM), θ is the angle of the TM vector with respect to the molecule-fixed a axis, and Φ_{Za} and Φ_{Zb} are the direction cosines between the laboratory Z axis and the molecular a and b axes.

Indole, the chromophore of 3-MI and 5-MI, shows axis reorientation upon electronic excitation [25]. The principal axis system rotates around the c axis (see Figure 2.1) and although the angle of rotation is small, only 0.5° , the effect on the intensities of the rotational transitions is very pronounced. For a correct calculation of the intensities all rotational wave functions of the ground and the excited state should be expressed in a common coordinate system. This can be achieved by transforming the excited state Hamiltonian *via* a rotation of \vec{J} around the c axis by an angle θ_T [25, 26]:

$$\begin{aligned} H_{v'\sigma'}^t = & (A' \cos^2 \theta_T + B' \sin^2 \theta_T) J_a'^2 + (A' \sin^2 \theta_T + B' \cos^2 \theta_T) J_b'^2 + C' J_c'^2 \\ & + (A' - B') \sin \theta_T \cos \theta_T (J_a' J_b' + J_b' J_a') \\ & + F' \sum_{n=1}^{\infty} W_{v'\sigma'}^{(n)} [(\rho_a' \cos \theta_T - \rho_b' \sin \theta_T) J_a' + (\rho_a' \sin \theta_T + \rho_b' \cos \theta_T) J_b']^n. \end{aligned} \quad (2.12)$$

In this way the excited state Hamiltonian is expressed in the coordinate system of the ground state and its eigenfunctions can therefore be given within the same basis set as the ground state functions.³ It is readily seen that the matrix elements of the transformed effective rotational Hamiltonian [Eq. (2.12)] are the same as those for the effective rotational Hamiltonian [Eq. (2.7)], with the exception that the constants A , B and C and ρ_a and ρ_b are replaced by variables depending on the transformation angle θ_T . The cross term $J_a J_b + J_b J_a$ however, gives rise to a new matrix element

$$\langle JK | (J_a J_b + J_b J_a) | JK \pm 1 \rangle = \frac{1}{2} (2K \pm 1) [J(J+1) - K(K \pm 1)]^{\frac{1}{2}}. \quad (2.13)$$

2.2.2 Effects on rotational spectra

The most apparent effect of the internal motion of the methyl group on the rotational spectra of the $S_1 \leftarrow S_0$ origin bands is the occurrence of two overlapping spectra arising from transitions between levels with different torsional symmetries ($0a_1 - 0a_1$ and $0e - 0e$ transitions). The two spectra can each be described by an effective rotational Hamiltonian, which accounts for the interaction between torsion and overall rotation [Eq. (2.7)]. The two origins will be shifted by:

$$\Delta v_0^{ae} = \Delta E'_{ae} - \Delta E''_{ae}, \quad (2.14)$$

where $\Delta E''_{ae}$ and $\Delta E'_{ae}$ are the torsional splittings between the $0a_1$ and $0e$ levels in the ground and excited state, respectively. The torsional level splitting is larger for lower barriers; hence, a lowering of the barrier upon excitation will cause a blue shift of the $0e - 0e$ origin with respect to the $0a_1 - 0a_1$ origin.

Since all the odd perturbation coefficients vanish for a levels, the effects of the internal rotation interaction are largest for the e levels. For these levels the rigid rotor wavefunctions are

³It should be kept in mind that the angle of the transition dipole moment θ is given with respect to the a'' axis, as well as the methyl top axis in the ground state, η'' , which is embedded in ρ_a and ρ_b , but the corresponding angle in the excited state, η' , is still defined with respect to the a' axis.

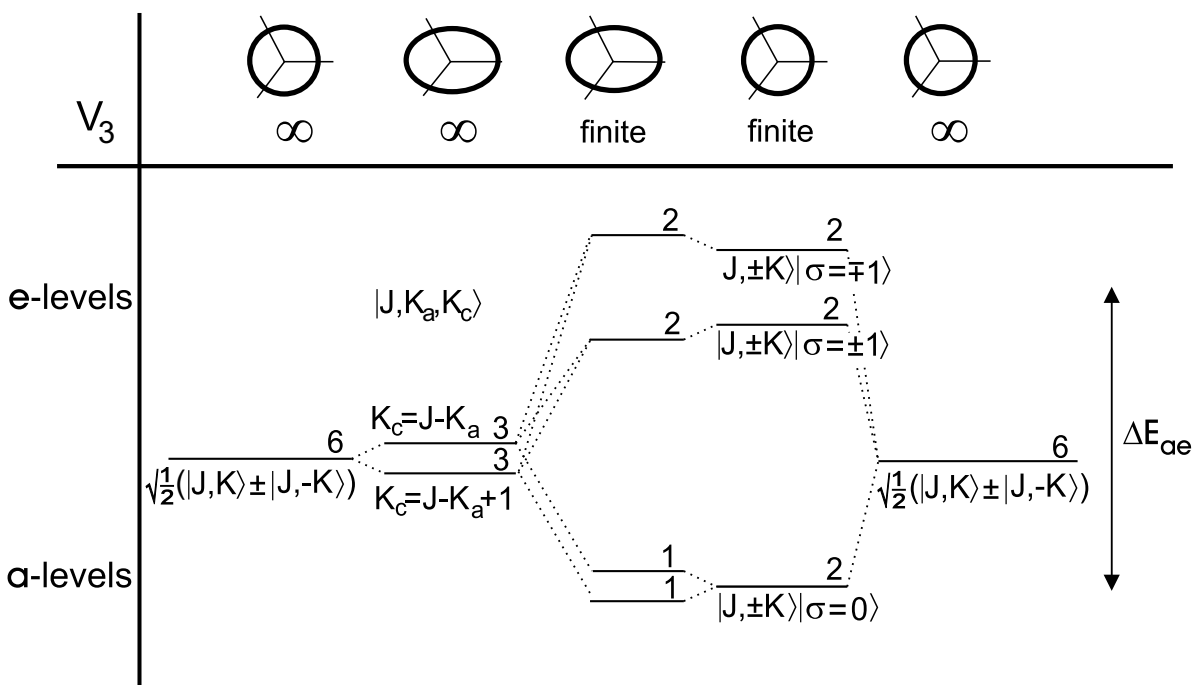


Figure 2.2: Correlation diagram, showing the effects of internal rotation on the energy and characterization of symmetric and asymmetric rotor levels. The figures on top of the diagram represent the symmetry of the rotor, while directly below the barrier height indicates whether there is internal rotation (finite barrier) or not (infinite barrier). The degeneracy of the levels is given by the numbers above each level. Where possible, a characterization of each level is given. ΔE_{ae} equals the torsional level splitting.

mixed. The mixing due to odd powers of J_a increases with increasing values of K_a and the mixing due to odd powers of J_b decreases with increasing values of K_a . Figure 2.2 schematically shows the effects of both asymmetry and internal rotation on the rigid symmetric rotor levels and displays the correlation of perturbed asymmetric rotor levels with rigid asymmetric rotor levels on the one hand and perturbed symmetric rotor levels on the other hand.

The mixing of K_c values causes a splitting of (almost) degenerate K doublets and the appearance of lines that are forbidden in the asymmetric rigid rotor limit, as illustrated in Figure 2.3. This is especially apparent in transitions involving high K_a levels of the $0e$ state, where the mixing of K_c values can be almost complete. The stronger the mixing of wavefunctions the more intense the 'forbidden' lines will be. For low K_a values there will be two strong rigid rotor allowed and two weak anomalous lines. For high K_a values there will be two weak 'allowed' and two strong anomalous lines. For some intermediate K_a value there will be four lines of comparable intensity.

Because rigid rotor wavefunctions of different K_a parity are mixed, as well, the line strength of a transition is no longer described by only one term in Eq. (2.11). A transition can be induced by both the a and b component of the TM (such a transition is no longer a pure a or pure b type

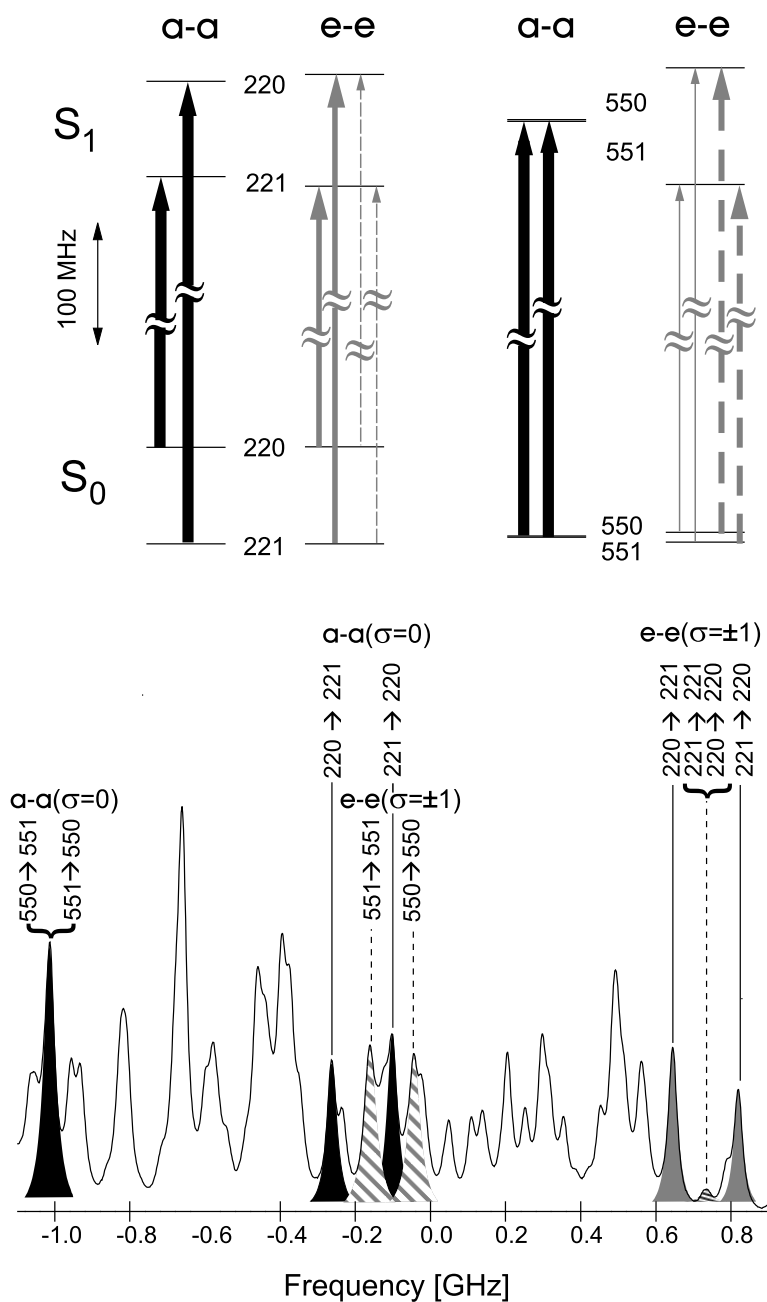


Figure 2.3: Effect of internal rotation on a type transitions in the Q branch of 3-methylindole. Upper panel: e levels with high J , K_a value are split by $FW_{0e}^{(1)} \rho_a K_a$. The width of the arrows corresponds (approximately) to the strength of the transitions; the $0e - 0e$ transitions show a change from 'normally allowed' transitions ($\Delta K_c = \pm 1$) for low K_a values, where the asymmetry splitting is large, to anomalous transitions ($\Delta K_c = 0$) for high K_a values, where the asymmetry splitting is much smaller. This is also illustrated by part of the experimental spectrum of 3-methylindole (lower panel), where the corresponding transitions are marked.

transition). The interference term in the line strength formula [Eq. (2.11)] makes it possible to distinguish positive and negative angles of the TM, as first discussed by Plusquellic *et al.* [27]. A change of the sign of this angle would change the sign of the interference term and therefore affects the intensities.

Axis reorientation also mixes the wavefunctions, as can be seen from Eq. (2.12). The term proportional to $(J_a J_b + J_b J_a)$ couples states with different K_a parities and therefore mixes the character of a and b type lines [26]. Unlike the internal rotation induced mixing, axis reorientation affects a and e symmetry levels in a similar way.

2.2.3 Computational Approach

All assigned rotational lines in the overlapping $0a_1 - 0a_1$ and $0e - 0e$ spectra were fit simultaneously with torsional frequencies from the literature if available. There are several advantages to this approach in comparison with the separate analysis of the $0a_1 - 0a_1$ and $0e - 0e$ spectra. (i) The perturbation coefficients and the torsional barrier heights are more accurate, since the vibrational band frequencies and rotational line frequencies are used in a self-consistent way. (ii) An important structural parameter, the angle of the methyl top axis is obtained directly from the fit. (iii) The ‘torsion-free’ rotational constants, which are directly related to the corresponding moments of inertia of the molecule, are immediately obtained. (iv) The assignment of extensively overlapping lines is much easier if the measured spectrum is directly compared with the composite $0a_1 - 0a_1/0e - 0e$ spectrum.

We start by fitting the frequencies of the rotational lines and torsional transitions to the torsional and effective rotational Hamiltonians [Eqs. (2.5) and (2.7)]. A maximum of 15 parameters can be determined, including the rotational constants A , B and C of the ground and electronically excited states, the torsional barrier heights in both states and the frequency of the $0a_1 - 0a_1$ band origin.

The constants resulting from the frequency fit are kept fixed in the intensity fit, where 10 additional parameters can be determined; the rotational population distribution parameters T_1 , T_2 , and w (see below), the transition dipole moment angle θ , the axis reorientation angle θ_T , the intensity ratio of the $0e - 0e$ and $0a_1 - 0a_1$ spectra I_e/I_a , the Lorentzian and the Gaussian contributions to the width of the Voigt-shaped lines, the background intensity, and an intensity scaling factor. The importance of these parameters has been extensively discussed in Ref. [25].

The intensity ratio of the $0e - 0e$ and $0a_1 - 0a_1$ spectra is given by:

$$\frac{I_e}{I_a} = \frac{g_e \cdot n_{S_e} \cdot S_e \cdot n_e}{g_a \cdot n_{S_a} \cdot S_a \cdot n_a}, \quad (2.15)$$

where g_e and g_a are the degeneracies of the $0a_1$ and $0e$ levels ($g_e = 2$ and $g_a = 1$), n_{S_e} and n_{S_a} are the nuclear spin statistical weights ($n_{S_e}/n_{S_a} = 1 : 2$ for molecules of G_6 symmetry [21, 28]), S_e and S_a are the strengths of the $0a_1 - 0a_1$ and $0e - 0e$ torsional bands (squared Franck-Condon factors), and n_e/n_a is the population ratio of $0a_1$ and $0e$ torsional states. Under the usual assumption of no collisional population redistribution between $0a_1$ and $0e$ levels during the expansion, the latter ratio is one.

The ground state rotational population, used to calculate the intensities, was described separately for each torsional level. It is given by a two-temperature distribution [25, 29]:

$$n_{J,K_a,K_c}(T_1, T_2, w) = e^{-E_{J,K_a,K_c}/kT_1} + w e^{-E_{J,K_a,K_c}/kT_2}, \quad (2.16)$$

where the energies E_{J,K_a,K_c} are pure rotational energies (relative to the lowest $0a_1$ and $0e$ rotational level respectively), and w is the weighting factor for the second temperature. The same weighting factors and rotational temperatures were used to describe the distribution over the $0a_1$ and $0e$ levels.

The final constants are obtained by averaging the results from different measurements of the same spectrum to reduce the errors due to a drift in the relative frequency calibration device. The errors of the constants reported are in most cases determined by the variations within different scans rather than by the statistical errors resulting from the fitting procedure. However, for several parameters the statistical error still dominates.

2.3 Experiment

Rotationally resolved fluorescence excitation spectra of 3-MI and 5MI were obtained using a narrow bandwidth UV laser system and a molecular beam apparatus [30]. 3-MI or 5-MI, obtained from Aldrich, was heated to *ca.* 75 °C, seeded in 0.6 bar argon, and expanded through a nozzle with a diameter of about 0.15 mm. The nozzle was kept at a slightly higher temperature than the sample vessel to prevent condensation of the sample in the orifice. The molecular beam was skimmed twice in a differential pumping system and was crossed perpendicularly with a UV laser beam at about 30 cm from the nozzle. The pressure in the detection chamber was below 10^{-6} mbar, assuring collision free conditions. The total undispersed fluorescence was imaged onto a photomultiplier connected to a photon counting system, interfaced with a computer.

UV radiation with a bandwidth of 3 MHz was generated by intracavity frequency doubling in a single frequency ring dye laser, operating on Rhodamine 110 and Rhodamine 6G for the 3-MI and 5-MI measurements, respectively. By using a 2 mm thick Brewster cut BBO crystal, 0.1 mW of tunable UV radiation was obtained. Light at the fundamental frequency was used for calibration and stabilization purposes. For relative frequency calibration a temperature stabilized Fabry–Perot interferometer was used with a free spectral range of 75 MHz. For absolute frequency calibration the iodine absorption spectrum [31] was recorded simultaneously. The scanning range is typically 2 cm^{-1} at the fundamental frequency.

The spectral resolution of the experimental setup is determined by the residual Doppler width in the molecular beam and the geometry of the fluorescence collection optics. Although the instrumental Doppler width is not known for specific molecules, it can be estimated to be ~ 16 MHz FWHM from the results of similar experiments on indole, indazole, and benzimidazole, measured previously using this setup [25].

2.4 Frequency analysis

2.4.1 3-methylindole

The observed spectrum of the $S_1 \leftarrow S_0$ origin band of 3-MI is presented in Figure 2.4. This spectrum is a composite of the $0a_1 - 0a_1$ and $0e - 0e$ spectra, whose simulations are given separately in the upper two panels. The $0e - 0e$ spectrum (of which the origin is indicated by an arrow in Figure 2.4) is blue shifted with respect to the $0a_1 - 0a_1$ spectrum, which means that

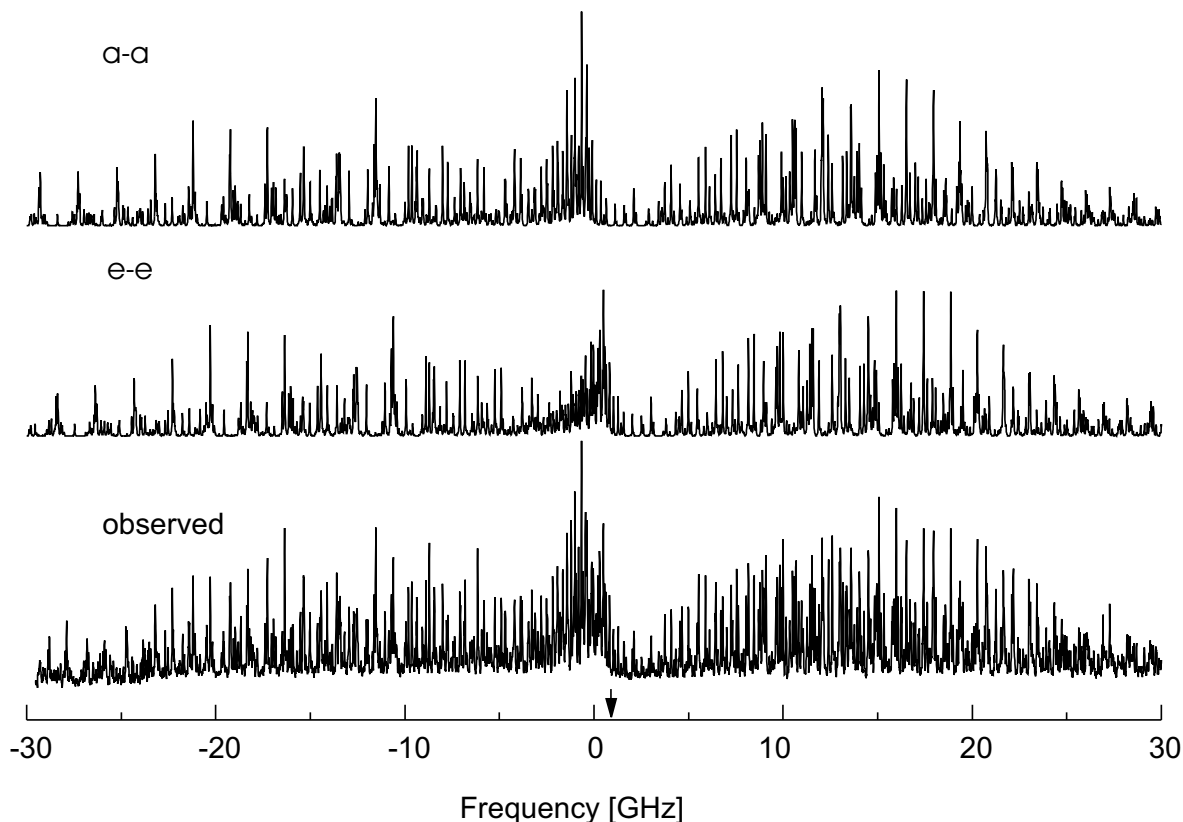


Figure 2.4: *Experimental spectrum of 3-methylindole (lower panel) together with simulations of the $0a_1-0a_1$ and $0e-0e$ transitions (upper two panels). The $0a_1-0a_1$ origin (0 on the scale of the figure) is located at $34\,874.69(1)\text{ cm}^{-1}$. The origin of the $0e-0e$ band is indicated by the arrow.*

the torsional barrier in the excited state is lower than that in the ground state. The separation between the origins of the $0a_1-0a_1$ and $0e-0e$ spectra, $\Delta\nu_0^{ae}$, was found to be 915 MHz. This separation appears in the spectrum as a spacing between $0a_1-0a_1$ and $0e-0e$ rotational transitions starting from low K_a levels. High K_a levels of the $0e$ states are disturbed by the torsion-rotation interaction, which causes this spacing to no longer be constant.

It was possible to reproduce all observed lines using terms up to $n = 2$ in the Hamiltonian of Eqs. (2.7) and (2.12). The analysis started with the simulation of a pure a type spectrum of a rigid asymmetric rotor, using rotational constants calculated from a 3-MI geometry obtained from the attachment of a methyl group to the calculated geometry of indole [32]. By comparison of this simulation with the observed spectrum several $0a_1-0a_1$ lines could be assigned. A fit of these lines provided improved rotational constants. Next, we simulated the complete spectrum containing all $0a_1-0a_1$ and $0e-0e$ lines, fixing the distance between the $0a_1-0a_1$ and $0e-0e$ origins to 915 MHz by adjusting the values of V_3'' and V_3' , taken from Ref. [8]. Eventually, about 400 $0a_1-0a_1$ and 400 $0e-0e$ lines were included in the fit, together with the excited state torsional frequencies of the $2a_1 \leftarrow 0a_1$ band at 188 cm^{-1} and the $2e \leftarrow 0e$ band at 197 cm^{-1} [8].

Table 2.1: Molecular constants of 3-methylindole. Fitted parameters are given in the upper part, derived parameters in the lower part.

	S_0	S_1		
$A'', A'-A''$	2603.6(9)	-37.45(3)	MHz	
$B'', B'-B''$	1268.6(2)	-18.30(2)	MHz	
$C'', C'-C''$	857.7(1)	-12.40(2)	MHz	
F_α		5.17(3)	cm ⁻¹	a)
V_3	500(40)	301(1)	cm ⁻¹	a)
η		50.1(9)	deg	a)
θ		$\pm 26.3(9)$	deg	b)
θ_T		$\pm 0.7(3)$	deg	b)
ν_0^{aa}		34874.69(1)	cm ⁻¹	
$\Delta \nu_0^{ae}$		914.7(4)	MHz	
ΔE_{ae}	90(40)	1005(40)	MHz	
I_α	3.26(2)	3.26(2)	amu Å ²	
F	5.23(3)	5.23(3)	cm ⁻¹	
$W_{0e}^{(1)}$	$-7(3) \times 10^{-4}$	$-77(3) \times 10^{-4}$		c)
$W_{0a}^{(2)}$	$8(4) \times 10^{-4}$	$93(3) \times 10^{-4}$		
$W_{0e}^{(2)}$	$-4(2) \times 10^{-4}$	$-47(2) \times 10^{-4}$		
$F W_{0e}^{(1)} \rho_a$	-1.2(5)	-12.9(6)	MHz	c),d)
$F W_{0e}^{(1)} \rho_b$	-0.7(3)	-7.5(3)	MHz	c),d)

a) $F''_\alpha = F'_\alpha$, $V''_6 = V'_6 = 0$, and $\eta'' = \eta'$ is assumed.

b) The signs of θ and θ_T cannot be independently determined from the fit. They are, however, coupled: both must either be positive or negative.

c) $W_{0e}^{(1)}$ is given for $\sigma = +1$. The value for $\sigma = -1$ is given by $-W_{0e}^{(1)}$.

d) $F W_{0e}^{(2)} \rho_g^2$, $g = a, b$ are < 0.02 MHz for S_0 , and < 0.2 MHz for S_1 .

Since the spectra did not contain enough information to determine all possible parameters, we made the following assumptions. First, it was assumed that the internal rotation constant of the methyl group does not change upon excitation; *i.e.*, the difference $F'_\alpha - F''_\alpha$ was fixed to zero. Since the torsion-rotation interaction in the ground state of 3-MI is very small, the calculated spectrum is relatively insensitive to large variations ($\sim 5^\circ$) of the ground state methyl top angle η'' , and it turned out to be impossible to fit η'' and $\eta' - \eta''$ simultaneously. We therefore also fixed $\eta' - \eta''$ to zero. The molecular constants obtained from the fit are listed in Table 2.1 together with the absolute center frequency of the $0a_1 - 0a_1$ spectrum ν_0^{aa} and several other constants calculated from the fit parameters.

Due to the high torsional barriers in both electronic states of 3-MI, the effective rotational constants for the $0a_1 - 0a_1$ and $0e - 0e$ spectra differ by less than 0.2 MHz from the 'torsion-free' values. This implies that the $0a_1 - 0a_1$ spectrum is practically that of a rigid asymmetric molecule with the same rotational constants and the perturbations of the $0e - 0e$ spectrum are mainly determined by the first-order terms in the effective rotational Hamiltonian.

As can be seen from Table 2.1, the torsion induced splittings of the $0e - 0e$ levels in the ground state ($\sim 2K_a F W_{0e}^{(1)} \rho_a$) reach a value that is comparable to the linewidth only at $K_a > 10$. Since the intensities of these lines are already negligible, it is impossible to obtain the ground state barrier height V_3'' directly from these splittings. V_3'' is determined via the excited state torsional parameters and the separation of the origins of the $0a_1 - 0a_1$ and $0e - 0e$ spectra, $\Delta\nu_0^{ae}$ [Eq. (2.14)]. This separation is directly determined from the observed spectrum, while V_3' is determined by a combination of the two torsional frequencies included in the fit and the perturbations of the $0e - 0e$ lines of the observed spectrum. It follows therefore that the uncertainties of both barrier heights V_3'' and V_3' largely depend on the torsional frequencies, which are accurate to 1 cm^{-1} .

2.4.2 5-methylindole

The spectrum of the $S_1 \leftarrow S_0$ origin band of 5-MI consists, like that of 3-MI, of a $0a_1 - 0a_1$ and a $0e - 0e$ spectrum. Figure 2.5 presents the observed spectrum (lower panel) together with simulations of the two separate $0a_1 - 0a_1$ and $0e - 0e$ spectra (upper panels). The $0e - 0e$ spectrum is again blue shifted with respect to the $0a_1 - 0a_1$ spectrum, indicating a lowering of the torsional barrier upon excitation, in this case by a substantially larger amount.

Terms up to $n = 4$ in the effective rotational Hamiltonian [Eqs. (2.7) and (2.12)] were necessary to reproduce the observed spectrum. The geometry of 5-MI was again constructed from the combination of a methyl group and an indole frame, which yielded the initial rotational constants. A hybrid asymmetric rotor spectrum was simulated and several $0a_1 - 0a_1$ lines were assigned. A fit of these lines provided the effective rotational constants for the $0a_1$ levels of the ground and the excited state of 5-MI. Assigning the $0e - 0e$ lines was more troublesome than for 3-MI, because the origin of the $0e - 0e$ spectrum is more shifted from the $0a_1 - 0a_1$ origin. Furthermore, the overall intensity of the $0e - 0e$ spectrum is about three times less than that of the $0a_1 - 0a_1$ spectrum. The distance between the origins was first crudely estimated and the values of the 3-fold barrier heights V_3'' and V_3' , taken from Ref. [7], were slightly adjusted to yield the correct $\Delta\nu_0^{ae}$ value ($\sim 0.9 \text{ cm}^{-1}$). These values enabled us to determine the perturbation coefficients from which we could calculate 'torsion-free' rotational constants for the ground and the excited state. In the next step these constants were used to simulate the composite spectrum of the $0a_1 - 0a_1$ and $0e - 0e$ bands. Finally, about 400 $0a_1 - 0a_1$ and 200 $0e - 0e$ transitions were included into the fit. The final parameters are given in Table 2.2.

Six excited-state torsional frequencies (39.5, 52, 74.6, 94.4, 155.5 and 203.1 cm^{-1}) [8], and six ground-state torsional frequencies (60.2, 101.3, 122.4, 166.7, 228.9, and 295.3 cm^{-1}) [7], were included into the fit. Thanks to this large number of torsional transitions also the 6-fold barrier heights V_6'' and V_6' could be determined. Within the errors η'' and η' yielded identical values in the attempt to fit both parameters. Therefore $\eta' - \eta''$ was fixed to zero. Furthermore, it was assumed that $F_\alpha' - F_\alpha'' = 0$.

As can be seen from Table 2.2 the difference between 'effective' A and 'torsion-free' A

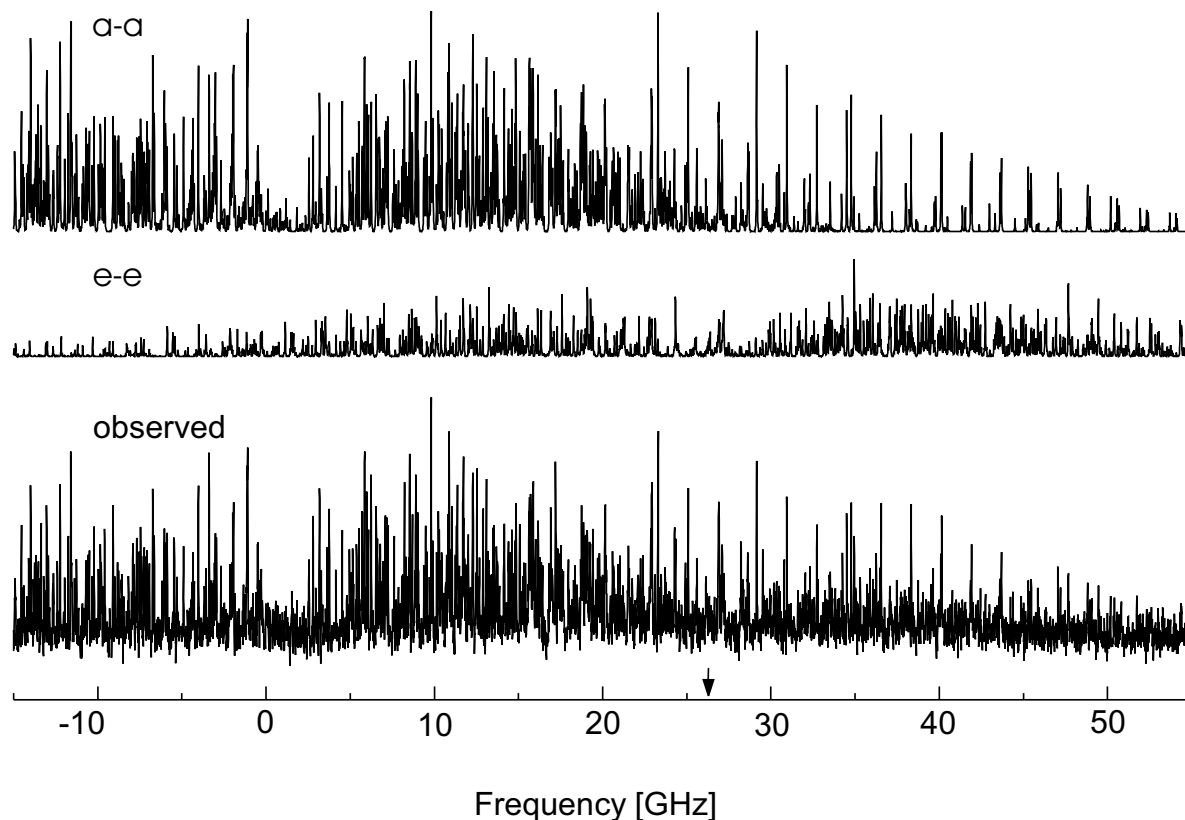


Figure 2.5: Experimental spectrum of 5-methylindole (lower panel) together with simulations of the $0a_1-0a_1$ and $0e-0e$ transitions (upper two panels). The $0a_1-0a_1$ origin (0 on the scale of the figure) is located at $34\,355.915(12)\text{ cm}^{-1}$. The origin of the $0e-0e$ band is indicated by the arrow.

constants, determined by $FW_{0a}^{(2)}\rho_a^2$ and $FW_{0e}^{(2)}\rho_a^2$, is quite significant (~ 25 MHz for the $0a_1$ states of S_1) and is different for $0a_1-0a_1$ and $0e-0e$ spectra. The difference for the B constants is less than 0.3 MHz.

2.5 Intensity analysis

With the parameters obtained from the frequency analysis kept fixed, the intensities of the rotational lines can now be analyzed. The results, which are averages of the results from fits of several measurements, are given in Table 2.1 and Table 2.2. Both molecules show an ab hybrid spectrum and undergo a reorientation of the inertial axes upon electronic excitation. For 5-MI it was possible to determine the signs of θ and θ_T . Information about the relative signs of the angles θ , θ_T , and η can only be obtained from the intensities. The $0a_1-0a_1$ spectrum behaves effectively as an ordinary asymmetric rotor spectrum and it is therefore only sensitive to the relative signs of θ and θ_T , as in indole [25]. The intensities of the $0e-0e$ lines, however, depend on the relative signs of angles θ , θ_T , and η . Therefore, since the sign of η is fixed by the

Table 2.2: Molecular constants of 5-methylindole. Fitted parameters are given in the upper part, derived parameters in the lower part.

	S_0	S_1		
$A'', A'-A''$	3459.9(1)	-132.85(4)	MHz	
$B'', B'-B''$	1034.06(5)	-0.81(1)	MHz	
$C'', C'-C''$	800.29(4)	-7.65(1)	MHz	
F_α		5.24(1)	cm^{-1}	a)
V_3	135(6)	85(1)	cm^{-1}	
V_6	-21(13)	-14(3)	cm^{-1}	
η		-16.9(4)	deg	a)
θ		53(1)	deg	
θ_T		0.4(2)	deg	
ν_0^{aa}		34355.915(12)	cm^{-1}	
$\Delta\nu_0^{ae}$		26325(2)	MHz	
ΔE_{ae}	18381(12)	44705(14)	MHz	
I_α	3.219(3)	3.219(3)	amu \AA^2	
F	5.348(6)	5.344(6)	cm^{-1}	
$W_{0e}^{(1)}$	-0.1431(3)	-0.3693(6)		b)
$W_{0a}^{(2)}$	0.1625(3)	0.3745(5)		
$W_{0e}^{(2)}$	-0.0809(2)	-0.1788(2)		
$FW_{0e}^{(1)}\rho_a$	-483.6(3)	-1199.6(4)	MHz	b)
$FW_{0e}^{(1)}\rho_b$	43.9(7)	113(2)	MHz	b)
$FW_{0a}^{(2)}\rho_a^2$	11.585(3)	24.667(3)	MHz	
$FW_{0e}^{(2)}\rho_a^2$	-5.764(2)	-11.773(3)	MHz	c)

a) F_α and η are assumed to be the same for S_0 and S_1 .

b) $W_{0e}^{(1)}$ is given for $\sigma = +1$. The value for $\sigma = -1$ is given by $-W_{0e}^{(1)}$.

c) $FW_{0a}^{(2)}\rho_b^2$ and $FW_{0e}^{(2)}\rho_b^2$ are < 0.1 MHz for S_0 , and < 0.3 MHz for S_1 .

geometry, the signs of θ and θ_T can be determined. For 5-MI this results in a TM angle θ that is $+53^\circ$, and a reorientation angle θ_T that is $+0.4^\circ$. The effect on the intensities of a change of θ and θ_T is demonstrated in Figure 2.6. For 3-MI the interference effects are not large enough to affect the intensities appreciably. It is therefore only possible to derive the relative signs of θ ($\theta = \pm 26.3^\circ$) and θ_T ($\theta_T = \pm 0.7^\circ$), yielding the same sign for both angles. The intensity ratio I_e/I_a found for 3-MI is approximately unity, in agreement with Eq. (2.15); the band strength ratio S_e/S_a is predicted to be 1.0, using the constants given in Table 2.1. For 5-MI a value of 0.25 ± 0.10 was found for the intensity ratio, again in agreement with the band strength ratio,

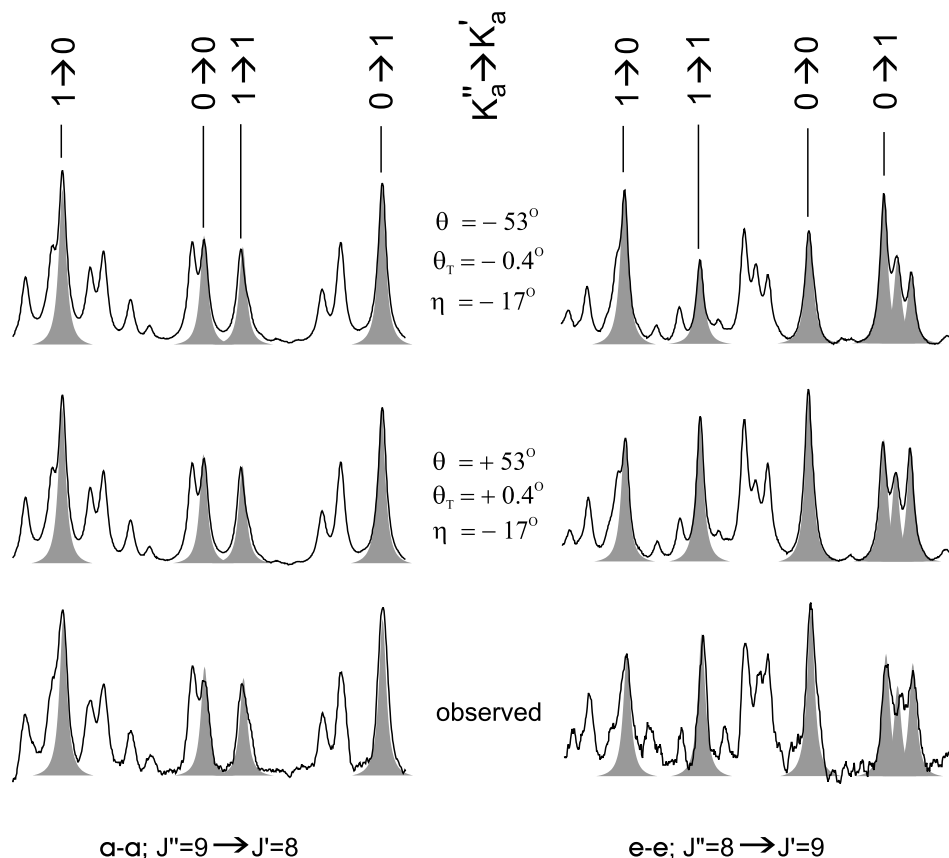


Figure 2.6: Parts of the $0a_1-0a_1$ and $0e-0e$ spectrum of 5-methylindole. The lower panels show the observed spectrum. The middle panels show simulations, using positive values for the transition moment and axis reorientation angle. A simultaneous change of sign of θ and θ_T does not affect the line positions but yields different intensities for the $0e-0e$ transitions, as can be seen from the upper panels.

which, using the constants given in Table 2.2, is predicted to be 0.304.

A Voigt line-profile was used in the fit of the observed spectrum. For 3-MI it was not possible to fit both the Lorentzian and Gaussian contributions to the linewidth. Therefore, we fixed the Gaussian contribution to 16 MHz, a value determined earlier for this experimental setup [25]. The resulting Lorentzian contribution to the linewidth was found to be 21 ± 3 MHz. Lifetime measurements of 3-MI by Demmer *et al.* [10] and Arnold *et al.* [3] yielded 12.3 ns and 13.8 ± 0.2 ns respectively. These result in Lorentzian contributions to the linewidth of only 12.9 MHz and 11.5 ± 0.2 MHz respectively. A similar line broadening, although less, was also found for indole and indazole [25]. For 5-MI we were able to fit both linewidth parameters, which yielded 17 ± 5 MHz and 10 ± 5 MHz for the Gaussian and the Lorentzian contribution respectively. This latter value corresponds to a lifetime of 15 ± 8 ns.

2.6 Discussion

The torsional barriers found for 3-MI are less accurate than those for 5-MI, but all values, where relevant, are in agreement with values found earlier [7, 8]. For both molecules the 3-fold barrier lowers by about a factor of 1.6 upon electronic excitation, which accounts for the blue shift of the $0e-0e$ origin with respect to the $0a_1-0a_1$ origin. 3-MI and 5-MI provide a nice example for comparing small and large internal rotation effects. The torsional barrier heights for 5-MI are about four times lower than those for 3-MI. This leads to larger torsional tunneling splittings (the $0a_1-0e$ distance ΔE_{ae}) for 5-MI, and larger distortions in the rotational spectrum of 5-MI compared to 3-MI. Therefore, fourth-order perturbation theory was necessary to describe the 5-MI spectrum while second-order theory was sufficient to describe the 3-MI spectrum. Despite this, the effects of K_c mixing can clearly be distinguished in the spectrum of 3-MI, as is illustrated in Figure 2.3.

The 3-fold barrier heights are related to the electron densities in the molecular frame at the site to which the methyl group is attached. In 3-MI the electron density is distributed asymmetrically around this site, which accounts for the large 3-fold barrier found for 3-MI. The much lower 3-fold and appreciable 6-fold barrier found for 5-MI can be explained by the much more symmetrical electron distribution in the benzene ring. The lowering of the 3-fold barrier upon electronic excitation indicates a shift of the electron distribution in the two molecules towards a more symmetrical distribution around the methyl group site.

Both 3-MI and 5-MI show hybrid type spectra. The 3-MI spectrum is predominantly a type ($|\theta| = 26^\circ$), while that of 5-MI is predominantly b type ($\theta = +53^\circ$). By virtue of the interference term in the intensity formula [Eq. (2.11)], arising from both axis reorientation and the interaction between internal and overall rotation, it was possible to determine the sign of the transition moment angle of 5-MI. This was found to be in agreement with several semi-empirical and *ab initio* calculations, which yield values between $+35^\circ$ and $+72^\circ$ for the TM angle of indole (for a review see Ref. [33]). It also agrees with the conclusion of Philips and Levy, who, after comparing the transition moment angles of tryptamine and indole, concluded that the transition moment angle of indole should be positive [34]. It is also consistent with the measurements of Albinsson *et al.* [17], who determined the angles θ of indole, 3-MI and 5-MI in polyethylene to be, respectively, $+42^\circ \pm 3^\circ$, $+30^\circ \pm 2^\circ$ and $+58^\circ \pm 2^\circ$. From this we conclude that, also for 3-MI, θ (and hence θ_T , which is found to have the same sign as θ) should be positive. Assuming that the direction of the TM with respect to the indole frame is the same in 3-MI and 5-MI as it is in indole, the TM angle in 3-MI and 5-MI can be calculated from the TM angle of indole. MP2/6-31G* geometry optimizations [35] were performed on 3-MI and 5-MI to ensure that the structure of the indole frame does not change significantly upon the attachment of a methyl group. This yielded 16° and 49° for the TM angles of 3-MI and 5-MI, respectively. The latter value is in reasonable agreement with the experimental value found for 5-MI, $53^\circ \pm 1^\circ$, implicating that the addition of a methyl group at C-5 only slightly influences the electron density changes in the indole frame upon excitation. For 3-MI however, the calculated value deviates much more from the experimental value, $26.3^\circ \pm 0.9^\circ$, implicating a larger influence of the methyl group.

The axis reorientation angles found for 3-MI and 5-MI (respectively 0.7° and 0.4°) are, as expected, comparable to the value found for indole (0.5° [25]). Geometry calculations on the first excited singlet state were performed by adding the excited state CIS/3-21G and ground

state HF/3-21G coordinate differences to the MP2/6-31G* ground state coordinates. The axis reorientation angle can subsequently be calculated using [22]:

$$\tan \theta_T = \frac{\sum_i m_i (a'_i b''_i - b'_i a''_i)}{\sum_i m_i (a'_i a''_i + b'_i b''_i)}, \quad (2.17)$$

where m_i are the atomic masses and a'_i, b'_i, a''_i, b''_i are the ground and excited state atomic coordinates, expressed in their inertial axis systems. For 5-MI this yielded a value of 0.4° , in good agreement with the measurements. For 3-MI calculations always converged into the 1L_a electronic state, which can be explained by the near degeneracy of the predicted 1L_a and 1L_b electronic states. No reorientation angle for excitation to the 1L_b state could therefore be determined.

2.7 Summary

The rotationally resolved excitation spectra of the $S_1({}^1L_b) \leftarrow S_0$ origin bands of 3-MI and 5-MI have been measured and analyzed. The rotational constants in the ground and electronically excited state have been determined for both molecules. These constants can be used to validate geometry calculations of these molecules. The transition moment angle was also determined from the spectra, consisting of two overlapping transitions between different torsional levels, which originate from the internal rotation of the methyl group. The spectra could be reproduced by describing the interaction between the overall rotation of the molecule and the internal rotation as a perturbation on the rotation. From the frequency analysis the rotational constants, the torsional barrier heights in the ground and electronically excited states, and the angle of the methyl top axis were determined. Intensity analysis of the spectra yielded values for the TM and axis reorientation angles.

Acknowledgments

Erko Jalviste gratefully acknowledges funding from the Nederlandse Organisatie voor Wetenschappelijk Onderzoek (NWO) and the Estonian Science Foundation (grant n.2270). Ivan Mistrík acknowledges the EPS/SOROS student mobility program for the financial support. This work was made possible by funding from the Dutch Foundation for Fundamental Research on Matter (FOM).

References

- [1] H. Lami and N. Glasser. *Indole's solvatochromism revisited*. *Journal of Chemical Physics* **84**:597–604, 1986.
- [2] P. R. Callis. *Molecular orbital theory of the 1L_b and 1L_a states of indole*. *Journal of Chemical Physics* **95**:4230–4240, 1991.

- [3] S. Arnold and M. Sulkes. *Spectroscopy of solvent complexes with indoles: Induction of $^1L_a - ^1L_b$ state coupling*. Journal of Physical Chemistry **96**:4768–4778, 1992. and references therein.
- [4] W. J. Hehre, J. A. Pople, and A. J. P. Devaquet. *Torsional potentials of methyl rotors attached to polar linkages*. Journal of the American Chemical Society **98**:664–668, 1976.
- [5] A. E. Dorigo, D. W. Pratt, and K. N. Houk. *Origin of methyl conformational preferences and rotational barriers in the ground states, excited triplet states, radical cations, and radical anion of molecules having $CH_3-C=X$ functionalities*. Journal of the American Chemical Society **109**:6591–6600, 1987.
- [6] L. H. Spangler and D. W. Pratt. in *Jet Spectroscopy and Molecular Dynamics*. edited by J. M. Hollas and D. Phillips, Blackie Academic & Professional, London, 1995.
- [7] G. A. Bickel, G. W. Leach, D. R. Demmer, J. W. Hager, and S. C. Wallace. *The torsional spectra of jet-cooled methyl substituted indoles in the ground and first excited states*. Journal of Chemical Physics **88**:1–8, 1988.
- [8] D. M. Sammeth, S. S. Siewert, P. R. Callis, and L. H. Spangler. *Methyl rotor effects in 3- and 5-methylindole*. Journal of Physical Chemistry **96**:5771–5778, 1992.
- [9] A. A. Rehms and P. R. Callis. *Resolution of L_a and L_b bands in methyl indoles by two-photon spectroscopy*. Chemical Physics Letters **140**:83–89, 1987.
- [10] D. R. Demmer, G. W. Leach, and S. C. Wallace. *$^1L_a - ^1L_b$ coupling in the excited state of 3-methylindole and its polar clusters*. Journal of Physical Chemistry **98**:12834–12843, 1994.
- [11] E. H. Strickland and C. Billups. *Oscillator strengths of the 1L_a and 1L_b absorption bands of tryptophan and several other indoles*. Biopolymers **12**:1989–1995, 1973.
- [12] J. R. Cable. *Polarization resolved two-photon resonant ionization spectroscopy of indole and 3-methylindole*. Journal of Chemical Physics **92**:1627–1633, 1990.
- [13] D. M. Sammeth, S. X. Yan, L. H. Spangler, and P. R. Callis. *2-photon fluorescence excitation spectra of indole in vapor and jet - 1L_a states*. Journal of Physical Chemistry **94**:7340–7342, 1990.
- [14] D. M. Sammeth, S. S. Siewert, L. H. Spangler, and P. R. Callis. *1L_a transitions of jet-cooled 3-methylindole*. Chemical Physics Letters **193**:532–538, 1992.
- [15] B. J. Fender, D. M. Sammeth, and P. R. Callis. *Site selective photoselection study of indole in argon matrix: Location of the 1L_a origin*. Chemical Physics Letters **239**:31–37, 1995.
- [16] B. J. Fender and P. R. Callis. *1L_a origin locations of methyl indoles in argon matrices*. Chemical Physics Letters **262**:343–348, 1996.

- [17] B. Albinsson and B. Nordén. *Excited-state properties of the indole chromophore. Electronic transition moment directions from linear dichroism measurements: Effect of methyl and methoxy substituents.* Journal of Physical Chemistry **96**:6204–6212, 1992.
- [18] X. Q. Tan, W. A. Majewski, D. F. Plusquellic, and D. W. Pratt. *Methyl group torsional dynamics from rotationally resolved electronic spectra. 1- And 2-methylnaphthalene.* Journal of Chemical Physics **94**:77217733, 1991.
- [19] G. Berden, W. L. Meerts, M. Schmitt, and K. Kleiner. *High resolution UV spectroscopy of phenol and the hydrogen bonded phenol-water cluster.* Journal of Chemical Physics **104**:972–982, 1996.
- [20] S. J. Humphrey and D. W. Pratt. *Hydrogen bonding in acid-base complexes: The trans-hydroquinone-NH₃ complex in its S₀ and S₁ electronic states.* Journal of Chemical Physics **106**:908–915, 1997.
- [21] C. C. Lin and J. D. Swalen. *Internal rotation and microwave spectroscopy.* Review of Modern Physics **31**:841–892, 1959.
- [22] J. T. Hougen, I. Kleiner, and M. Godefroid. *Selection rules and intensity calculations for a C_s asymmetric top molecule containing a methyl group internal rotor.* Journal of Molecular Spectroscopy **163**:559–586, 1994.
- [23] E.W. Gordy and R. L. Cook. *Microwave Molecular Spectra.* John Wiley & Sons, New York, 3rd edition, 1984.
- [24] D. R. Herschbach. *Calculation of energy levels for internal torsion and over-all rotation. III.* Journal of Chemical Physics **31**:91–108, 1959.
- [25] G. Berden, E. Jalviste, and W. L. Meerts. *Rotationally resolved ultraviolet spectroscopy of indole, indazole, and benzimidazole: Inertial axis reorientation in the S₁(¹L_b) – S₀ transitions.* Journal of Chemical Physics **103**:9596–9606, 1995.
- [26] A. A. Held, B. B. Champagne, and D. W. Pratt. *Inertial axis reorientation in the S₁ – S₀ electronic transition of 2-pyridone. A rotational duschinsky effect. Structural and dynamical consequences.* Journal of Chemical Physics **95**:8732–8743, 1991.
- [27] D. F. Plusquellic and D. W. Pratt. *Exploiting quantum interference effects for the determination of the absolute orientation of an electronic transition moment vector in an isolated molecule.* Journal of Chemical Physics **97**:8970–8976, 1992.
- [28] L. H. Spangler and D. W. Pratt. *Laser-induced phosphorescence spectroscopy in supersonic jets. The lowest triplet states of glyoxal, methylglyoxal, and biacetyl.* Journal of Chemical Physics **84**:4789–4796, 1986.
- [29] Y. R. Wu and D. H. Levy. *Determination of the geometry of deuterated tryptamine by rotationally resolved electronic spectroscopy.* Journal of Chemical Physics **91**:5278–5284, 1989.

- [30] W. A. Majewski and W. L. Meerts. *Near-UV spectra with fully resolved rotational structure of naphthalene and perdeuterated naphthalene*. Journal of Molecular Spectroscopy **104**:271–281, 1984.
- [31] S. Gerstenkorn and P. Luc. *Atlas du Spectroscopie d’Absorption de la Molecule d’Iode*. (CNRS, Paris, 1978).
S. Gerstenkorn and P. Luc. *Absolute iodine (I_2) standards measured by means of fourier-transform spectroscopy*. Reviews of Physical Applications **14**:791–794, 1979.
- [32] L. S. Slater and P. R. Callis. *Molecular orbital theory of the 1L_a and 1L_b states of indole. 2. An ab initio study*. Journal of Physical Chemistry **99**:8572–8581, 1995.
- [33] P. R. Callis. 1L_a and 1L_b transitions of tryptophan: Applications of theory and experimental observations to fluorescence of proteins. in *Methods in Enzymology* volume 278, chapter 7, pages 113–150 edited by L. Brand and M. L. Johnson, Academic Press, New York, 1997.
- [34] L. A. Philips and D. H. Levy. *Determination of the transition moment and the geometry of tryptamine by rotationally resolved electronic spectroscopy*. Journal of Physical Chemistry **90**:4921–4923, 1986.
- [35] *GAUSSIAN 94 Revision D.3*. M. J. Frisch, G. W. Trucks, H. B. Schlegel, P. M. W. Gill, B. G. Johnson, M. A. Robb, J. R. Cheeseman, T. A. Keith, G. A. Petersson, J. A. Montgomery, K. Raghavachari, M. A. Al-Laham, V. G. Zakrzewski, J. V. Ortiz, J. B. Foresman, J. Cioslowski, B. B. Stefanov, A. Nanayakkara, M. Challacombe, C. Y. Peng, P. Y. Ayala, W. Chen, M. W. Wong, J. L. Andres, E. S. Replogle, R. Gomperts, R. L. Martin, D. J. Fox, J. S. Binkley, D. J. Defrees, J. Baker, J. P. Stewart, M. Head-Gordon, C. Gonzalez, and J. A. Pople. Gaussian, Inc., Pittsburgh PA, 1995.

Chapter 3

Structural information on the S_0 and S_1 state of *o*-fluorophenol by hole burning and high resolution ultraviolet spectroscopy

Abstract

The electronic transitions of *o*-fluorophenol situated at $36\,799.382\text{ cm}^{-1}$ and $36\,906.710\text{ cm}^{-1}$, denoted the A and B bands respectively, have been investigated by high resolution fluorescence excitation spectroscopy. Hole burning studies together with the high resolution spectroscopy results show, that both bands originate in the same ground state and can be fitted to the rotational constants of the *cis* isomer. The rotational constants for the excited states are found to be $A' = 3231.80\text{ MHz}$, $B' = 2207.92\text{ MHz}$ and $C' = 1313.97\text{ MHz}$ for the A band and $A' = 3226.95\text{ MHz}$, $B' = 2211.24\text{ MHz}$ and $C' = 1321.03\text{ MHz}$ for the B band. The planarity of the ground state is lost upon electronic excitation, which enhances the activity of an out-of-plane vibration. The A and B band transitions arise from excitations to respectively the zero and first overtone levels in the double-minimum potential of this out-of-plane vibration, which shows similarities to the so-called butterfly mode observed in other benzene derivatives.

3.1 Introduction

Phenol and naphthol derivatives, substituted in ortho-position by a proton accepting group, provide model systems for studying the influence of intramolecular hydrogen bonding on the spectroscopic properties of the system [1–7]. However, these systems have two different isomers, differing by the direction of the hydroxyl group, as shown in Figure 3.1 for *o*-fluorophenol. In the *cis* isomer an intramolecular hydrogen bond is formed between the hydroxyl group and the proton accepting group, which will stabilize it over the *trans* isomer [8]. The influence of rotamerism on the spectroscopy and dynamics of the S_1 state has especially been studied in ortho-halophenols, such as chlorophenol [2] and fluorophenol [1], whose $S_0 - -S_1$ electronic transition displays two strong bands in the region of the origin, denoted A and B hereafter.

In the past decades there has been much discussion about the nature of the A and B band in *o*-fluorophenol. First measurements of the electronic spectrum in the gas-phase were done by Tripathi in 1971 [9]. Tripathi assigned the A band to the origin of the $A' \leftarrow A'$ transition, corresponding to the $B_{2u} \leftarrow A_{1g}$ transition of benzene, and the B band to a vibronic band, corresponding to an excited state fundamental of 109 cm^{-1} , since a vibration of this magnitude was also seen in *o*-fluoroanisole [10].

Since the dispersed fluorescence spectrum, obtained by exciting the B band, failed to show a strong band corresponding to a fundamental vibration of around 109 cm^{-1} , Oikawa *et al.* [1] assigned the two bands to the origins of the two different isomers. The greater stability of the *cis* isomer was used as an argument to assign the (stronger) A band to the *cis* and the B band to the *trans* isomer.

Measurements of the OH stretching vibration by Omi *et al.* [11] contradicted these results. Using IR dip spectroscopy, they measured the OH stretching vibration via excitation of both the A and B states and in both cases found the same value (3634 cm^{-1}). This implies that both bands belong to the same isomer, since the intramolecular hydrogen bond in the *cis* isomer will cause a difference between the OH stretching frequency of the two isomers. A redshift to the phenol frequency (3658 cm^{-1}) of 24 cm^{-1} was observed. This is a typical shift for weakly hydrogen bonded OH and leads to the conclusion that both bands originate from the *cis* isomer. Fujii *et al.* [12, 13] reached the same conclusion from the OH stretching vibration of the *o*-fluorophenol ion. Although no splitting in the OH stretching mode has been observed in the

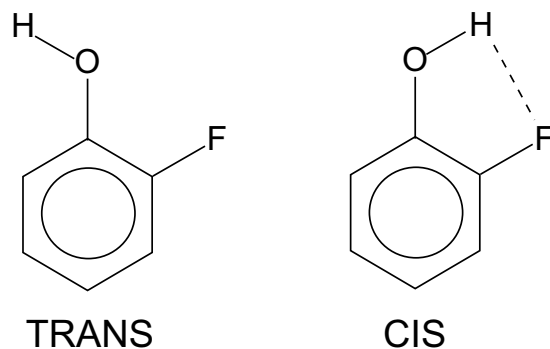


Figure 3.1: The two different isomers of *o*-fluorophenol.

vapor phase, a splitting of the OH torsional frequency has been related to the presence of the two different isomers [14].

The microwave spectra of *o*-fluorophenol and its deuterated derivative only show the presence of the *cis* isomer [15]. However, the authors did not rule out the existence of a *trans* isomer, since the lines due to the *trans* form could be weaker than the detection limit.

In recent measurements [16] on clusters of *o*-fluorophenol with benzene and water the signal arising from clusters of molecules associated with the A band was found to be much stronger than that from clusters associated with the B band. The *trans* isomer is expected to form clusters more easily than the *cis* isomer. So if both excited states have comparable fluorescence lifetimes, the A band should be associated with the *trans*, and the B band with the *cis* isomer, respectively.

To decide unambiguously whether the A and B bands arise from the same ground state species, we have applied ground state depletion (hole burning) spectroscopy to *o*-fluorophenol. Since the rotational constants of a given state contain much information on the structure of the molecule in that state, we also studied the rotationally resolved ultraviolet excitation spectra of the A and B band. These spectra enabled us to determine unambiguously the structure of *o*-fluorophenol in both the ground and the excited state.

3.2 Experiment

The experimental setup that was used for the low resolution experiments has been described previously [4]. Briefly, the molecules under study are cooled down in a continuous expansion and excited with a frequency-doubled dye laser (Coumarin 540A) pumped by the third harmonic of a YAG Laser (BM Industries or Quantel). The fluorescence is observed at right angle through a WG 285 or WG 310 cut-off filter by a Hamamatsu R2059 photomultiplier. The signal is monitored by a Camac ADC (LeCroy 2249W), connected to a PC.

Lipert and Colson were the first to report hole burning experiments in a supersonic jet [17]. The experiments involve a pump-probe excitation scheme: an intense pump laser beam is scanned through the wavelength region of interest while a counterpropagating probe laser, that is delayed in time, is fixed on a selected resonance. The resulting fluorescence is a measure of the population of the probed ground state level. When both lasers excite transitions which arise from the same ground state species, the pump beam induced depopulation manifests itself by a decrease in the intensity of the fluorescence excited by the probe (spectral hole). If both lasers excite different ground state levels, no spectral hole is observed.

The apparatus that was used to measure the rotationally resolved fluorescence excitation spectra of *o*-fluorophenol has extensively been described elsewhere [18]. A molecular beam was formed by expanding *o*-fluorophenol (Aldrich, 98%), seeded in 0.6 bar argon, through a quartz nozzle with a diameter of about 0.15 mm. The molecular beam was skimmed twice in a differential pumping system, and was crossed perpendicularly with a UV laser beam at about 30 cm from the nozzle. The pressure in the detection chamber was below 10^{-6} mbar, assuring collision free conditions. The total undispersed fluorescence was collected by two spherical mirrors and imaged onto a photomultiplier, which was connected to a photon counting system, interfaced with a computer.

Intracavity frequency doubling in a single frequency ring dye laser, operating on Rhodamine 110, was used to generate UV radiation with a bandwidth of 3 MHz. By using a 2 mm

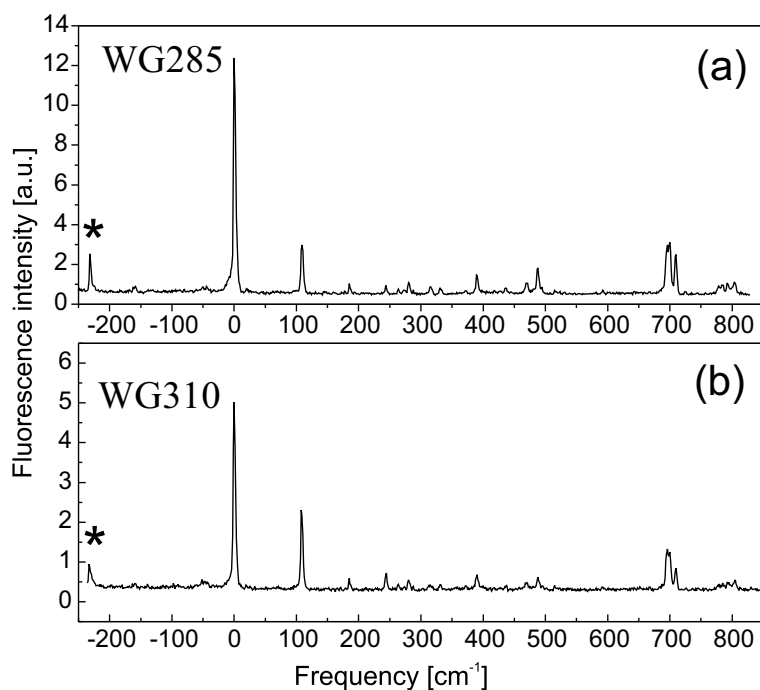


Figure 3.2: Fluorescence excitation spectrum of *o*-fluorophenol taken by monitoring the fluorescence through a WG 285 (a) and a WG 310 filter (b). The frequency scale is relative to the A band transition, which is at $36\,799\text{ cm}^{-1}$. The bands marked with an asterisk are due to the *o*-fluorophenol dimer.

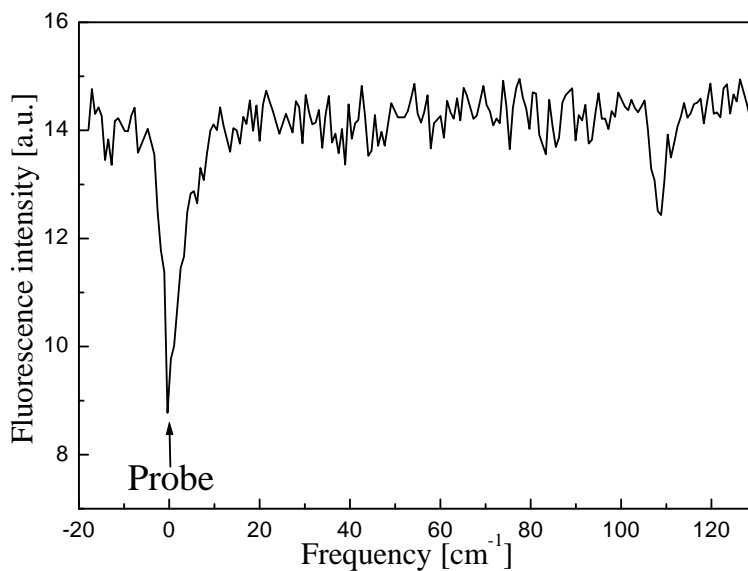


Figure 3.3: Hole burning spectrum of *o*-fluorophenol. The probe laser is fixed to the A band transition at $36\,799\text{ cm}^{-1}$, while the pump laser is scanned over both transitions. Frequencies are relative to the A band transition.

thick Brewster cut BBO crystal, 0.15 mW of tunable UV radiation was obtained. A temperature stabilized Fabry–Perot interferometer with a free spectral range of 75 MHz was used for relative frequency calibration, while the iodine absorption spectrum [19] was recorded simultaneously for absolute frequency calibration.

The spectral resolution of the experimental setup is about 16 MHz and is determined by the residual Doppler width in the molecular beam and the geometry of the fluorescence collection optics.

3.3 Results

3.3.1 Low resolution measurements

The fluorescence excitation spectrum of *o*-fluorophenol is shown in Figure 3.2(a) (observation through a WG 285 filter) and Figure 3.2(b) (observation through a WG 310 filter). The origin, denoted as band A, is located at 36799 cm^{-1} [1] and is followed by a weaker band, located at 109 cm^{-1} (band B). The hole burning spectrum, recorded by fixing the probe laser on the A band and scanning the pump laser, is shown in Figure 3.3 and shows unambiguously that the A band and the B band are due to the same ground state.

The dispersed fluorescence spectra obtained by exciting the A and B bands are given in Figure 3.4. Vibrations that can be assigned to the ring deformation 18a, 6b, and 1 (Wilson’s notation [20]), appear in both the excitation and the emission spectra. However, as already noticed by Oikawa *et al.* [1], the 109 cm^{-1} frequency has no clear counterpart in the emission spectrum. The emission spectra resulting from excitation of the A and B bands show the same frequencies, *i.e.* both bands act as origin for the emission spectrum with the lowest frequency mode at 297 cm^{-1} . However, the peak observed around 440 cm^{-1} seems to consist of two transitions at 436 and 468 cm^{-1} , respectively. The latter is much more prominent in the emission spectrum from excitation to the B band.

In addition to the resonant fluorescence that both emission spectra show the B band exhibits a redshifted emission broadened by a spectral congestion, which peaks around 3000 cm^{-1} from excitation. This is confirmed by the excitation spectra recorded through the WG 285 and the WG 310 filter (Figure 3.2), which show that the A band emits much more to the blue (resonant emission only) than the B band.

A more careful study of the excitation spectra clearly demonstrates that also the 248 cm^{-1} band displays a redshifted emission. These bands (the B band at 109 cm^{-1} and the 248 cm^{-1} band) are assigned as excitations of the same vibrational mode with a negative anharmonicity. A similar negative anharmonicity was also found for one of the S_1 modes in catechol and its deuterated species [5, 6]. In that molecule intense low-frequency vibrations have been observed in both resonance enhanced two-photon ionization and hole burning spectra. For *d*2-catechol a 105 cm^{-1} mode was found in the $S_0 \rightarrow S_1$ excitation spectrum, while the lowest mode observed in the emission spectrum is at 289 cm^{-1} . This has been explained in terms of a torsion of (one of) the hydroxyl groups, moving in a harmonic potential in the ground state and a double-minimum potential in the electronically excited state. Out-of-plane vibrations were also found in perfluoronaphthol derivatives [4]. The inversion motion of the C–F bonds with respect to the aromatic ring (“butterfly motion”) can also be described by a harmonic potential for the ground

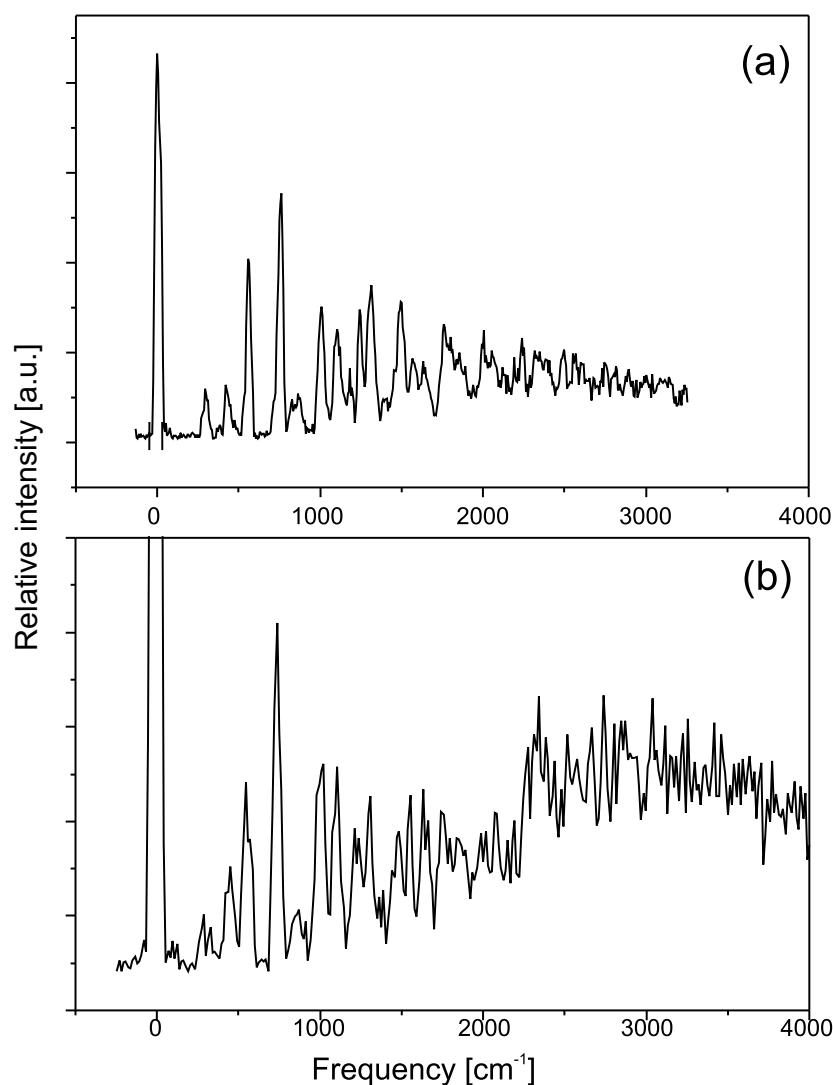


Figure 3.4: Comparison of the dispersed fluorescence spectra after exciting the A band at $36\,799\text{ cm}^{-1}$ (a) and the B band at $36\,907\text{ cm}^{-1}$ (b).

state and a double-minimum potential for the excited state.

The lifetimes of both the A and the B band are within the laser pulsewidth. However, the intensity ratio of the two bands in the fluorescence excitation spectrum (~ 2) is smaller than the intensity ratio in the REMPI spectrum (~ 15) [12]. This shows that the lifetime of the B band is shorter than that of the A band. The difference in lifetimes cannot be attributed to a difference in the intersystem crossing efficiency, because no difference in the laser induced fluorescence spectrum and the sensitized phosphorescence spectrum has been observed [2].

3.3.2 High resolution measurements

The rotationally resolved UV spectrum of the A band of *o*-fluorophenol is given in Figure 3.5. It is a *ab*-hybrid type spectrum with its origin situated at $36\,799.382\text{ cm}^{-1}$. The rotationally

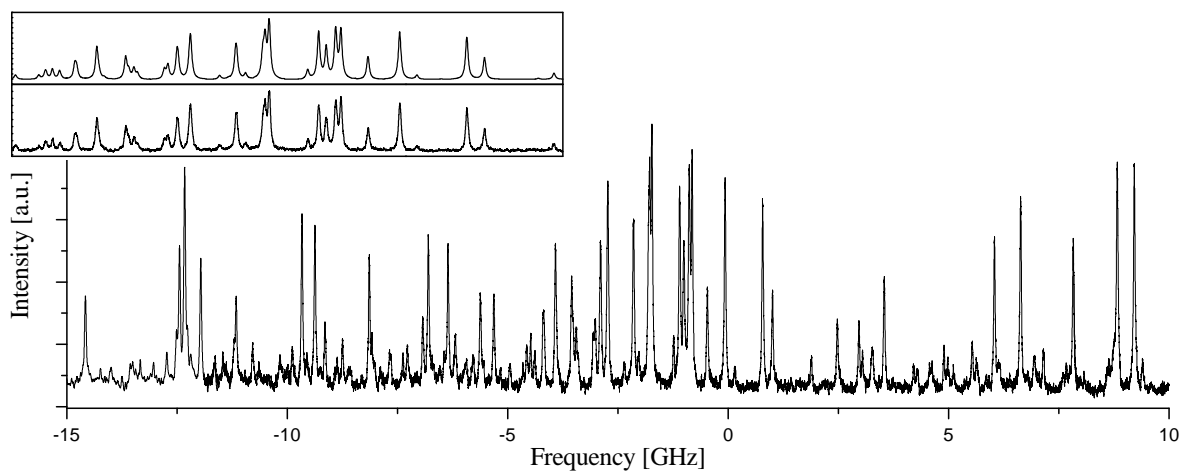


Figure 3.5: High resolution spectrum of the A band of *o*-fluorophenol. The origin (0 on the scale of the figure) is located at $36\,799.382(6)\text{ cm}^{-1}$. The inset ranges from -5 to 2 GHz and shows the Q branch of the spectrum, together with a simulation of this part.

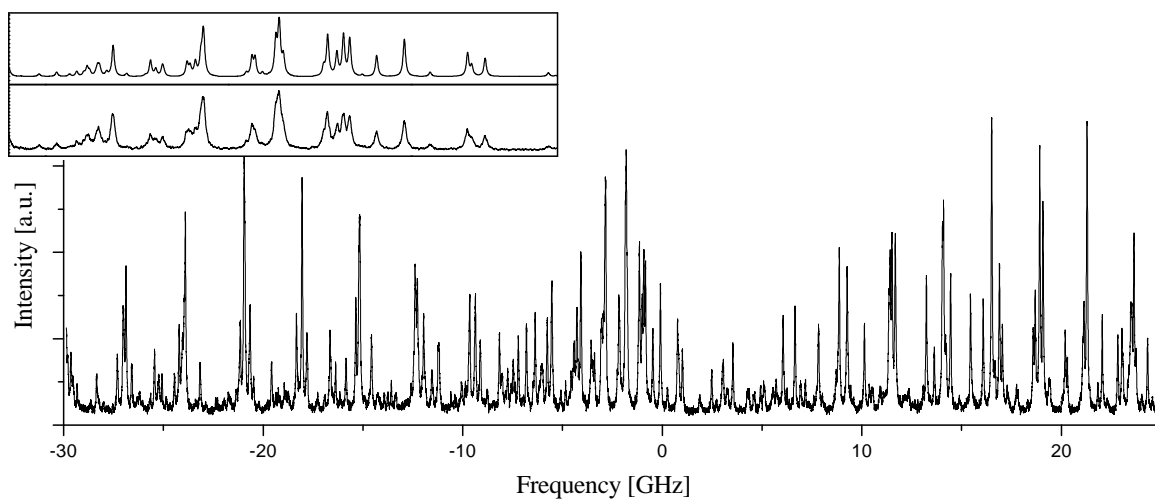


Figure 3.6: High resolution spectrum of the B band of *o*-fluorophenol. The origin (0 on the scale of the figure) is located at $36\,906.710(8)\text{ cm}^{-1}$. The inset ranges from -5.5 to 2 GHz and shows the Q branch of the spectrum, together with a simulation of this part.

resolved UV spectrum of the B band is given in Figure 3.6. This is also a *ab*-hybrid type spectrum with its origin situated at $36906.710 \text{ cm}^{-1}$. The lines in the latter spectrum are broader than those in the A band transition, indicating a shorter lifetime. An estimation of the lifetimes will be given below.

The analysis of the measured spectra was started with a Gaussian94 [21] calculation (using a Becke3LYP functional with the gen basis) of the rotational constants for the ground state of both the *cis* and *trans* isomer. The two sets of calculated rotational constants were used to simulate two spectra from the asymmetric top rigid rotor Hamiltonian. The simulated spectra were compared with the two measured transitions. For both spectra a first assignment was made for some of the lines, which was used as input to a frequency fitting procedure. The ground state rotational constants that resulted from the fits of both transitions were closer to the rotational constants of the *cis* isomer than to those calculated for the *trans* isomer. The difference between the ground state rotational constants of the two transitions was much smaller than the calculated difference between the rotational constants of the *cis* and *trans* isomer. This made us decide to record the hole burning spectrum described in the preceding section. The result of these measurements clearly indicated that both bands indeed originate from the same ground state.

By improving the fits of both spectra, all rotational lines could eventually be assigned, with the result that the rotational constants for the ground state were, within their errors, identical to the ground state rotational constants of the *cis* isomer, as determined by microwave spectroscopy [15]. In the next step we performed new fits of our data, fixing the ground state rotational constants to the microwave data of the *cis* isomer. This yielded more accurate constants for the excited state. The results of these fits are given in Table 3.1.

Keeping the rotational constants from the frequency fit fixed, several parameters, that determine the intensities of the individual lines, were varied in an intensity fit. The population

Table 3.1: *Molecular constants of o-fluorophenol in its ground, excited A, and excited B state. For the ground state the rotational constants A'' , B'' , and C'' are given, while for the excited states the differences $\Delta A = A' - A''$, $\Delta B = B' - B''$, and $\Delta C = C' - C''$, with the ground state values are given.*

	S_0 state ^{a)}	A state	B state	
A	3337.86(2)	-106.065(10)	-110.915(11)	MHz
B	2231.92(1)	-24.00(5)	-20.684(15)	MHz
C	1337.52(1)	-23.55(3)	-16.492(4)	MHz
θ_{TM}		$\pm 23.4(4)$	$\pm 21.74(13)$	degree
ν_0		36799.382(6)	36906.710(8)	cm^{-1}
$\Delta I^b)$	0.008(3)	-0.65(1)	-2.597(4)	amu \AA^2

^{a)} From Ref. [15]

^{b)} Inertial defect: $\Delta I = I_c - I_b - I_a$, with I_a , I_b , and I_c the moments of inertia along the *a*, *b* and *c* axis respectively.

distribution was described by three parameters T_1 , T_2 , and w in a two-temperature model, where w is the weighting factor for the second temperature [22, 23]:

$$n(T_1, T_2, w) = e^{-E/kT_1} + we^{-E/kT_2}. \quad (3.1)$$

Other parameters that were determined in the intensity fit are the transition moment angle θ_{TM} , that determines the intensity ratio between the a - and b -type lines, and the Lorentzian contribution to the linewidth $\Delta\nu_L$. The Gaussian contribution to the linewidth was fixed to 16 MHz, the spectral resolution of the experimental setup. The results of the intensity fits are added in Table 3.1.

From the Lorentzian contribution to the linewidth, the lifetimes can be estimated. We found 4.6 ± 0.2 ns and 2.8 ± 0.1 ns for the excited A state and B state, respectively. This is in agreement with the preceding section, where it was concluded that the lifetime of the B state is shorter than that of the A state. To our knowledge, no lifetimes have been reported before for these states.

3.4 Discussion

3.4.1 Structural information deduced from the high resolution measurements

As can be seen from the inertial defect, the *cis* isomer is planar in its ground state. The inertial defect is even smaller than that of phenol in its ground state ($\Delta I'' = -0.0309$ amu \AA^2) [24], which might be a result of the intramolecular hydrogen bond between the hydroxyl-group and the fluorine-atom keeping the hydrogen-atom in plane. Evidence for this hydrogen bond is also found if we consider the OH \cdots F distance determined from electron diffraction studies [25]. The OH group is pulled towards the F atom, which results in an OH \cdots F distance that is shorter than the sum of their van der Waals radii.

An increase of the nonplanarity upon electronic excitation was already found for phenol [24]. However, while the inertial defect of the S_1 state of phenol is only -0.18 amu \AA^2 , in *o*-fluorophenol it is much larger: -0.65 amu \AA^2 . A large change like that is quite unusual for aromatic derivatives, and it clearly indicates that the molecule is nonplanar in the S_1 state. An even larger inertial defect in the B band (-2.6 amu \AA^2) yields unambiguous confirmation that an out-of-plane vibration is involved.

Also catechol is found to be nonplanar in the excited electronic state [5–7]. In that molecule the free OH group rotates over 24° out of the aromatic plane [7]. Nonplanarity of the electronically excited state seems to be a general propensity of fluorinated aromatic species. A coupling between the excited $\pi\pi^*$ state and a $\pi\sigma^*$ state, localized on the C–F bond, has been observed in fluorinated naphthalene derivatives [4, 26], in tetrafluorobenzene [27] and in difluorobenzene [28, 29] and has been shown to lead to out-of-plane distortion of the excited state. The latter results in activity of an out-of-plane vibration. In tetrafluorobenzene and the fluorinated naphthalene derivatives, this vibration has been identified as the so-called butterfly mode. The nonplanarity of the S_1 state in *o*-fluorophenol most likely also originates from a coupling between the S_1 state and a $\pi\sigma^*$ state, localized on the C–F bond.

There are several ways in which the ground state structure of *o*-fluorophenol can be modified, so that the rotational constants and inertial defect of the vibrationless S_1 state are repro-

duced. The first possibility that comes to mind, is rotation of the hydroxyl-group around the C–O axis, resulting in an out-of-plane position of the hydrogen atom. A rotation of the OH group over 30° results in a inertial defect of -0.42 amu \AA^2 . In catechol a similar rotation of the free OH group describes its nonplanarity in the S_1 state. The remaining contributions to the inertial defect in *o*-fluorophenol can be attributed to smaller out-of-plane displacements of the other atoms, and hence explain the inertial defect in the A state of *o*-fluorophenol.

However, quantitative information on the structural changes upon excitation is difficult to obtain. Many possible geometries reproduce the observed rotational constants. Starting from the ground state structure derived from gas-phase electron diffraction by Vajda *et al.* [25], various excited state structures have been calculated. The rotational constants of the A state could well be reproduced by rotating the hydroxyl group over 30° and, similar to phenol [22], simultaneously decreasing the C–O and C–F bondlengths and increasing the bonds of the ring. All angles and other bondlengths are kept fixed to the ground state values. The different ring bonds are increased with 0.049 to 0.058 \AA (several different combinations are possible), while the C–O and C–F bondlengths are decreased with 0.048 to 0.119 \AA . As a result the OH \cdots F distance increases by approximately 0.1 \AA , which indicates a weakening of the hydrogen bond. In the ionic state of *o*-fluorophenol, the hydrogen bond is stronger than in the ground state [12, 13]. From this, one would expect to find a similar strengthening of the intramolecular hydrogen bond in the S_1 state, although somewhat less than for the ion. Possibly, the increase of acidity, that strengthens of the hydrogen bond, has to compete with the out-of-plane distortion, which weakens the hydrogen bond. However, we have to stress here, that the proposed change in structure is not unique, and an unambiguously conclusion cannot be drawn on the strength of the hydrogen bond in the electronically excited state.

As mentioned before, the inertial defect of the B state is even larger than that of the A state, and it will require much larger out-of-plane displacements to satisfy this value (-2.6 amu \AA^2). The large increase in the inertial defect of the B state gives strong evidence that excitation to this state involves excitation of an out-of-plane vibration.

The directions of the transition moments of the A and B band transition are almost equal, and make an angle of respectively $\pm 23.4^\circ$ and $\pm 21.7^\circ$ with the *a* axis of the molecule (see Figure 3.7). Substitutions are found to be of large influence on the transition moment direction of benzene derivatives. The transition moment of the $S_1 \leftarrow S_0$ transition in phenol lies along the *b* axis almost perpendicular to the C–O bond [24]. The transition moment of the $S_1 \leftarrow S_0$ transition in *o*-difluorobenzene is directed along the *a* axis [29], which in this case lies in between the two substituted fluorine atoms and intersects the C–C bond perpendicular. Based on these findings, we favor the minus sign for the direction of the transition moments in *o*-fluorophenol. This results in a transition moment direction almost parallel to the C–F bond.

3.4.2 Out-of-plane deformation

It is concluded in the preceding section that *o*-fluorophenol is nonplanar in the excited state. If we assume that the aromatic ring is still planar, the nonplanarity indicates that there are two equivalent minima on the potential energy surface at either side of the aromatic plane. An out-of-plane rocking motion of the nonplanar group of atoms from one minimum to the other can be described by a double minimum potential along the vibrational coordinate. This is schematically shown in Figure 3.8. If we assume that the hydroxyl group dominates the nonplanarity

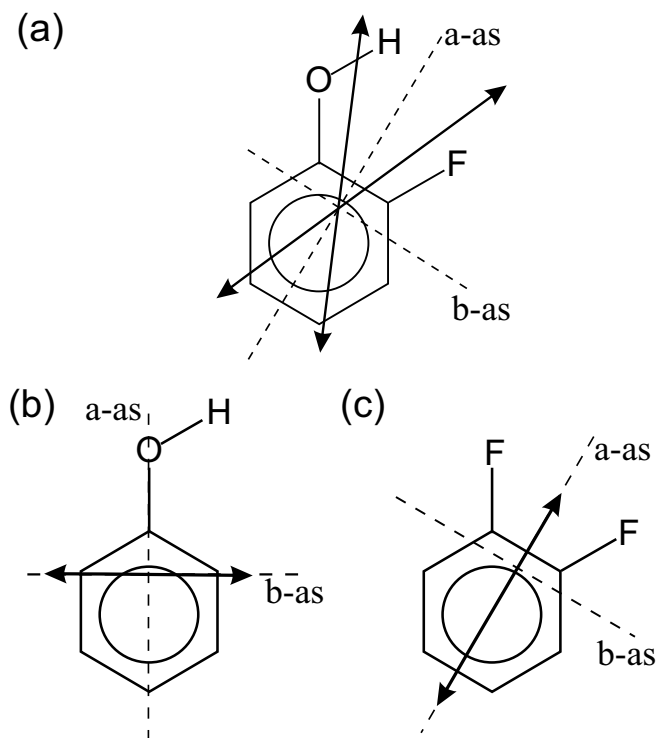


Figure 3.7: Direction of the transition moment of the A band of *o*-fluorophenol ($\pm 23.4^\circ$, determined from the high resolution measurements) (a), compared with the transition moments of phenol (Ref. [24]) (b) and difluorobenzene (Ref. [29]) (c).

by undergoing a torsional-like motion around the C-O bond, the vibrational coordinate is described by the angle between the hydroxyl group and the aromatic plane. The minima in the double minimum potential will be around 30° above and below the aromatic plane (see section 3.4.1).

The low frequency modes that we have observed in absorption (109 cm^{-1}) and in emission (297 cm^{-1}), behave exactly like the corresponding modes in catechol [5, 6]. This is a strong indication that the out-of-plane deformation in *o*-fluorophenol is located on the substituents. Leutwyler and coworkers indeed assigned the 113 cm^{-1} band in catechol to the torsion of (mostly) the hydrogen-bonded OH group. Kleinermanns and co-workers later assigned the 113 cm^{-1} band to the excitation of one quantum of the torsion of the free OH. The hydrogen bond in *o*-fluorophenol is quite weak, as can be inferred from the small displacement of the OH stretching mode relative to phenol (24 cm^{-1} [12, 13]). However, it would be surprising that the torsion frequencies of free OH in catechol and bound OH in *o*-fluorophenol are almost identical.

A harmonic ground state potential, and a double-minimum excited state potential of the form $V(\tau) = ae^{-2\tau^2} + b\tau^2 + c\tau^4$, have been fitted to the spectroscopic data for catechol [5]. The C-F butterfly vibrations in the electronically excited states of perfluorinated naphthalene, naphthol [4, 26], and tetrafluorobenzene [27] have also been fitted to such a Gaussian type double-minimum potential [30]. Since the potential in the planar ground state can be described

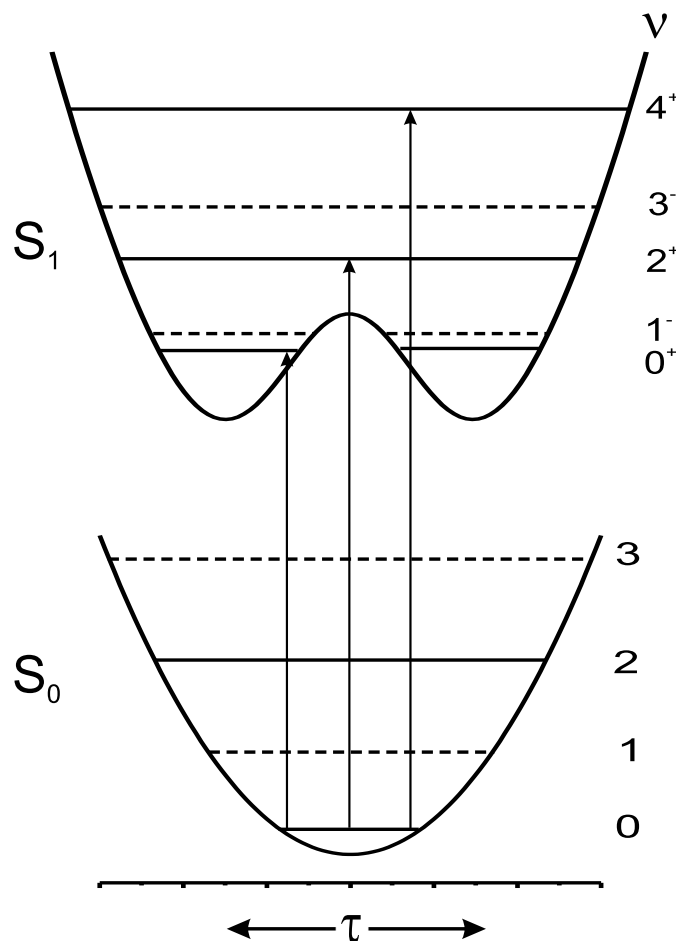


Figure 3.8: *Harmonic ground state and double-minimum excited state potential along the out-of-plane coordinate τ , together with allowed transitions.*

by a single minimum potential, there exists substantial overlap between the ground state and higher vibronic levels in the electronically excited state. Since all out-of-plane motions are of a'' symmetry, and both the ground and the electronically excited state are of A' symmetry, only transitions with $\Delta\nu$ is even, are allowed. A similar fit to our data can only be performed after it has been established which of the frequencies and overtones belong to the out-of-plane mode. As argued before, the excited state 109 cm^{-1} and 248 cm^{-1} frequencies are overtones (τ_0^2 and τ_0^4) of that mode. However, it is difficult to decide which of the ground state frequencies are their counterparts, since both A and B band seem to behave like origins for the emission spectra. In other words, in emission, no clear $\Delta\nu = 0$ transition is observed upon excitation of the τ^2 band. This peculiar distribution of Franck–Condon factors has previously been observed in the butterfly mode of tetrafluorobenzene [27]. After excitation of the 11^2 band the 11_2^2 transition is much weaker in emission than the 11_0^2 transition. This could also be described by a double minimum potential in the electronically excited state.

To further complete the analysis of the ground and excited state frequencies, we performed

Table 3.2: *Experimental and calculated vibrational frequencies (cm^{-1}) of the ground state.*

Experiment	<i>Ab initio</i>	
	Becke3LYP/D95(<i>d, p</i>)	Symmetry
	190	a''
	289	a''
297	293	a' (OH...F stretch)
	402	a'' (OH torsion)
436	440	a'
468 ^{a)}	453	a''
	551	a'
	559	a''
561	577	a' ($6b_1^0$ ring vibration in benzene)
589 ^{a)}		τ_2
	707	a''
	755	a''
758	772	a' (1_1^0 ring vibration in benzene)

^{a)} Most prominent in the emission spectrum resulting from excitation to the B band.

ab initio calculations using Gaussian 94 [21]. Table 3.2 lists the strongest experimental ground state frequencies below 800 cm^{-1} , as well as the calculated frequencies (using a Becke3LYP functional with the D95(*d, p*) basis set). Most of the observed frequencies are very well reproduced by the calculated a' symmetry vibrations.

Table 3.3 displays the measured frequencies in the excited state, together with results from CIS/D95(*d, p*) *ab initio* calculations. As common practice for these type of calculations, the calculated frequencies are by scaled 0.89. The observed frequencies below 270 cm^{-1} cannot be explained by a' symmetry vibrations, since there are no a' symmetry vibrations calculated below this frequency. Moreover, the correspondence with calculated a'' symmetry vibrations is also poor. This is not at all surprising if any of these frequencies belong to an out of the plane double-minimum vibration, since in that case, we observe the overtones, τ_0^2 , τ_0^4 , etc., with a negative anharmonicity.

The lowest calculated modes in the excited electronic state are at 74 cm^{-1} and 151 cm^{-1} . The relative motion of the atoms for these vibrations is given in Figure 3.9. The 74 cm^{-1} mode corresponds to the 289 cm^{-1} mode in the ground state, while the 151 cm^{-1} mode corresponds to the 190 cm^{-1} ground state mode. In the dispersed spectra, we expect to observe the overtone τ_2 , which, if one of two above-mentioned vibrations is involved, is predicted around 580 cm^{-1} or 280 cm^{-1} , respectively.

There are several candidates in the emission spectra that can be assigned to the overtone τ_2 . The mode at 297 cm^{-1} shows up in the emission spectra originating from both the A and the

Table 3.3: *Experimental and calculated vibrational frequencies (cm⁻¹) in the excited state. Calculated frequencies are scaled by 0.89.*

Experiment	<i>Ab initio</i>	
	CIS/D95(<i>d, p</i>)	Symmetry
109	74	<i>a</i> ''
	152	τ_0^2
186		
248		τ_0^4
283	285	<i>a</i> ' (OH ··· F stretch)
	296	<i>a</i> ''
	345	<i>a</i> ''
389	386	<i>a</i> '
	418	<i>a</i> '' (OH torsion)
	475	<i>a</i> ''
486	479	<i>a</i> ' ($6b_0^1$ ring vibration in benzene)
	500	<i>a</i> ''
	503	<i>a</i> '
	573	<i>a</i> ''
	692	<i>a</i> ''
697		
700		
725	716	<i>a</i> ' (1_0^1 ring vibration in benzene)

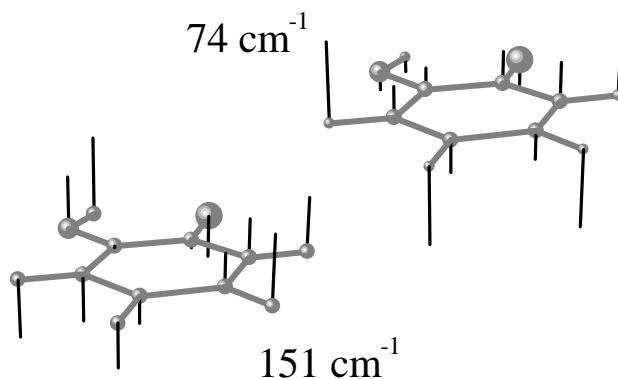


Figure 3.9: *The two lowest frequency vibrations of o-fluorophenol in the excited state as calculated by Gaussian94 (Ref. [21]), using a CIS functional.*

B band. The most likely assignment for this mode is the totally symmetric OH...F stretching mode, calculated at 293 cm^{-1} . Another possible candidate is the 468 cm^{-1} transition, that is observed in the emission spectrum of the B band. This mode would correspond to a harmonic vibration of 234 cm^{-1} in the ground state. However, no vibration is calculated around this frequency. A mode around 580 cm^{-1} would be very close to the totally symmetric ring vibration (6b), observed at 561 cm^{-1} in the emission spectra. Nevertheless, a shoulder seems to appear at the high frequency side of this transition in the emission spectrum of the B band. This might be attributed to the overtone τ_2 .

A large redshift of the active out-of-plane vibration upon electronic excitation was found in catechol [5], perfluoronaphthalene [26], tetrafluorobenzene [27] and perfluoronaphthol [4]. The 74 cm^{-1} mode (289 cm^{-1} in the ground state) therefore, is the most likely candidate for the observed out-of-plane vibration in *o*-fluorophenol.

A more striking feature in the emissive properties of *o*-fluorophenol, is a clear redshift in the fluorescence after excitation of the overtones of the torsion modes at 109 and 248 cm^{-1} . Besides the narrow bands located near the origin, there exists a broad fluorescence maximum, peaking at 3000 cm^{-1} from the excitation. Such a redshift has been observed before in compounds that contain a OH and a F substituent in ortho position, like perfluorophenols [4] and 2,6-difluorophenol [6]. It should be noted that in the latter case, the redshift is even more prominent than in *o*-fluorophenol. This redshift is thus related to the presence of the interaction between a fluorine atom and an adjacent OH group. Since, in contrast to the ground state, the molecule is not planar in the excited state, the principal axes change upon excitation. The excited state modes are, therefore, described as a "mixture" of ground state modes (Duschinsky effect). The large redshift in an out-of-plane mode upon electronic excitation is most likely due to the presence of high frequency modes in the emission spectrum. These modes gain activity through the Duschinsky effect and have strongly displaced Franck–Condon factors, caused by the difference in geometry between the planar ground and nonplanar excited state.

Isotope studies of the molecule would be of great help to determine, firstly, which group of atoms is responsible for the out-of-plane motion, and secondly, which of the remaining frequencies can be attributed to this out-of-plane motion. However, attempts to perform these measurements have failed so far.

3.5 Summary

The transitions A and B of *o*-fluorophenol, studied by hole burning spectroscopy and rotationally resolved UV spectroscopy, both originate in the ground state of the *cis* isomer. The ground state is found to be planar, while it is clearly established that the S_1 state is nonplanar. The inertial defect of the B state is four times that of the A state. The nonplanarity of the S_1 state induces the activity of an out-of-plane vibration, which shows some similarity to the so-called butterfly mode observed in other benzene derivatives. In the ground state this mode is harmonic, while in the S_1 state it is described by a double-minimum potential with a negative anharmonicity in the vibrational progression. The overtone of this vibration, τ_0^2 , is responsible for the strong B band at 109 cm^{-1} to the blue of the $S_1 \leftarrow S_0$ origin.

Acknowledgments

Authors would like to thank Dr. Gert von Helden for carrying out some of the *ab initio* calculations. This work was made possible by funding from the Dutch Foundation for Fundamental Research on Matter (FOM). A. Z. is grateful to the CNRS/NWO program for international cooperation for financing her stay in Nijmegen.

References

- [1] A. Oikawa, H. Abe, N. Mikami, and M. Ito. *Electronic spectra and ionization potentials of rotational isomers of several disubstituted benzenes*. *Chemical Physics Letters* **116**:50–54, 1985.
- [2] S. Yamamoto, T. Ebata, and M. Ito. *Rotational isomers of *o*-chlorophenol and their different emission properties*. *Journal of Physical Chemistry* **93**:6340–6345, 1989, and references therein.
- [3] H. Lampert, W. Mikenda, and A. Karpfen. *Molecular geometries and vibrational spectra of phenol, benzaldehyde, and salicylaldehyde: Experimental versus quantum chemical data*. *Journal of Physical Chemistry A* **101**:2254–2263, 1997.
- [4] F. Lahmani, A. Zehnacker, G. Denisov, and G. G. Furin. *Laser-induced fluorescence study of the $S_0 - S_1$ transition of 1- and 2-perfluoronaphthol in a supersonic jet*. *Journal of Physical Chemistry* **100**:8633–8639, 1996.
- [5] T. Bürgi and S. Leutwyler. *O-H torsional vibrations in the S_0 and S_1 states of catechol*. *Journal of Chemical Physics* **101**:8418–8429, 1994.
- [6] M. Gerhards, W. Perl, S. Schumm, U. Henrichs, C. Jacobi, and K. Kleinermanns. *Structure and vibrations of catechol and catechol·H₂O(D₂O) in the S_0 and S_1 state*. *Journal of Chemical Physics* **104**:9362–9375, 1996.
- [7] M. Gerhards, S. Schumm, C. Unterberg, and K. Kleinermanns. *Structure and vibrations of catechol in the S_1 state and ionic ground state*. *Chemical Physics Letters* **294**:65–70, 1998.
- [8] P. George, C. W. Bock, and M. Trachtman. *Hydrogen-bonding in 2-fluorophenol, and rotation about the C-O bond - A molecular orbital study*. *Journal of Molecular Structure (THEOCHEM)* **152**:35–53, 1987.
- [9] G. N. R. Tripathi. *Electronic absorption spectrum of ortho-fluorophenol in vapor state*. *Journal of Molecular Spectroscopy* **37**:486–493, 1971.
- [10] L. N. Tripathi. *Near ultraviolet absorption spectrum of *o*-fluoroanisole*. *Indian Journal of Pure Applied Physics*, **7**:357, 1969.

- [11] T. Omi, H. Shitomi, N. Sekiya, K. Takazawa, and M. Fujii. *Nonresonant ionization detected IR spectroscopy for the vibrational study in a supersonic jet*. Chemical Physics Letters **252**:287–293, 1996.
- [12] A. Fujii, A. Iwasaki, and N. Mikami. *Observation of intramolecular hydrogen bonds of o-fluorophenol ions by using autoionization detected infrared spectroscopy*. Chemistry Letters **11**:1099–1100, 1997.
- [13] A. Fujii, A. Iwasaki, T. Ebata, and N. Mikami. *Autoionization-detected infrared spectroscopy of molecular ions*. Journal of Physical Chemistry A **101**:5963–5965, 1997.
- [14] G. L. Carlson, W. G. Fateley, A. S. Manocha, and F. F. Bentley. *Torsional frequencies and enthalpies of intramolecular hydrogen bonds of o-halophenols*. Journal of Physical Chemistry **76**:1553–1557, 1972.
- [15] A. Dutta, A. I. Jaman, and R. N. Nandi. *Microwave spectral study of 2-fluorophenol: cis conformer*. Journal of Molecular Spectroscopy **114**:274–279, 1985.
- [16] A. Zehnacker-Rentien and F. Lahmani. *unpublished results*.
- [17] R. J. Lipert and S. D. Colson. *Low frequency vibrations in phenol-(H₂O)₂ revealed by hole-burning spectroscopy in a supersonic jet*. Chemical Physics Letters **161**:303–307, 1989.
- [18] W. A. Majewski and W. L. Meerts. *Near-UV spectra with fully resolved rotational structure of naphthalene and perdeuterated naphthalene*. Journal of Molecular Spectroscopy **104**:271–281, 1984.
- [19] S. Gerstenkorn and P. Luc. *Atlas du Spectroscopie d’Absorption de la Molecule d’Iode*. (CNRS, Paris, 1978).
S. Gerstenkorn and P. Luc. *Absolute iodine (I₂) standards measured by means of fourier-transform spectroscopy*. Reviews of Physical Applications **14**:791–794, 1979.
- [20] E. B. Wilson. Physical Reviews **45**:706–714, 1934.
- [21] GAUSSIAN 94 Revision D.2. M. J. Frisch, G. W. Trucks, H. B. Schlegel, P. M. W. Gill, B. G. Johnson, M. A. Robb, J. R. Cheeseman, T. A. Keith, G. A. Petersson, J. A. Montgomery, K. Raghavachari, M. A. Al-Laham, V. G. Zakrzewski, J. V. Ortiz, J. B. Foresman, J. Cioslowski, B. B. Stefanov, A. Nanayakkara, M. Challacombe, C. Y. Peng, P. Y. Ayala, W. Chen, M. W. Wong, J. L. Andres, E. S. Replogle, R. Gomperts, R. L. Martin, D. J. Fox, J. S. Binkley, D. J. Defrees, J. Baker, J. P. Stewart, M. Head-Gordon, C. Gonzalez, and J. A. Pople. Gaussian, Inc., Pittsburgh PA, 1995.
- [22] G. Berden, E. Jalviste, and W. L. Meerts. *Rotationally resolved ultraviolet spectroscopy of indole, indazole, and benzimidazole: Inertial axis reorientation in the S₁(¹L_b) – S₀ transitions*. Journal of Chemical Physics **103**:9596–9606, 1995.
- [23] Y. R. Wu and D. H. Levy. *Determination of the geometry of deuterated tryptamine by rotationally resolved electronic spectroscopy*. Journal of Chemical Physics **91**:5278–5284, 1989.

- [24] G. Berden, W. L. Meerts, M. Schmitt, and K. Kleinermanns. *High resolution UV spectroscopy of phenol and the hydrogen bonded phenol-water cluster*. Journal of Chemical Physics **104**:972–982, 1996.
- [25] E. Vajda and I. Hargittai. *Molecular structure of 2-fluorophenol and 2,6-difluorophenol from gas-phase electron diffraction*. Journal of Physical Chemistry **97**:70–76, 1993.
- [26] T. Chakraborty, D. Nath, and M. Chowdhury. *Study of butterfly inversion of perfluoronaphthalene by laser-induced fluorescence in supersonic jet*. Journal of Chemical Physics **96**:6456–6463, 1992.
- [27] K. Okuyama, F. Kakinumo, M. Fujii, N. Mikami, and M. Ito. *Electronic spectra of 1,2,4,5-tetrafluorobenzene in a supersonic jet: Butterfly tunneling in the excited state*. Journal of Physical Chemistry **90**:3948–3952, 1986.
- [28] Y. Tsuchiya, K. Takazawa, M. Fujii, and M. Ito. *Vibronic coupling in S_0 of *o*- and *m*-difluorobenzene*. Chemical Physics Letters **183**:107–112, 1991.
- [29] A. K. Swinn and S. H. Kable. *The $S_1(^1A_1) - S_0(^1A_1)$ electronic transition of jet-cooled *o*-fluorobenzene*. Journal of Molecular Spectroscopy **191**:49–67, 1998.
- [30] J. B. Coon, N. W. Naugle, and R. D. McKenzie. *The investigation of double-minimum potentials in molecules*. Journal of Molecular Spectroscopy **20**:107–129, 1966.

Chapter 4

Proton tunneling in the benzoic acid dimer studied by high resolution ultraviolet spectroscopy

Abstract

High resolution ultraviolet spectroscopy has been used to investigate the rotationally resolved excitation spectrum of the first singlet-singlet transition in the benzoic acid dimer. The measured spectrum consists of two overlapping components. The corresponding lines in the two components are shown to originate in different levels of the ground state potential, separated by a tunneling splitting produced by concerted proton exchange between the two sub-units forming the dimer. The frequency separation between the two components is equal to the difference between the tunneling splittings in the ground and the excited electronic state. This frequency separation is found to be 1107 ± 7 MHz. From the analysis, it is estimated that the barrier for proton tunneling changes by about 20% upon electronic excitation. The structure of the dimer in the ground state is determined to be linear, while in the excited S_1 state it is slightly bent ($3.4^\circ \pm 1.7^\circ$).

4.1 Introduction

Hydrogen bonded systems play an important role in many chemical and biological processes. These processes are often governed by proton transfer, which has been extensively studied throughout the last decades. Of special interest is the issue of proton tunneling and how much it contributes to these processes. Carboxylic dimers are well suited systems to study intermolecular proton tunneling since the constituents in these dimers are connected by two intermolecular hydrogen bonds. The displacement of the two protons occurs in concert, and can be described by a single transfer coordinate in a double minimum potential, which is symmetric for an isolated dimer. From infrared measurements, the barrier for proton transfer has been determined to lie between 6400 and 6900 cm^{-1} for both formic acid and acetic acid dimers [1]. Because these barriers are so high, the tunneling splittings are small, and their measurement will require high resolution. Microwave spectroscopy has been used to measure the rotational spectra of several hydrogen bonded bimolecules, two different molecules combined by two intermolecular hydrogen bonds to form an asymmetric polar complex [2]. Unfortunately, cyclic carboxylic dimers are centrosymmetric, and have no permanent dipole moment. Therefore, they cannot be studied by microwave spectroscopy.

The benzoic acid dimer as well consists of two monomer units connected by two hydrogen bonds. The two hydrogen bonds stabilize the dimer by about 6000 cm^{-1} [3, 4]. Consequently, at low temperatures, only dimers are present. The dimer structure is illustrated in Figure 4.1. When the dimer is formed, the structure of the monomers is assumed to remain unchanged. The two monomer units are co-planar. In the ground electronic state, the molecule is linear: that is, the a axes of the monomers are co-linear. The structure of the dimer can then be characterized by a single distance r , which is here taken to be the distance between the centre of mass of the dimer and the centre of mass of either monomer unit. The two tautomers of the benzoic acid dimer can be interconverted by concerted proton transfer.

In the description of a general asymmetric proton-transfer potential, it is necessary to introduce two constants: an asymmetry parameter and a tunneling matrix element. The asymmetry parameter is defined to be the energy difference between the lowest level in one potential well and that in the other in the limit that the tunneling matrix element vanishes. The tunneling matrix element couples these two lowest levels, and is defined so that it equals the tunneling splitting in the limit that the asymmetry parameter vanishes.

The benzoic acid dimer has been extensively studied in various condensed phase environments [5–21]. In these cases, the two benzoic acid units will experience different local environments, and the double-minimum potential will be asymmetric. In pure benzoic acid crystals, the asymmetry parameter is found to be 60 cm^{-1} [20]. Due to the asymmetry, the population at very low temperatures will be highly concentrated in the deeper potential well. It is only in cases where the tunneling matrix element is comparable to (or larger than) the asymmetry parameter that both wells will be populated. In such cases, the tunneling matrix element can be determined. This has been done for benzoic acid crystals doped with dye molecules. In that case, the asymmetry is reduced to about 1 cm^{-1} for the benzoic acid dimers that are nearest neighbor to a dye molecule [11]. The tunneling matrix element is found to be relatively independent of the nature of the dopant. For thioindigo-doped benzoic acid crystals, a value of 8.4 GHz was found, while a value of 6.5 GHz was obtained if selenoindigo was the dopant [11, 21]. No value has been reported yet for the tunneling splitting in an isolated benzoic acid dimer. The

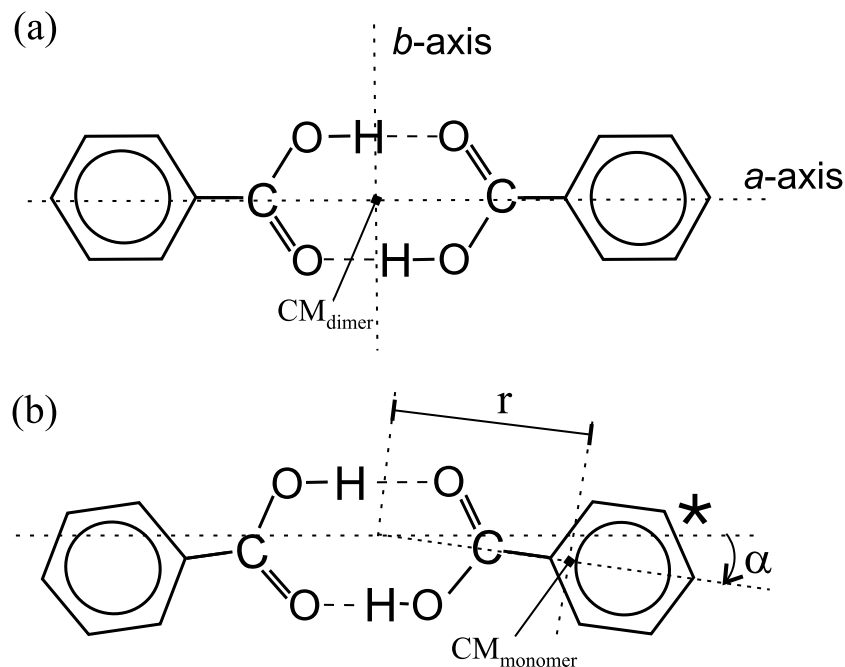


Figure 4.1: The structure of the benzoic acid dimer in the ground (a) and electronically excited state (b). The star denotes the monomer unit that has been excited. Also shown in (b) are the definition of the parameters that are used to characterize the structure of the benzoic acid dimer; α is the angle between the longitudinal axis of the dimer and that of the monomer unit, while r is the distance from the center of mass of the monomer unit to the center of rotation (i.e. the center of mass of the dimer having a linear configuration).

benzoic acid monomer has been studied by microwave spectroscopy [22]. But since the dimer is centrosymmetric it cannot be studied with the same technique.

Comparison of experimental results with theoretical studies shows that the proton transfer is strongly coupled to motion of the heavy nuclei, i.e. the whole benzoic acid frame rearranges itself slightly as the protons tunnel between the two benzoic acid units. From experimental results (activation energy and OH stretching vibration frequency), the potential barrier has been estimated to be 1850 cm^{-1} [4]. In performing several *ab initio* calculations, geometry optimization of the transition state, a step which lowers the calculated potential barrier, was found to be necessary to reproduce the estimated potential barrier [4, 23]. This implies that a multidimensional potential is necessary to reproduce the observed features [15, 24–26].

Very few studies on isolated benzoic acid dimers have been reported [27–30]. For free dimers, the two constituents are equivalent and consequently the potential describing the proton tunneling is symmetric. The lowest singlet-singlet transition, $S_1 \leftarrow S_0$, is located at $35\,724\text{ cm}^{-1}$. This is a $\pi^* \leftarrow \pi$ transition, analogous to the ${}^1B_{2u} \leftarrow {}^1A_{1g}$ transition in benzene. Isotope studies show that the excitation is essentially localized in one of the monomer units [5, 27]. The two constituents are no longer equivalent after electronic excitation, thus the

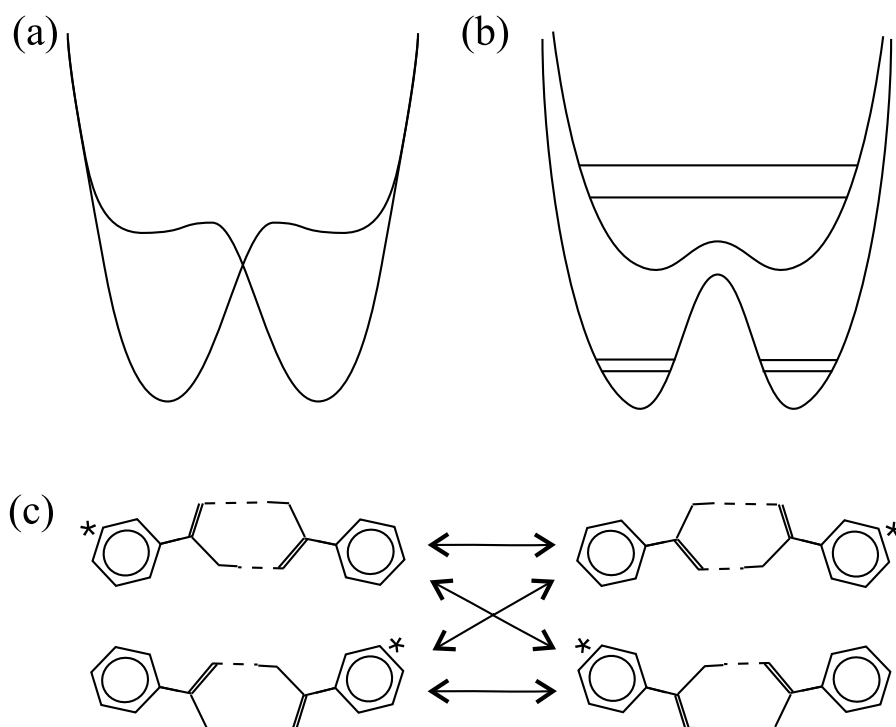


Figure 4.2: The potential describing double proton transfer in the benzoic acid dimer. Localized excitation breaks the symmetry of the potential (a), but coupling between the two asymmetric potentials leads to two symmetric potentials (b). The coupling shown in (c) can be induced by excitation exchange (horizontal arrows) or by v_3'' inversion (diagonal arrows).

symmetry of the dimer is broken in S_1 . The potential for proton transfer will be given by an asymmetric potential, schematically given in Figure 4.2(a). However, since no distinction can be made as to which of the two molecules in the dimer is excited, the symmetry in the potential surface must be restored. In general, the two potentials are coupled, which gives rise to a symmetric potential depicted in Figure 4.2(b). This is similar to the description of the interconversion tunneling in $(\text{HF})_2$ and $(\text{HCCH})_2$ [31] and of the tunneling dynamics in the ammonia dimer [32].

The coupling in the benzoic acid dimer can be induced by exchange of the excitation from one unit to the other; see Fig. 4.2(c). Also inversion along the in-plane intermolecular v_3'' coordinate can induce coupling between the two potentials. The localized excitation increases the basicity of the excited unit and decreases its acidity so that it will act as a proton acceptor, while the non-excited unit will act as a proton donor. This causes the dimer to bend along the v_3'' coordinate, as is shown in Figure 4.1(b) [5, 29]. As a result of the bend, an angular parameter is required (in addition to r) to characterize the structure of the dimer in the S_1 state. Here this parameter, denoted α , is taken to be the angle between the a axis of the dimer and the a axis of the excited monomer.

4.2 Experiment

A molecular beam in combination with a high resolution UV excitation source was used to measure the rotationally resolved fluorescence excitation spectrum of the benzoic acid dimer. The apparatus has been extensively described elsewhere [33]. In brief, the molecular beam is formed by flowing a carrier gas over the benzoic acid sample (Fluka), which is kept at 120°C. The beam is subsequently expanded through a 0.15 mm quartz nozzle, which is kept at a slightly higher temperature. In the expansion region, the dimers are formed. Neon rather than argon was used as the carrier gas. This choice was made to avoid consuming too high a percentage of the benzoic acid monomers in the formation of clusters with the carrier gas. At the same time, use of neon insures that sufficient rotational cooling is achieved.

The molecular beam is skimmed twice in a differential pumping system and crosses the UV laser beam at right angles at about 30 cm from the nozzle. To insure collision-free conditions, the pressure in the detection chamber is kept below 10^{-6} mbar. The total undispersed fluorescence is imaged onto a photomultiplier, which is connected to a photon counting system interfaced with a computer.

UV radiation at 280 nm is generated by intracavity frequency doubling of a cw single frequency ring dye laser operating with Rhodamine 110. By using a 2 mm thick Brewster cut BBO crystal, 0.15 mW of tunable UV radiation is obtained with a bandwidth of 3 MHz. For relative frequency calibration, a temperature-stabilized Fabry–Perot interferometer with a free spectral range of 75 MHz is used. For absolute frequency calibration, the iodine absorption spectrum [34] was recorded simultaneously.

The resolution of the spectrometer is determined by the geometry of the fluorescence collection optics and by the residual Doppler width arising from the angular spread of the molecular beam. The latter depends on the carrier gas used to form the molecular beam, and is about 16 MHz when argon is used. Since neon is about twice as light as argon, we expect a Gaussian contribution to the linewidth of 23 MHz.

4.3 Results

The high resolution UV excitation spectrum of the $S_1 \leftarrow S_0$ transition of the benzoic acid dimer is given in the lower panel of Figure 4.3. It can be clearly identified as a composite of two b type components with selection rules $\Delta K_a = \pm 1$. The frequency separation between corresponding lines in the two components is here denoted by Δ (defined to be positive). This separation appears to be constant in the spectrum for all pairs of corresponding lines. As is shown in Figure 4.4, the two tunneling states in the ground state potential have opposite parities; the same is true for the two tunneling states in the excited state potential. Each of the two b type components arises from transitions originating in a different tunneling level of the ground state potential. Since the parity must change in an electric dipole transition, it is clear that the transitions for the two different components must also end on different tunneling states in the excited state potential. Consequently, if the energy ordering of the two parity levels in the ground and excited states is the same, as is the case for the higher energy transitions given in Figure 4.4, then Δ will be the sum of the tunneling splittings in the two electronic states. On the other hand, if the energy ordering is reversed, then Δ will be the difference of

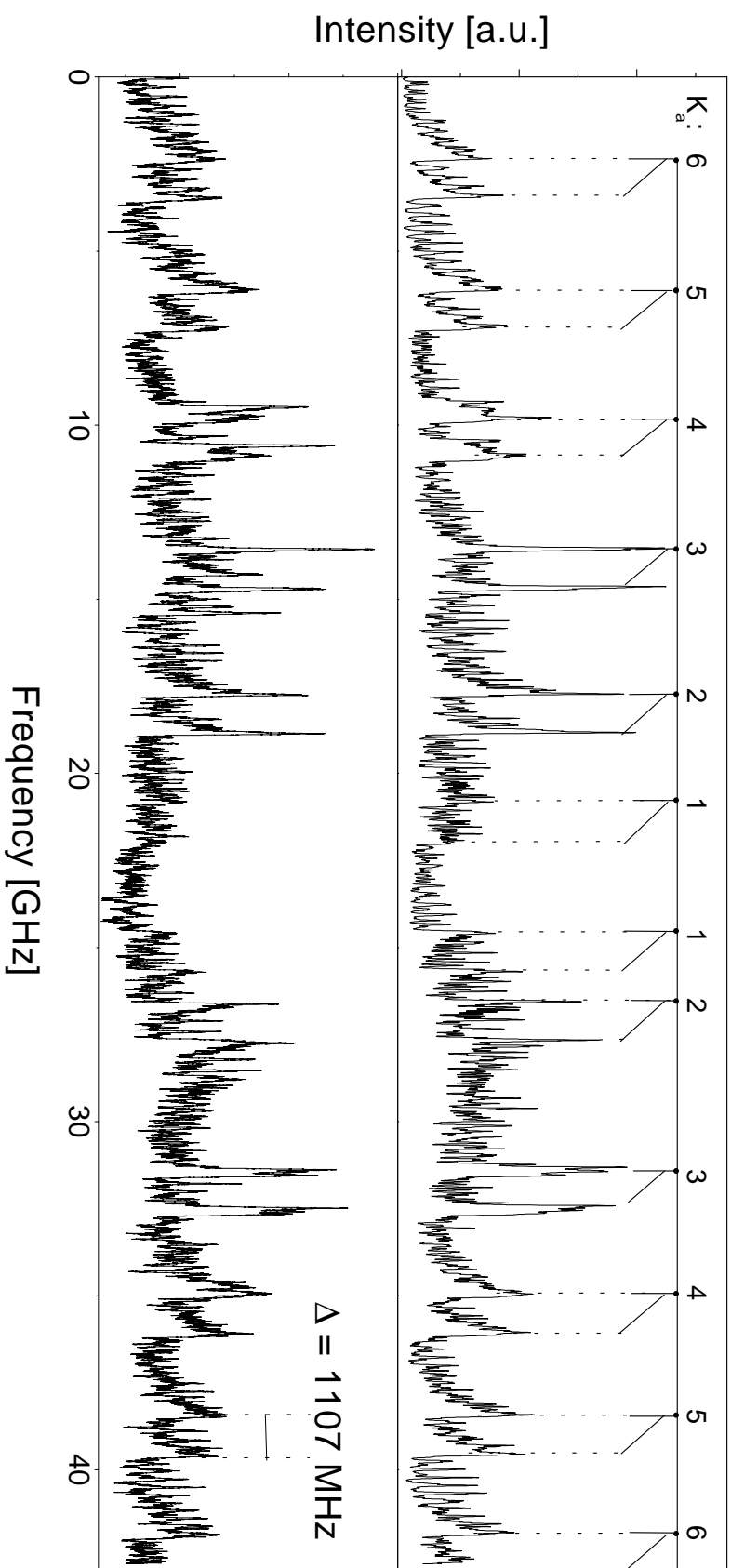


Figure 4.3: The experimental spectrum of the benzoic acid dimer (lower panel), compared with a simulation using rotational constants that are calculated from rotational constants of the benzoic acid monomer (upper panel). The upper panel shows the labeling of the K_a -stacks.

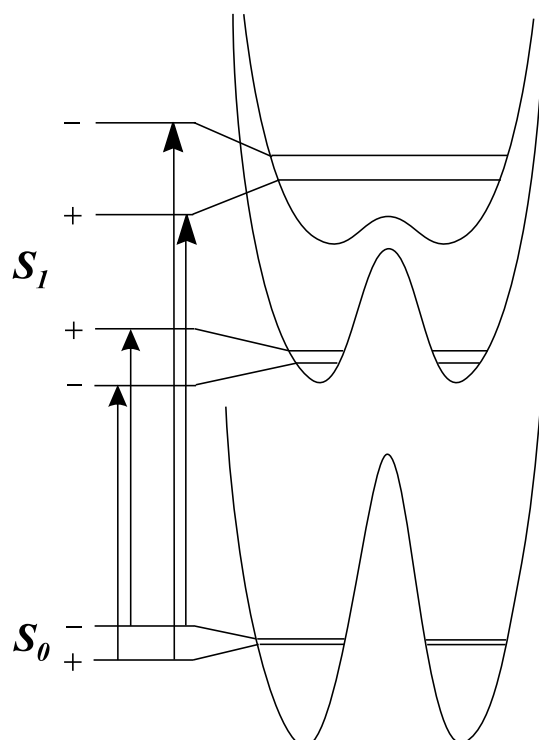


Figure 4.4: Allowed transitions between tunneling levels in the ground and electronically excited state potentials. The parity has to change upon electronic excitation. For illustration purposes, parities as well as barrier heights (and tunneling splittings) are chosen arbitrarily.

the tunneling splittings in the upper and lower electronic states. This is the case for the lower energy transitions in Figure 4.4. Whether Δ is the sum or difference depends on the symmetry of the upper state (relative to that of the ground state).

To determine the value of Δ accurately, the autocorrelation of the spectrum is calculated using the correlation theorem [35]. The experimental spectrum is correlated with itself and the area of overlap between the two spectra is calculated as a function of the relative shift of the two spectra [36]. The autocorrelation spectrum, given in Figure 4.5, shows three sharp maxima: at zero frequency shift, where the spectra overlap exactly, and at $+1107$ MHz as well as at -1107 MHz, where the frequency shift between the two components equals $+\Delta$ and $-\Delta$. From this analysis, it was determined that $\Delta = 1107 \pm 7$ MHz.

The observed excitation spectrum is very dense and no single transition can be distinguished. It is therefore impossible to make a full assignment of the spectrum and fit the rotational constants of the ground and the electronically excited state in the conventional manner. However, the spectrum shows some very characteristic features. In the autocorrelation spectrum, a series of broad peaks appear with an approximately constant spacing; see Figure 4.5. Each of these peaks is formed from a particular K -stack; that is, it is formed from a series of blended Q branch transitions originating in ground state levels with the same K_a ; these transitions have the same

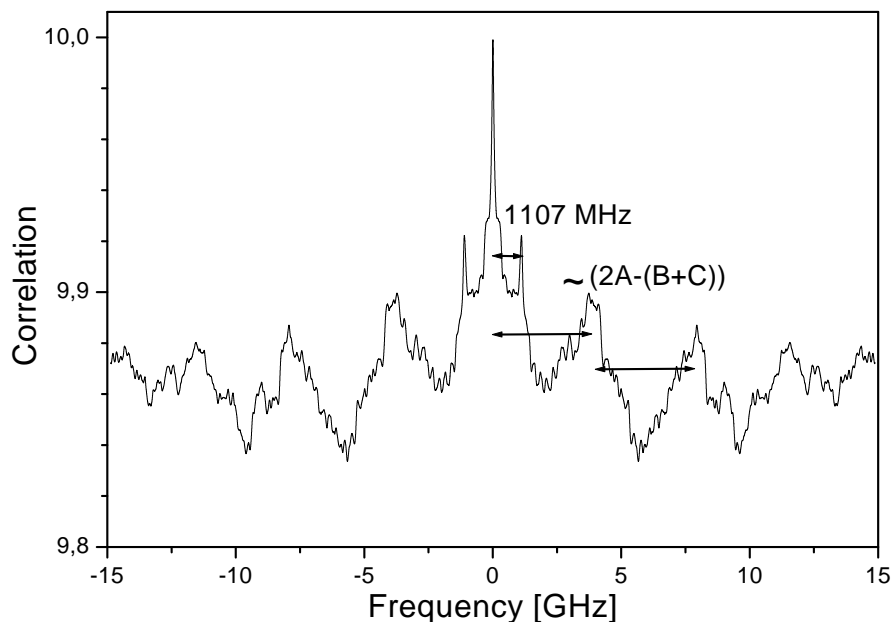


Figure 4.5: The autocorrelation spectrum of the $S_1 \leftarrow S_0$ transition of the benzoic acid dimer. The spacing between the sharp peaks in the middle is the frequency separation Δ (1107 MHz) between corresponding transitions in the two different components that make up the spectrum. The separation between neighboring broad peaks is approximately equal to $[2A - (B + C)]$.

value of ΔK_a . The spacing between K -stacks is approximately equal to $[2A - (B + C)]$, but it also depends weakly on ΔA . The width of each stack is determined by $\Delta(B + C)$. Throughout the spectrum, a number of lines can be found with an almost constant spacing corresponding to P and R branch transitions that originate from levels with the same K_a and have the same ΔK_a . The interval between these lines depends on $(B'' + C'')$ and $\Delta(B + C)$. Consequently, in spite of the fact that it is not possible to assign individual transitions in the spectrum, a great deal of information can be extracted. By comparing the experimental spectrum with spectra simulated for various values of the molecular parameters, a range of acceptable values has been determined for each rotational constant except for ΔB and ΔC , for which a value for the sum $\Delta(B + C)$ has been determined instead. The results for the rotational constants are given in Table 4.1. The origin of the transition that has the lowest frequency has been determined at $35\,723.82 \pm 0.05 \text{ cm}^{-1}$.

By using the experimental results in Table 4.1 and the rotational constants of the monomer as determined by microwave spectroscopy [22], values for r and α can be estimated for both the S_0 and S_1 states and considerable insight into the structure can be obtained.

As was indicated in Section 4.1, the ground state is assumed to be linear. The value of r can be determined from its effects on B'' and C'' ; from the values of these constants given in Table 4.1 it was found that $r = 3.62 \pm 0.15 \text{ \AA}$. This result is in very good agreement with the value for r of 3.58 \AA deduced from the $\text{O} \cdots \text{O}$ distance determined by Brougham *et al.* [17]. In order to check the linearity of the ground state, the angle α defined in Figure 4.1 was varied. If the

Table 4.1: *Rotational constants of the benzoic acid dimer in the ground and electronically excited state. The calculated constants are determined for a linear configuration with $r = 3.58 \text{ \AA}$ in the ground state, and a bent configuration with $\alpha = 3.4^\circ$ and $r = 3.60 \text{ \AA}$ in the excited state. See text. All values are given in MHz.*

		Experiment	Calculation
S_0 state	A''	1923(16)	1928.9
	B''	127(8)	127.9
	C''	114(8)	120.0
S_1 state	ΔA	-15(10)	-12.48
	$\Delta(B + C)$	-1.5(7)	-1.16

rotational constants for the S_0 state are to be consistent with those given in Table 4.1, then the dimer cannot be bent by more than 5.1° in the ground state.

For the excited state, a bent structure has been suggested [5, 29]. For this state, both r and α were varied. As compared to the ground state values, both parameters must be increased in order to reproduce the experimental determinations of the rotational constants. The larger α is in the ground state, the smaller is the increase required in α upon electronic excitation.

If a linear ground state is assumed, then the excited state value of α must fall in the range from 1.7° to 5.1° in order to obtain rotational constants that are in agreement with those given in Table 4.1. The value of r increases by from 0.01 to 0.03 \AA .

Very good agreement with the experimental spectrum is obtained for a linear ground state structure with r equal to 3.58 \AA and an excited state structure that is bent by 3.4° with a distance r of 3.60 \AA . The rotational constants that are calculated from these structures are given in Table 4.1, while the upper part of Figure 4.3 shows a simulation using these constants.

4.4 Conclusion

The experimental spectrum of the benzoic acid dimer clearly reveals a tunneling splitting due to proton transfer in the ground and electronically excited state. A spectrum consisting of two rigid rotor components is found, with a frequency separation of $\Delta = 1107 \pm 7 \text{ MHz}$. No gas phase measurements of the tunneling splittings in the benzoic acid dimer have been previously reported. As mentioned in section 4.1, the tunneling matrix element equals the tunneling splitting in the limit that the asymmetry parameter vanishes. The tunneling matrix element for the ground state of benzoic acid crystals doped with different dye molecules was determined to be 8.4 GHz and 6.5 GHz respectively [11, 21]. If these values are used as an estimate of the tunneling splitting in the ground state of the isolated dimer, the frequency separation Δ equals the *difference* in the tunneling splittings in the ground and electronically excited states. It follows

that transitions are made between the lower tunneling level in the ground state potential and the lower tunneling level in the excited state potential. (Upper-to-upper transitions form the other component of the spectrum.) This can occur only if the energy ordering of the two parity levels in the excited state is inverted as compared to the ordering in the ground state. If it is further assumed that the tunneling path and effective tunneling mass do not change upon excitation, the value of 1107 MHz for Δ implies a change in the potential barrier of about 20% upon electronic excitation (from the approximation that the logarithm of the tunneling splitting is proportional to $\sqrt{V_0}$ [37]; see also Ref [38]). It is not known whether the barrier increases or decreases. Only an absolute value for Δ has been determined from the spectrum. In case the barrier in the excited state is smaller than in the ground state (i.e. the tunneling splitting in the excited state is larger than in the ground state), the lower frequency component in the spectrum corresponds to the lower-to-lower transitions and the higher frequency component to the upper-to-upper transitions, whereas if the barrier in the excited state is larger the lower frequency component in the spectrum corresponds to the upper-to-upper transitions.

The simulated spectrum using calculated rotational constants is in good agreement with the measured spectrum. For the ground electronic state, it is concluded that the dimer has a linear structure with r equal to 3.58 Å, yielding a distance of 7.16 Å between the centers of mass of the two monomers. For the excited electronic state, it is concluded that the dimer is bent by about 3.4° with r being equal to 3.60 Å.

It would be very interesting to see how the tunneling splitting evolves in the different vibrational modes of the dimer, especially in the bending mode ν_3'' , which is expected to couple efficiently to the proton tunneling. Such measurements are currently on the way in our laboratory.

Acknowledgments

Authors would like to thank Prof. Dr. Gerard Meijer for suggesting this experiment. This work was made possible by funding from the Dutch Foundation for Fundamental Research on Matter (FOM). One of the authors (I.O.) would like to thank the University of Nijmegen for its hospitality during the period November, 1997 to February, 1998.

References

- [1] H. Morita and S. Nagakura. *O-H overtone bands and potential energy curves of the hydrogen-bonded formic and acetic acids*. *Journal of Molecular Spectroscopy* **42**:536–546, 1972.
- [2] C. C. Costain and G. P. Srivastava. *Microwave rotation spectra of hydrogen-bonded molecules*. *Journal of Chemical Physics* **41**:1620–1627, 1964.
- [3] G. Allen, J. G. Watkinson, and K. H. Webb. *An infra-red study of association of benzoic acid in vapour phase and in dilute solution in non-polar solvents*. *Spectrochimica Acta* **22**:807, 1966.

- [4] S. Nagaoka, N. Hirota, T. Matsushita, and K. Nishimoto. *An ab initio calculation on proton transfer in the benzoic acid dimer*. Chemical Physics Letters **92**:498–502, 1982.
- [5] J. C. Baum and D. S. McClure. *The ultraviolet transitions of benzoic acid. 4. High-resolution spectral studies of hydrogen bonding in the excited states of the benzoic acid dimer*. Journal of the American Chemical Society **102**:720–727, 1980.
- [6] S. Nagaoka, T. Terao, F. Imashiro, A. Saika, and N. Hirota. *An NMR relaxation study on the proton transfer in the hydrogen bonded carboxylic acid dimers*. Journal of Chemical Physics **79**:4694–4703, 1983.
- [7] J. M. Clemens, R. M. Hochstrasser, and H. P. Trommsdorff. *Direct studies of proton tunneling in hydrogen bonded mixed molecular crystals by optical excitation*. Journal of Chemical Physics **80**:1744–1753, 1984.
- [8] G. R. Holtom, H. P. Trommsdorff, and R. M. Hochstrasser. *Impurity-induced double proton transfer in benzoic acid crystals*. Chemical Physics Letters **131**:44–50, 1986.
- [9] R. M. Hochstrasser and H. P. Trommsdorff. *Observation of delocalized states of the proton in carboxylic acid dimers in condensed matter*. Chemical Physics **115**:1–6, 1987.
- [10] C. Rambaud, A. Oppenländer, M. Pierre, H. P. Trommsdorff, and J. Vial. *Tunneling dynamics of delocalized protons in benzoic acid dimers: A study of the temperature dependence by time and frequency domain optical spectroscopy*. Chemical Physics **136**:335–347, 1989.
- [11] A. Oppenländer, C. Rambaud, H. P. Trommsdorff, and J. Vial. *Translational tunneling of protons in benzoic-acid crystals*. Physical Review Letters **63**:1432–1435, 1989.
- [12] A. Stöckli, B. H. Meier, R. Kreis, R. Meyer, and R. R. Ernst. *Hydrogen bond dynamics in isotopically substituted benzoic acid dimers*. Journal of Chemical Physics **93**:1502–1520, 1990.
- [13] A. J. Horsewill, P. J. McDonald, and D. Vijayaraghavan. *Hydrogen bond dynamics in benzoic acid dimers as a function of hydrostatic pressure measured by nuclear magnetic resonance*. Journal Chemical Physics **100**:1889–1894, 1994.
- [14] S. G. Stepanian, I. D. Reva, E. D. Radchenko, and G. G. Sheina. *Infrared spectra of benzoic acid monomers and dimers in argon matrix*. Vibrational Spectroscopy **11**:123–133, 1996.
- [15] C. Scheurer and P. Saalfrank. *Hydrogen transfer in vibrationally relaxing benzoic acid dimers: Time-dependent density matrix dynamics and infrared spectra*. Chemical Physics **104**:2869–2882, 1996.
- [16] C. C. Wilson, N. Shankland, and A. J. Florence. *Direct determination of the temperature dependence of proton transfer in the benzoic acid dimer by single crystal neutron diffraction*. Chemical Physics Letters **253**:103–107, 1996.

- [17] D. F. Brougham, A. J. Horsewill, A. Ikram, R. M. Ibberson, P. J. McDonald, and M. Pinter-Krainer. *The correlation between hydrogen bond tunneling dynamics and the structure of benzoic acid dimers*. Journal of Chemical Physics **105**:979–982, 1996.
- [18] D. F. Brougham, A. J. Horsewill, and R. I. Jenkinson. *Proton transfer dynamics in the hydrogen bond: A direct measurement of the incoherent tunnelling rate by NMR and the quantum-to-classical transition*. Chemical Physics Letters **272**:69–74, 1997.
- [19] J. Seliger and V. Zagar. *^{17}O nuclear quadrupole resonance study of proton disorder in solid benzoic acid, 4-hydroxybenzoic acid and 4-nitrobenzoic acid*. Chemical Physics **234**:223–230, 1998.
- [20] M. Neumann, D. F. Brougham, C. J. McGloin, M. R. Johnson, A. J. Horsewill, and H. P. Trommsdorff. *Proton tunneling in benzoic acid crystals at intermediate temperatures: Nuclear magnetic resonance and neutron scattering studies*. Journal of Chemical Physics **109**:7300–7311, 1998.
- [21] Ch. Rambaud and H. P. Trommsdorff. *Cooperative proton transfer and tunneling in dye doped benzoic acid crystals*. Chemical Physics Letters **306**:124–132, 1999.
- [22] M. Onda, M. Asai, K. Takise, K. Kuwae, K. Hayami, A. Kuroe, M. Mori, H. Miyazaki, N. Suzuki, and I. Yamaguchi. *Microwave spectra of benzoic acid*. Journal of Molecular Structure **482-483**:301–303, 1999.
- [23] F. Graf, R. Meyer, T. K. Ha, and R. R. Ernst. *Dynamics of hydrogen bond exchange in carboxylic acid dimers*. Journal of Chemical Physics **75**:2914–2918, 1981.
- [24] R. Meyer and R. R. Ernst. *Transitions induced in a double minimum system by interaction with a quantum mechanical heat bath*. Journal of Chemical Physics **93**:5518–5532, 1990.
- [25] V. P. Sakun, M. V. Vener, and N. D. Sokolov. *Proton tunneling assisted by the intermolecular vibration excitation. temperature dependence of the proton spin-lattice relaxation time in benzoic acid powder*. Journal of Chemical Physics **105**:379–387, 1996.
- [26] D. Antoniou and S. D. Schwartz. *Proton transfer in benzoic acid crystals: Another look using quantum operator theory*. Journal of Chemical Physics **109**:2287–2293, 1998.
- [27] D. E. Poeltl and J. K. McVey. *Laser induced fluorescence excitation spectrum of jet-cooled benzoic acid dimers*. Journal of Chemical Physics **78**:4349–4355, 1983.
- [28] Y. Tomioka, H. Abe, N. Mikami, and M. Ito. *Electronic spectra of benzoic acid in a supersonic free jet*. Journal of Physical Chemistry **88**:2263–2270, 1984.
- [29] D. E. Poeltl and J. K. McVey. *Excited-state dynamics of hydrogen-bonded dimers of benzoic acid*. Journal of Chemical Physics **80**:1801–1811, 1984.
- [30] G. Meijer, M. S. de Vries, H. E. Hunziker, and H. R. Wendt. *Laser desorption jet-cooling spectroscopy of the benzoic acid monomer*. Journal of Physical Chemistry **94**:4394–4396, 1990.

-
- [31] G. T. Fraser. *Vibrational exchange upon interconversion tunneling in (HF)₂ and (HCCH)₂*. *Journal of Chemical Physics* **90**:2097–2108, 1989.
- [32] H. Linnartz, W. L. Meerts, and M. Havenith. *The ammonia dimer: New infrared-far infrared double resonance results*. *Chemical Physics* **193**:327–338, 1995.
- [33] W. A. Majewski and W. L. Meerts. *Near-UV spectra with fully resolved rotational structure of naphthalene and perdeuterated naphthalene*. *Journal of Molecular Spectroscopy* **104**:271–281, 1984.
- [34] S. Gerstenkorn and P. Luc. *Atlas du Spectroscopie d’Absorption de la Molecule d’Iode*. (CNRS, Paris, 1978).
S. Gerstenkorn and P. Luc. *Absolute iodine (I₂) standards measured by means of fourier-transform spectroscopy*. *Reviews of Physical Applications* **14**:791–794, 1979.
- [35] W. H. Press, S. A. Teukolsky, W. T. Vetterling, and B. P. Flannery. *Numerical Recipes in C: The Art of Scientific Computing*. Cambridge University Press, Cambridge, 1992.
- [36] R. M. Helm, H. P. Vogel, and H. J. Neusser. *Highly resolved UV spectroscopy: Structure of S₁ benzonitrile-argon by correlation automated rotational fitting*. *Chemical Physics Letters* **270**:285–292, 1997.
- [37] T. Horsewill, M. Johnson, and H. P. Trommsdorff. *Proton tunnelling in intermolecular hydrogen bonds*. *Europhysics News* **28**:140–142, 1997.
- [38] J. Brickmann. *Proton motions in hydrogen bonds*. in *The Hydrogen Bond -recent developments in theory and experiments* Volume I, chapter 4, pages 217–243 edited by P. Schuster, G. Zundel, and C. Sandorfy North-Holland Publishing Company, Amsterdam, 1992.

Chapter 5

Rotational contour and gas-phase infrared spectroscopy on the lowest triplet state of pyrazine, the pyrazine-argon complex and its deuterated substituents

Abstract

The infrared absorption spectrum of the jet-cooled pyrazine-argon Van der Waals complex in its lowest triplet state is measured. Vibrational excitation of the laser prepared triplet state by infrared absorption causes dissociation of the complex, which is monitored via the depletion of the pyrazine-argon ion-signal. A total of 10 vibrational transitions is detected in the 500 to 1500 cm^{-1} region. The vibrational spectrum of the pyrazine- d_4 -argon complex is also reported. Comparison of these data with *ab initio* calculations might help to elucidate the nature of the distortion of the lowest triplet state by other electronically excited states. The rotational contour spectra of the $T_1 \leftarrow S_0$ transitions in pyrazine, the pyrazine-argon complex, and its deuterated substituents were measured by two-color multiphoton ionization spectroscopy. It is found that higher resolution is necessary to observe the effect of the fine structure splitting in the lowest triplet state of these molecules.

5.1 Introduction

Pyrazine is the most symmetric of the three diazabenzenes. It has been studied extensively, using various spectroscopic techniques [1]. Of special interest is the lowest triplet state of pyrazine, which is found to play an important role in the photophysics of this molecule [2–10]. In the description of intersystem crossing (ISC) three different groups can be distinguished. In the small molecule limit an excited energy level couples to only a few 'dark' triplet levels. The fluorescence decay from this level will be exponential with a decay rate that is determined by the radiative lifetime of the excited state and a fluorescence quantum yield that is (almost) unity. In the large molecule limit the singlet level couples to a continuum of dark states. The fluorescence will still decay exponentially but with a yield that is less than unity, since energy is transferred to the coupled triplet states. Intermediate type behavior is found when the excited singlet level couples to a limited number of triplet states. In that case, the observed fluorescence decay is nonexponential [11]. This has been explained by level mixing, yielding levels with both singlet and triplet character, the so-called eigenstates [11].

Pyrazine has become the prototype of intermediate case molecules. In pyrazine the energy gap between the S_1 and T_1 state is equal to 4056 cm^{-1} [1]. This ensures the density of triplet levels at the S_1 origin to be low enough not to act as a continuum. Time domain experiments, in which a number of states are excited simultaneously, have revealed nonexponential decay of excited singlet levels [2, 3]. Besides a slow and a fast component in the fluorescence decay also quantum beats have been observed [5, 11]. With the setup described in Chapter 1, a narrow band UV excitation source in combination with a molecular beam setup, van der Meer *et al.* have been able to resolve the individual eigenstates [4]. From these frequency domain measurements the observed quantum beats could be reconstructed. With the use of absorption intensities, it was possible to deconvolute the molecular eigenstates into zero-order states [12, 13]. A characterization of the levels in terms of J , K_a , K_c values of the original singlet rotational levels has also been given [13].

In the non-rotating molecule the triplet state is split into three spin sublevels, T_x , T_y and T_z . Studies in solid low temperature matrices have shown that each spin sublevel has a different spin-orbit coupling strength, resulting in different lifetimes for the different sublevels. In a benzene crystal the lifetimes of the different spin sublevels in the lowest triplet state of pyrazine are 163, 6 and 284 ms for the T_x , T_y , and T_z level, respectively [14]. The energy separation between the sublevels T_x and T_z is only 0.5 GHz, with the T_x level having the higher energy. The T_y sublevel is about 10 GHz lower in energy and it is found that only this level is radiative, due to spin-orbit coupling between this level and a singlet state of B_{1u} symmetry [14]. In the gas phase the three spin sublevels will be mixed by the overall rotation of the molecule. The upper limit for the gas phase phosphorescence lifetime at the T_1 origin is found to be only 2.5 ms [15] with a lower limit of 1.45 ms [16]. The reason for this much smaller lifetime in the gas phase is not yet understood.

Although the triplet state has been extensively studied, little is known about the triplet levels that are involved in the singlet-triplet mixing. The T_1 state has been identified as a ${}^3B_{3u}$ state of $n\pi^*$ character [17]. It has, however, not yet indisputably been established whether or not the potential surface of this state is distorted and what its symmetry is. Just like for the S_1 state [1], it has been suggested that the lowest triplet state of pyrazine is distorted due to vibronic coupling with one or more higher lying B_{1u} or B_{2u} states of $\pi\pi^*$ character [16, 18–20]. On the basis

of studies on the $T \rightarrow S$ emission and $T \leftarrow S$ excitation spectra of pyrazine in different crystals, Nishi *et al.* concluded that the potential surface of the triplet state should be described by a double minimum potential along the ν_5 and ν_{10a} normal coordinates in the crystal [18]. Several other groups also use vibronic coupling between the ${}^3B_{3u}(n\pi^*)$ state and higher lying $\pi\pi^*$ states via the ν_5 or ν_{10a} mode to explain their observations [16, 19]. Kokai and Azumi suggested a distortion along the ν_4 coordinate, to explain the observed phosphorescence spectra of pyrazine in a benzene crystal [20]. Nevertheless, more recent experiments failed to show any evidence for vibronic coupling to a ${}^3\pi\pi^*$ state, or for a second low-lying triplet state [21, 22]. This seems to be validated by *ab initio* calculations that predict the ${}^3B_{1u}$ state to be $\sim 1000 \text{ cm}^{-1}$ higher in energy than the S_1 state [23].

Detailed information on the vibrational structure of the lowest triplet state is essential in order to validate any calculation on the triplet state, but, despite extensive studies, most assignments are restricted to the totally symmetric modes, although some overtones and combination bands of non-totally symmetric modes have been observed [19, 21, 24]. Recently, Kok *et al.* [25] measured the infrared spectrum of the ${}^3B_{3u}(n\pi^*)$ state of pyrazine in a dodecane matrix, using a free-electron laser. However, the nature of these experiments makes it difficult to determine which of the observed bands can be assigned to IR transitions in the triplet state. Furthermore, only gas-phase experiments can insure that the observed distortions are not matrix-induced.

The free-electron laser as a widely tunable infrared source, in combination with mass-selective double-resonance ionization spectroscopy, has proven to be a powerful tool to do gas-phase infrared spectroscopy on jet-cooled polyatomic molecules [26–28]. Experimentally it is often found to be easier to do measurements on complexes of these molecules with an inert gas. IR-laser-induced vibrational predissociation of such weakly bonded complexes can be used to measure their IR spectra [27–32]. Up to now this technique has been used to measure the IR spectra of the ground state of neutral and ionized Van der Waals complexes [27, 28], but it can, as will be demonstrated, also be applied to measure pure IR gas-phase spectra of long-lived electronically excited states. The 'matrix-shift', induced by the additional argon-atom, of vibrational transitions of the argon-clusters compared to transitions in the bare molecule will, in general, be limited to a fraction of a percent of the corresponding frequency [33–35], and the spectra can well be simulated using *ab initio* calculations on the bare molecule [27, 28]. So, instead of measuring the vibrational spectrum of the lowest triplet state of pyrazine, the spectrum of the triplet state of the pyrazine-argon complex is measured. The pure IR frequencies and intensities that follow from these measurements can be compared to calculations on the ${}^3B_{3u}(n\pi^*)$ state of pyrazine to yield more information on the symmetry of this state and the possible coupling mechanisms that are involved. For comparison also the pyrazine-*d*4-argon complex was measured.

The effect of the fine structure splitting on the singlet-triplet transition $T_1 \leftarrow S_0$ in pyrazine, the pyrazine-argon complex, and its deuterated substituents was further examined by rotational contour spectroscopy.

5.2 Experiment

The molecular beam machine used for the experiments, is described elsewhere [36]. It is currently installed at the "Free-Electron Laser for Infrared eXperiments" (FELIX) user facility in Nieuwegein, the Netherlands [37, 38], and consists of a molecular beam apparatus, two tunable pulsed dye laser systems and a differentially pumped Wiley-McLaren-type linear time-of-flight mass spectrometer. Pyrazine is put in the sample compartment of a pulsed valve (R.M. Jordan Co.), heated to 40°C and seeded in argon (2 bar backing pressure). Gas pulses are formed by expansion through a 0.5 mm diameter orifice into vacuum of 10^{-6} Torr. The molecular beam is skimmed about 4 cm downstream upon entering the interaction region. In this region the molecules can be excited and subsequently ionized by two separately pumped dye lasers. To do the infrared experiments the output of FELIX enters the interaction region counterpropagating the two dye laser beams via a vacuum tube that is connected to the molecular beam spectrometer. It is aligned, both in space and time, in between the two dye lasers. The laser beam axis, the molecular beam axis and the time-of-flight-tube axis are mutually perpendicular. Ions generated in the interaction region are extracted and accelerated to a microchannel plate detector, the signal of which is amplified and fed into a digital oscilloscope (LeCroy 9430), connected to a PC. A four-channel digital delay/pulse generator (SRS DG535) is used to synchronize the molecular beam spectrometer to the FELIX output to ns precision. The whole system runs at a 10 Hz repetition rate.

FELIX consists of two lasers, the first, FEL-1, generating infrared radiation with an energy between 40 and 400 cm^{-1} and the second, FEL-2, generating radiation between 300 and 2000 cm^{-1} . This radiation appears in the form of macropulses of about 4 μs duration, containing up to 100 mJ of energy. Each of these pulses is made up of a train of micropulses that are 0.3-5 ps long and 1 ns apart. For the experiments reported here only FEL-2 is used, at a macropulse repetition rate of 10 Hz and a bandwidth of typically 0.5-1.0% of the central frequency. To induce the $T_1 \leftarrow S_0$ transition in the pyrazine-argon complex, laser radiation at 373 nm, generated by frequency doubling the output of a Nd:YAG pumped pulsed dye laser system, operating on DCM, in a KDP crystal, is used. For subsequent ionization of the laser-prepared triplet state of the complex, laser radiation at 208 nm is used. This is generated by frequency mixing the fundamental and the doubled frequency of the second dye laser system, which is operating on LDS-751.

First, an attempt was made to measure the infrared absorption spectrum of the lowest triplet state of bare pyrazine. For this the first dye-laser excites the vibrationless triplet state, the origin of which is at 26820 cm^{-1} for pyrazine, and at 26974 cm^{-1} for pyrazine-*d4* [1], while the ionization laser is tuned to further excite the molecule to just below the ionization potential (which is at 74908 cm^{-1} for pyrazine, determined via the S_1 origin [39]). Since in the first step a long-lived triplet state is excited, the time-delay between the two dye lasers can be as long as 5 μs . Ionization can only be achieved if an additional resonant infrared photon excites a vibration in the triplet state, that subsequently can be ionized by the ionization laser. This scheme, however, did not yield any detectable ion-signal, probably due to unfavorable Franck-Condon overlap between excited vibrations in the triplet state and the ionic ground state.

We then decided to do measurements on the pyrazine-argon complex instead, by using the excitation scheme given in Figure 5.1. Again, the first dye-laser excites the vibrationless triplet state (shifted by about 16 cm^{-1} from the $T_1 \leftarrow S_0$ transition of pyrazine) [19], but now the

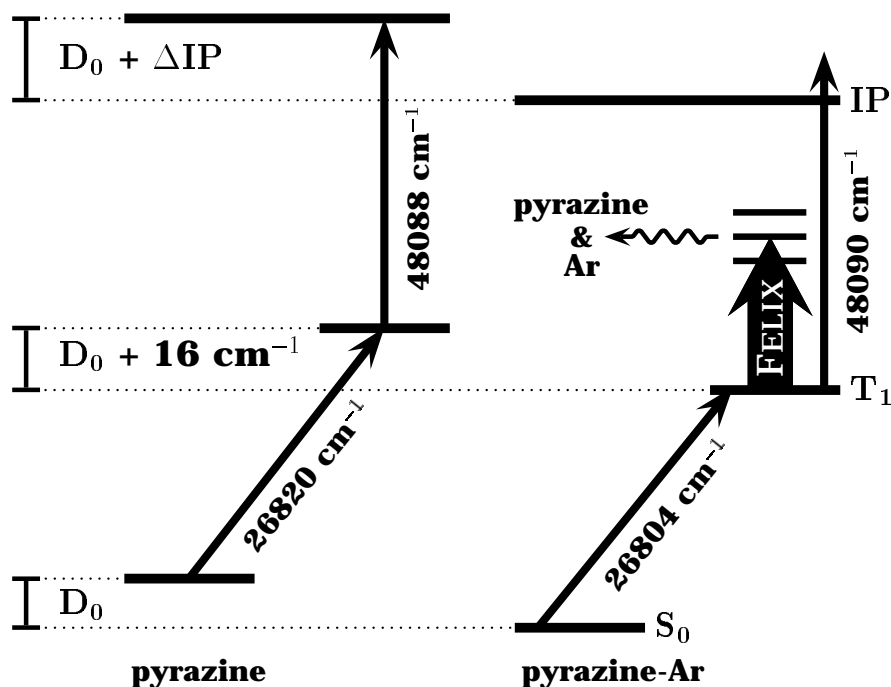


Figure 5.1: Energy level scheme of pyrazine and pyrazine-argon, indicating the experimental detection method. IR-laser induced pre-dissociation of the pyrazine-argon clusters in their triplet state is monitored via depletion of the ion-signal on the parent mass of the complex.

ionization laser ionizes the cluster to yield a pyrazine-argon ion-signal. The excitation laser is set on the central part of the rotational contour of the complex. Whenever the infrared laser, that is fired in between the two dye-lasers, excites a vibrational level above the dissociation limit in the triplet state, the pyrazine-argon cluster dissociates, and the ion-signal will decrease. Thus, the infrared absorption spectrum of the triplet state is measured as a depletion of the pyrazine-argon ion-signal. The infrared absorption spectrum of the triplet state of the pyrazine-*d*4-argon complex is measured in a similar way.

The rotational contour spectra of the $T_1 \leftarrow S_0$ transitions in pyrazine, the pyrazine-argon complex and its deuterated compounds were measured using two-color ($1+1'$)-resonance enhanced multiphoton ionization (REMPI) spectroscopy. The first dye laser is scanned over the $T_1 \leftarrow S_0$ transition, while the second dye laser is used for subsequent ionization of the laser-prepared triplet state and is fixed above the ionization potential. From a rough simulation of the rotational contour spectra, which yields the relative origins, the origin of the $T_1 \leftarrow S_0$ transition in the pyrazine-argon complex is found to be 16.6 cm^{-1} red-shifted from the same transition in pyrazine ($26\,820 \text{ cm}^{-1}$ [1]). The origin of the $T_1 \leftarrow S_0$ transition in the deuterated cluster is found to be 17 cm^{-1} red-shifted from the same transition in pyrazine-*d*4 ($26\,974 \text{ cm}^{-1}$ [1]).

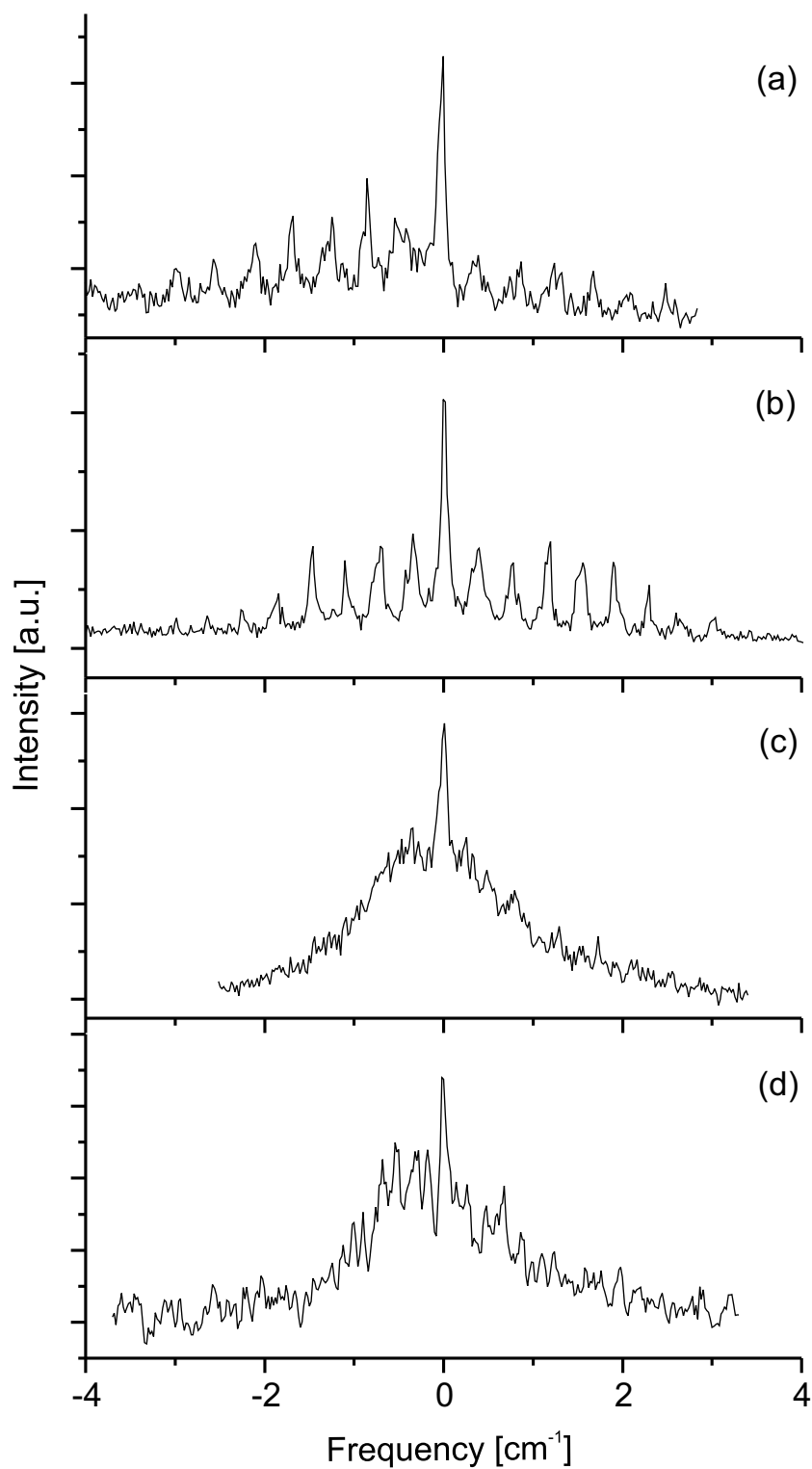


Figure 5.2: *The rotational contour spectra of pyrazine (a), pyrazine- d_4 (b), the pyrazine-argon complex (c) and the pyrazine- d_4 -argon complex (d). Experimental resolution is 0.07 cm^{-1} , while the rotational temperature is estimated at 5 K.*

5.3 Results and discussion

5.3.1 Rotational contour spectra

The observed rotational contour spectra of the $T_1 \leftarrow S_0$ transitions of pyrazine, pyrazine-*d*4 and its argon clusters, using double resonance multiphoton ionization, are given in Figure 5.2. The experimental resolution is about 0.07 cm^{-1} for all spectra, while the rotational temperature is estimated to be 5 K.

The analysis of rotational singlet-triplet transitions is in several ways different from that of singlet-singlet transitions. In condensed phases each triplet level is split into three spin sublevels by spin-spin interaction. This is described by the Hamiltonian:

$$H_{SS} = D(S_x^2 - \frac{1}{3}S^2) + E(S_z^2 - S_y^2), \quad (5.1)$$

where D and E are the fine structure splitting constants. However, unlike condensed phases, where rotations are frozen out, in the gas phase the rotational angular momentum \vec{N} will couple with spin momentum \vec{S} , and this spin-rotation interaction has to be included in the calculations. This will mix all three spin sublevels of the triplet state. If the fine structure splittings are large compared to the rotational energy splittings of the molecule, each spin sublevel will have its own rotational ladder. This is similar to Hund's Case (a) coupling [40]. Hund's Case (b) describes the situation, where the fine structure splittings are small compared to the rotational energy splittings of the molecule. Each rotational level will be split into three spin sublevels, labeled by N and J , where J can take on the values $N, N \pm 1$. A transition from Hund's Case (a) to (b) can occur for moderate values of D and E . For low values of the rotational angular momentum N , where the pure rotational level splittings are still larger than the fine structure splittings, Hund's Case (a) applies, while for higher rotational levels, the rotational frequency can become larger than the spin nutation frequency, and Hund's Case (b) is approached. This is called spin uncoupling [40]. This spin uncoupling occurs in pyrazine, for which the rotational and fine structure splitting constants are given in table 5.1. (Since in the non-rotating pyrazine molecule two spin sublevels are closely spaced, while the third one is much lower in energy, actually a transition from Hund's Case (ab) to Hund's Case (b) should be seen [41, 42].)

The principle axes of pyrazine are shown in Figure 5.3. Pyrazine is a near-symmetric oblate top, with rotational constant C much smaller than A and B , which makes the c axis the top axis of the molecule.¹ Pyrazine-*d*4 is also a near-symmetric oblate top with rotational constants given in table 5.1. Compared to pyrazine the a and b axes are interchanged. Pyrazine-argon and pyrazine-*d*4-argon are both near-symmetric prolate tops. The top axis now becomes the a axis, as is shown in Figure 5.3. This implicates that, with the proper choice of axis representation, the symmetry of the triplet state remains unchanged and the analysis is similar for these molecules.

Medvedev and Pratt derived a general analytical expression for the calculation of individual spin-rotational transitions between a singlet and triplet electronic state in a polyatomic molecule [41]. Singlet-triplet transitions can only occur through singlet contamination into the triplet, or

¹The top axis is defined as the near-symmetry axis of the molecule, *i.e.* the principal axis with the smallest rotational constant for a near-oblate and the principal axis with the largest rotational constant for a near-prolate molecule.

Table 5.1: *Rotational and fine structure splitting constants of pyrazine and pyrazine-d4 in the ground and lowest triplet state (MHz).*

	pyrazine		pyrazine-d4
	$S_0^{\text{a)}}$	$T_1^{\text{b)}}$	$S_0^{\text{a)}}$
A	6381	6355	5513
B	5926	5876	5247
C	3073	3028	2688
D		10358	
E		-211	

a) Ref. [1].

b) Rotational constants are from Ref. [43]; D and E are taken from Ref. [1].

triplet contamination into the singlet state. The intensities of singlet-triplet transitions are thus not governed by a single transition dipole moment between the two electronic states, but are governed by spin-orbit coupling of one of the two states with a state of different multiplicity. For pyrazine in condensed phases, only the lowest spin sublevel, which is of B_{3g} symmetry, is found to be radiative through spin-orbit coupling with a higher lying singlet state of B_{1u} symmetry. (We have to note, that the symmetry labeling used here is different from that used by Medvedev *et al.* [41]. This is caused by a difference in the choice of axes.) The selection rules that follow from the intensity formula derived using this spin-orbit coupling, as it is given in Ref. [41], are $\Delta J = 0, \pm 1$, $\Delta N = 0, \pm 1, \pm 2$ and $\Delta K = 0, \pm 2$. The derived expressions were used to calculate the singlet-triplet transitions of pyrazine, pyrazine-d4 and the pyrazine-

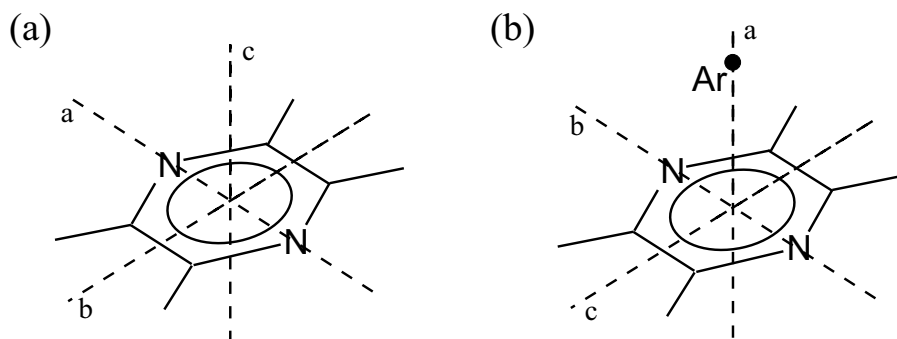


Figure 5.3: *The structure and principal axes of pyrazine (a) and the pyrazine-argon complex (b). For pyrazine-d4 the a and b axes are interchanged compared to pyrazine.*

argon complex. For pyrazine, the rotational constants given in Table 5.1 were used to calculate the spectra, while the rotational constants of the argon complexes were calculated using the constants of the bare molecule and attaching an argon atom at 3.5 Å above the middle of the pyrazine plane, taking this value from the argon–ring distance in benzene-argon [44] and *s*-tetrazine-argon [45]. Simulations of the singlet-triplet transitions of pyrazine, pyrazine-*d*4 and the pyrazine-argon complex, calculated using these selection rules, are in agreement with the measured spectra. Thus, these transitions are induced by spin-orbit coupling between the B_{3g} sublevel and a singlet state of B_{1u} symmetry, leading to $\Delta K = 0, \pm 2$ selection rules.

The effect of spin-spin interaction is more pronounced in pyrazine-*d*4 and the pyrazine-argon complex. This is due to their smaller rotational constants compared to pyrazine, which makes the coupling between spin and rotation deviate more from Hund’s Case (b) coupling, especially at low N . With high enough resolution it should therefore be possible to observe a transition from Hund’s Case (a) (or rather (ab)) at low N to Hund’s Case (b) at high N . This will show in nicely stacked rotational transitions at high N values, while at low N values the pattern will look ‘messy’. Unfortunately, the resolution of the measured spectra, especially for the argon clusters, is not high enough to resolve the fine structure splittings in singlet-triplet transitions.

From these rotational contour spectra, it is found that the origin of the pyrazine-argon complex is shifted 16.6 cm^{-1} to the red of the pyrazine origin. The shift between the origins of pyrazine-*d*4 and its argon complex is 17 cm^{-1} , with the cluster transition again being on the low-frequency side of the transition in the bare molecule. The $T_1 \leftarrow S_0$ transition of pyrazine-*d*4 is located 156 cm^{-1} to the blue of the $T_1 \leftarrow S_0$ transition in pyrazine. This situates the origin of the $T_1 \leftarrow S_0$ transition in pyrazine-*d*4 at 26976 cm^{-1} .

5.3.2 Vibrational spectra

The measured IR spectrum of the lowest triplet state of the pyrazine-argon complex, recorded via the scheme given in Figure 5.1, is given in the upper panel of Figure 5.4. The spectrum shown in Figure 5.4 is the result of several different scans. Since the IR spectrum is measured as a depletion of the pyrazine-argon signal, the signal S of each of the scans is given by:

$$S(\nu) = ae^{-\sigma(\nu)I(\nu)}, \quad (5.2)$$

where I is the IR laser power, σ the absorption cross section and a is the pyrazine-argon signal generated by the UV lasers when no IR light is present. Each scan is corrected for fluctuations in IR laser power to yield a pure absorption spectrum. One scan was taken with a laser power attenuation of 30 dB to avoid saturation of the strong absorption line around 700 cm^{-1} .

For comparison a calculated absorption spectrum of bare pyrazine is shown in the lower panel of Figure 5.4. This calculation is performed with GAUSSIAN 94 [46], using a Becke3LYP functional with the D95(d,p) basis set. Calculations assuming D_{2h} symmetry did not yield a minimum on the potential energy surface at this level of theory, so C_{2h} symmetry was assumed for the ${}^3B_{3u}$ state. The calculated frequencies are given in Table 5.2, together with assignments of previously measured vibrations and their irreducible representations in the C_{2h} point group. The frequencies and relative intensities of the measured IR transitions are also given in this table. Since the measurements concern the pyrazine-argon complex, we might expect to see Van der Waals modes showing up as sidebands of the strong transitions. The rather weak modes at

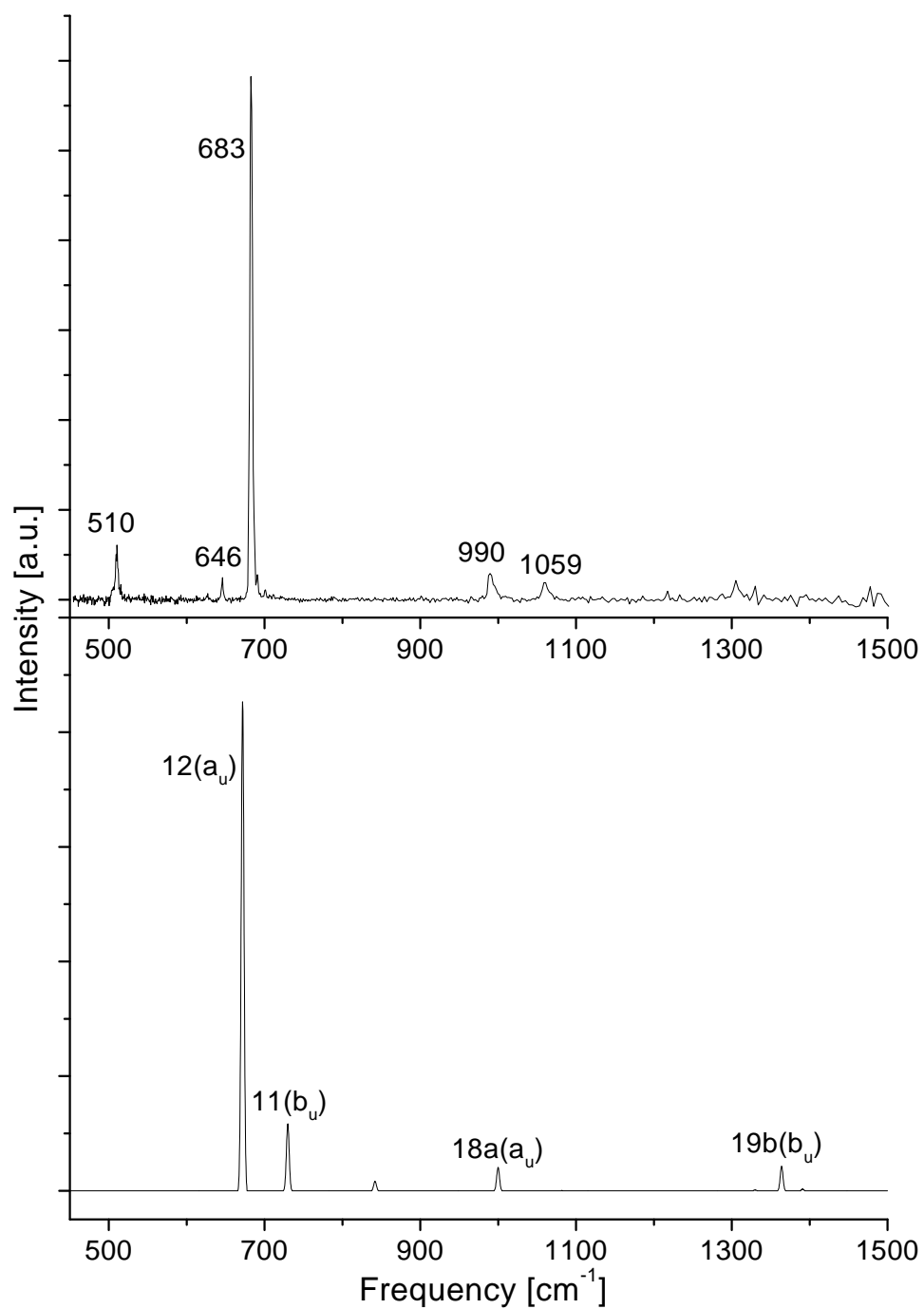


Figure 5.4: Observed absorption spectrum of pyrazine-argon as a function of IR laser frequency (upper panel), compared to the calculated IR spectrum of pyrazine in its triplet state (lower panel).

691 or 701 cm^{-1} might be attributed to this. Besides this, still more vibrational transitions show up in the spectrum than are predicted by the calculations, where, using C_{2h} symmetry, a total of 8 a_u and b_u vibrations are infrared active in this frequency range, but only five of them are calculated to have reasonable intensity. Possibly, vibronic coupling of the ${}^3B_{3u}(n\pi^*)$ state to higher lying ${}^3\pi\pi^*$ states will have to be taken into account in the calculations in order to fully reproduce all the observed transitions. Possible Fermi-resonances could further complicate the spectrum. Based on the calculations reported here, which at least reproduce the strong transition observed at 683 cm^{-1} , we assign this transition to the ν_{12} mode of a_u symmetry.

Table 5.2: *Experimental and calculated vibrational frequencies (cm^{-1}) in the lowest triplet state of pyrazine. Calculations were performed using GAUSSIAN 94 (Becke3LYP/D95(d,p)). The intensity of the strongest observed IR transition is taken to be the same as the strongest calculated transition, which is given in km mol^{-1} .*

Frequency [cm^{-1}]		IR intensity [km mol^{-1}]		Assignment
Exp.	Calc.	Exp.	Calc.	
237 ^{a)}	272		34	16b(b_u)
406 ^{b)}	440		0.2	16a(a_u)
440 ^{a)}	208			10a(a_g)
510 ^{c)}		89		
522 ^{a)}	809			5(b_g)
557 ^{a)}	374			4(b_g)
563 ^{b)}	730		117	11(b_u)
620 ^{a)}	614			6a(a_g)
	621			6b(b_g)
646 ^{c)}		36		
683 ^{c)}	672	853	853	12(a_u)
691 ^{c)}		41		VdW?
701 ^{c)}		16		VdW?
	842		17	17a(a_u)
	1000		41	18a(a_u)
980 ^{a)}	1019			1(a_g)
990 ^{c)}		43		
	1016			3(b_g)
1059 ^{c)}		28		
	1082		1	18b(b_u)

a) Ref. [21]

b) Ref. [24]

c) This work

continued on next page

Table 5.2 continued

Frequency [cm^{-1}]		IR intensity [km mol^{-1}]		Assignment
Exp.	Calc.	Exp.	Calc.	
1146 ^{a)}	1199			9a(a _g)
	1306			8b(b _g)
	1330		2	19b(b _u)
	1364		43	14(b _u)
	1391		2	19a(a _u)
1230 ^{a)}	1558			8a(a _g)
1305 ^{c)}		31		
1330 ^{c)}		22		
1478 ^{c)}		21		
	3197			7b(b _g)
	3199		12	13(a _u)
	3228		1	20b(b _u)
	3229			2(a _g)

^{a)} Ref. [21]

^{b)} Ref. [24]

^{c)} This work

The measured IR spectrum of the lowest triplet state of the pyrazine-*d*4-argon complex is very similar to that of the pyrazine-argon complex. It is given in Figure 5.5 together with the results of a calculation of the IR absorption spectrum of bare pyrazine-*d*4. Less vibrations are observed than in the non-deuterated spectrum. However, also in this case the agreement between observed and calculated spectrum is poor and we only assign the transition observed at 643 cm^{-1} to the ν_{12} mode of a_u symmetry.

5.4 Conclusion

The observed rotational contour spectra of the $T_1 \leftarrow S_0$ transitions of pyrazine, pyrazine-*d*4 and its argon clusters, using double resonance multiphoton ionization, are in agreement with the simulated spectra given in Ref. [41], where it has to be noted that these spectra are simulated using different rotational temperatures and, except for pyrazine, higher resolution than apply to our measured spectra. For the complexes an argon distance of 3.5 \AA to the pyrazine plane compares well to the measured spectra. The transitions are induced by spin-orbit coupling between the lowest spin sublevel of B_{3g} symmetry and a higher lying singlet state of B_{1u} symmetry. The resolution obtained here, is not high enough to observe the fine structure splittings in the singlet-triplet transitions of these molecules.

IR absorption spectra of jet-cooled Van der Waals complexes in their triplet state can be measured using a 'standard' molecular beam apparatus in combination with a free-electron

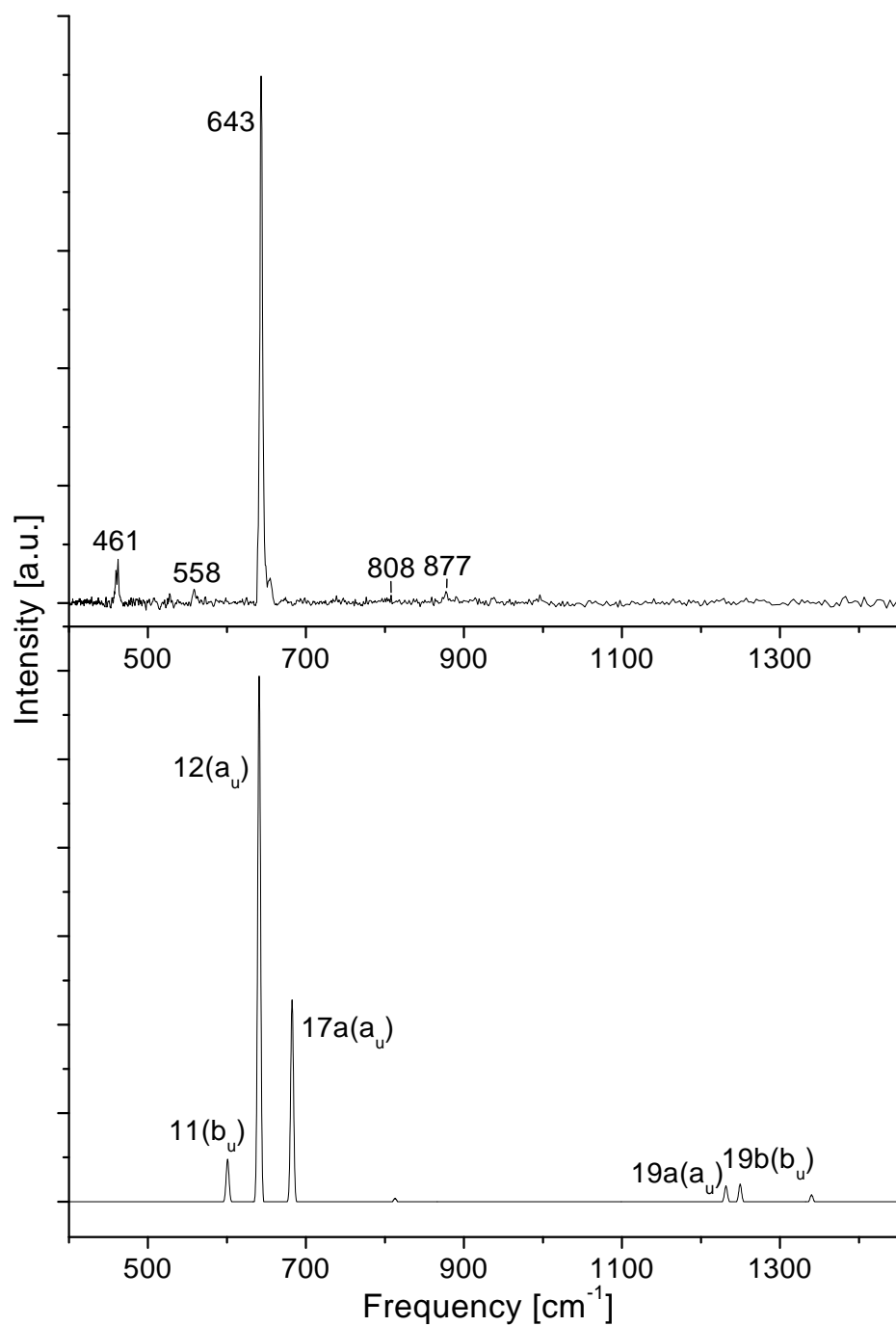


Figure 5.5: Observed absorption spectrum of pyrazine-*d*4-argon as a function of IR laser frequency (upper panel), compared to the calculated IR spectrum of pyrazine-*d*4 in its triplet state (lower panel).

laser, as demonstrated here by recording the pure IR absorption spectrum of the pyrazine-argon complex in its lowest triplet state. A total of 10 IR transitions is observed in the range from 500 to 1500 cm^{-1} . The strongest of these transitions is assigned to the ν_{12} mode of a_u symmetry, but so far no other assignments can be made. Due to a distortion of the potential energy surface of the triplet state of pyrazine, caused by vibronic coupling to other electronic states, the Becke3LYP/D95(d,p) calculations, performed using C_{2h} symmetry for the triplet state, are unable to reproduce all the observed features in the IR absorption spectrum. Comparing the spectrum to the IR absorption spectrum of the pyrazine- d_4 -argon complex in its lowest triplet state, does not lead to new insights in the spectrum, as was the case for the benzene-argon cation [47]. The two absorption spectra are very similar. The reported spectra, however, are expected to make an essential contribution to the validation of *ab initio* calculations on the triplet state of pyrazine.

In future experiments, the information obtained from the IR spectrum of the lowest triplet state of pyrazine will be used to access the vibrational levels of the lowest triplet state of pyrazine, via its eigenstates in the lowest singlet state, in a UV-IR double resonance experiment.

Acknowledgments

The authors gratefully acknowledge the support by the Stichting voor Fundamenteel Onderzoek der Materie (FOM) in providing the required beam time on FELIX and highly appreciate the skillful assistance by the FELIX staff and the expert technical assistance by A. J. A. van Roij. This research is part of the research program of FOM and is in part financially supported by the Council for Chemical Sciences, both of which are financially supported by the Nederlandse Organisatie voor wetenschappelijk Onderzoek (NWO), and receives direct support from the NWO via PIONIER grant 030-66-89.

References

- [1] K. K. Innes, I. G. Ross, and W. R. Moomaw. *Electronic states of azabenzenes and azanaphthalenes: A revised and extended critical review*. Journal of Molecular Spectroscopy **132**:492–544, 1988.
- [2] A. Frad, F. Lahmani, A. Tramer, and C. Tric. *Luminescence and radiationless transitions from single vibronic levels of the isolated pyrazine molecule in the $S_1(n, \pi^*)$ state of pyrazine*. Journal of Chemical Physics **60**:4419–4430, 1974.
- [3] A. E. W. Knight and C. S. Parmenter. *Radiative and non-radiative processes in the first excited singlet state of azabenzene vapors*. Chemical Physics **15**:85–102, 1976.
- [4] B. J. Van der Meer, H. Th. Jonkman, J. Kommandeur, W. L. Meerts, and W. A. Majewski. *Spectrum of the molecular eigenstates of pyrazine*. Chemical Physics Letters **92**:565–569, 1982.

- [5] P. M. Felker, Wm. R. Lambert, and A. H. Zewail. *Picosecond excitation of jet-cooled pyrazine: Magnetic field effects on the fluorescence decay and quantum beats*. Chemical Physics Letters **89**:309–314, 1982.
- [6] A. Amirav and J. Jortner. *Rotational and vibrational state dependence on intramolecular coupling and dynamics in the S_1 state of pyrazine*. Journal of Chemical Physics **84**:1500–1507, 1986.
- [7] J. Kommandeur, W. A. Majewski, W. L. Meerts, and D. W. Pratt. *Pyrazine: An "exact" solution to the problem of radiationless transitions*. Annual Review of Physical Chemistry **38**:433–462, 1987.
- [8] W. M. Van Herpen, W. L. Meerts, K. E. Drabe, and J. Kommandeur. *High resolution lifetime measurements of the perturbed $J' \neq 0$ levels of the $^1B_{3u}$ state of pyrazine*. Journal of Chemical Physics **86**:4396–4400, 1987.
- [9] H. Bitto and P. R. Willmott. *The dynamics and its power dependence of $S_1(1B_{3u})$ pyrazine studied with transform-limited nanosecond laser pulses*. Chemical Physics **165**:113–121, 1992.
- [10] E. S. Medvedev and D. W. Pratt. *Fast and slow fluorescence decays in pyrazine under nanosecond excitation conditions: A resolution of the enigma*. Journal of Chemical Physics **105**:3366–3375, 1996.
- [11] S. Okajima, H. Saigusa, and E. C. Lim. *Quantum beats in the fluorescence of jet-cooled diazabenzenes*. Journal of Chemical Physics **76**:2096–2098, 1982.
- [12] W. D. Lawrance and A. E. W. Knight. *Direct convolution of extensively perturbed spectra: The singlet-triplet molecular eigenstate spectrum of pyrazine*. Journal of Physical Chemistry **89**:917–925, 1985.
- [13] W. Siebrand, W. L. Meerts, and D. W. Pratt. *Analysis and deconvolution of some $J' \neq 0$ rovibronic transitions in the high resolution $S_1 \leftarrow S_0$ fluorescence excitation spectrum of pyrazine*. Journal of Chemical Physics **90**:1313–1316, 1989.
- [14] D. M. Burland and J. Schmidt. *The dynamic properties of the lowest triplet states of pyrazine and pyrimidine in zero magnetic field*. Molecular Physics **22**:19–31, 1971.
- [15] I. Becker and O. Cheshnovsky. *The decay of triplet pyrazine and pyrazine-d4 in supersonic jets: Isotope effects*. Journal of Chemical Physics **101**:3649–3655, 1994.
- [16] O. Sneh, D. Dünn-Kittenplon, and O. Cheshnovsky. *The decay of triplet pyrazine in supersonic jets*. Journal of Chemical Physics **91**:7331–7339, 1989.
- [17] L. Goodmann and M. Kasha. Journal of Molecular Spectroscopy **2**:85, 1958.
- [18] N. Nishi, M. Kinoshita, T. Nakashima, R. Shimada, and Y. Kanda. *Study on the molecular geometry of phosphorescent pyrazine by optical detection of zero-field magnetic resonance and $T \leftarrow S$ excitation spectroscopy*. Molecular Physics **33**:31–52, 1977.

- [19] E. Villa, M. Terazima, and E. C. Lim. *MPI detection of single-trig-tharrow-triplet transitions in a supersonic jet: Evidence for T_1 potential energy distortion in pyrazine and related molecules.* Chemical Physics Letters **129**:336–341, 1986.
- [20] F. Kokai and T. Azumi. *Sublevel phosphorescence spectra of pyrazine. interpretation of "anomalous" behavior of the radiative rate constant ratios for totally symmetric vibrations and the reinvestigation of the triplet state geometry.* Journal of Chemical Physics **75**:1069–1073, 1981.
- [21] J. L. Tomer, K. W. Holtzclaw, D. W. Pratt, and L. H. Spangler. *Phosphorescence excitation spectroscopy in supersonic jets. The lowest triplet state of pyrazine.* Journal of Chemical Physics **88**:1528–1538, 1988.
- [22] M. C. J. M. Donckers, A. M. Schwencke, E. J. J. Groenen, and J. Schmidt. *An electron-nuclear double resonance study of the lowest triplet state of pyrazine.* Journal of Chemical Physics **97**:110–117, 1992.
- [23] I. C. Walker and M. H. Palmer. *The electronic states of the azines. 4. Pyrazine, studied by VUV absorption, near-threshold electron energy-loss spectroscopy and ab initio multireference configuration-interaction calculations.* Chemical Physics **153**:169–187, 1991.
- [24] G. Fisher. *The triplet ${}^3B_{3u}(n) \leftarrow {}^1A_g(x)$ absorption spectrum of pyrazine vapour.* Chemical Physics Letters **79**:573–577, 1981.
- [25] P. Kok, E. J. J. Groenen, P. W. Van Amersfoort, and A. F. G. Van der Meer. *The infrared spectrum of pyrazine in its metastable triplet state. A free-electron-laser study.* Journal of Chemical Physics **106**:2984–2986, 1997.
- [26] M. Putter, G. Von Helden, and G. Meijer. *Mass selective infrared spectroscopy using a free electron laser.* Chemical Physics Letters **258**:118–122, 1996.
- [27] J. A. Piest, G. Von Helden, and G. Meijer. *Infrared spectroscopy of jet-cooled neutral and ionized aniline-Ar.* Journal of Chemical Physics **110**:2010–2015, 1999.
- [28] J. A. Piest, G. Von Helden, and G. Meijer. *Infrared spectroscopy of jet-cooled cationic polyatomic hydrocarbons: Naphthalene⁺.* The Astrophysical Journal **520**:L75–L78, 1999.
- [29] M. Okumura, L. I. Yeh, and Y. T. Lee. *The vibrational predissociation spectroscopy of hydrogen cluster ions.* Journal of Chemical Physics **83**:3705–3706, 1985.
- [30] M. Okumura, L. I. Yeh, J. D. Myers, and Y. T. Lee. *Infrared spectra of the solvated hydronium ion - vibrational predissociation spectroscopy of mass-selected $H_3O^+(H_2O)_n \cdot (H_2)_m$.* Journal of Physical Chemistry **94**:3416–3427, 1990.
- [31] R. V. Olkhov, S. A. Nizkorodov, and O. Dopfer. *Infrared photodissociation spectra of CH-Ar_n complexes (n = 1-8).* Journal of Chemical Physics **108**:10046–10060, 1998.

- [32] K. Kleinermanns, Ch. Janzen, D. Spangenberg, and M. Gerhards. *Infrared spectroscopy of resonantly ionized (phenol)(H₂O)_n⁺*. *Journal of Physical Chemistry A* **103**:5232–5239, 1999.
- [33] M. Takahashi, H. Ozeki, and K. Kimura. *Vibrational spectra of aniline-Ar_n Van der Waals cations (n=1 and 2) observed by two-color "threshold photoelectron" [zero kinetic energy (ZEKE)-photoelectron] spectroscopy*. *Journal of Chemical Physics* **96**:6399–6406, 1992.
- [34] X. Zhang, J. M. Smith, and J. L. Knee. *High resolution threshold photoelectron spectroscopy of aniline and aniline Van der Waals complexes*. *Journal of Chemical Physics* **97**:2843–2860, 1992.
- [35] W. E. Sinclair and D. W. Pratt. *Structure and vibrational dynamics of aniline and aniline-Ar from high resolution electronic spectroscopy in the gas phase*. *Journal of Chemical Physics* **105**:7942–7956, 1996.
- [36] M. G. H. Boogaarts, G. Von Helden, and G. Meijer. *A study on the structure and vibrations of diphenylamine by resonance-enhanced multiphoton ionization spectroscopy and ab initio calculations*. *Journal of Chemical Physics* **105**:8556–8568, 1996.
- [37] D. Oepts, A. F. G. Van der Meer, and P. W. Van Amersfoort. *The free-electron-laser user facility FELIX*. *Infrared physics & technology* **36**:297–308, 1995.
- [38] G. M. H. Knippels, R. F. X. A. M. Mols, A. F. G. Van der Meer, D. Oepts, and P. W. Van Amersfoort. *Intense far-infrared free-electron laser pulses with a length of six optical cycles*. *Physical Review Letters* **75**:1755–1758, 1995.
- [39] L. Zhu and P. Johnson. *Vibrations of pyrazine and its ion as studied by threshold ionization spectroscopy*. *Journal of Chemical Physics* **99**:2322–2331, 1993.
- [40] G. Herzberg. *Molecular Spectra and Molecular Structure, volume I. Spectra of diatomic molecules*. Van Nostrand Reinhold Company, New York, N. Y. 10001, second edition, 1950.
- [41] E. S. Medvedev and D. W. Pratt. *Hund's case (a)- case (b) transition in the singlet-triplet absorption spectrum of pyrazine in a supersonic jet*. *Journal of Experimental and Theoretical Physics* **87**:35–50, 1998.
- [42] F. Creutzberg and J. T. Hougen. *Triplet-state rotational energy levels for near-symmetric rotor molecules of symmetry C_{2v}, D₂ and D_{2h}*. *Canadian Journal of Physics* **45**:1363–1387, 1967.
- [43] K. W. Holtzclaw, L. H. Spangler, and D. W. Pratt. *A rotational resolved phosphorescence excitation spectrum of the lowest triplet state of pyrazine*. *Chemical Physics Letters* **161**:347–352, 1989.
- [44] Th. Weber, A. Von Bargaen, E. Riedle, and H. J. Neusser. *Rotationally resolved ultraviolet spectroscopy of the benzene-Ar complex by mass-selected resonance-enhanced 2-photon ionization*. *Journal of Chemical Physics* **92**:90–96, 1990.

- [45] P. M. Weber and S. A. Rice. *Intramolecular vibrational relaxation in the S_0 state of s-tetrazine- X ($X=AR, KR, XE$)*. Journal of Chemical Physics **88**:6120–6133, 1988.
- [46] *GAUSSIAN 94 Revision D.3*. M. J. Frisch, G. W. Trucks, H. B. Schlegel, P. M. W. Gill, B. G. Johnson, M. A. Robb, J. R. Cheeseman, T. A. Keith, G. A. Petersson, J. A. Montgomery, K. Raghavachari, M. A. Al-Laham, V. G. Zakrzewski, J. V. Ortiz, J. B. Foresman, J. Cioslowski, B. B. Stefanov, A. Nanayakkara, M. Challacombe, C. Y. Peng, P. Y. Ayala, W. Chen, M. W. Wong, J. L. Andres, E. S. Replogle, R. Gomperts, R. L. Martin, D. J. Fox, J. S. Binkley, D. J. Defrees, J. Baker, J. P. Stewart, M. Head-Gordon, C. Gonzalez, and J. A. Pople. Gaussian, Inc., Pittsburgh PA, 1995.
- [47] R. G. Satink, J. A. Piest, G. von Helden, and G. Meijer. *The infrared spectrum of the benzene- Ar cation*. Journal of Chemical Physics **111**:10750–10753, 2000.

Samenvatting

Kleine aromatische moleculen bestudeerd met behulp van spectroscopie.

-Wat fundamenteel onderzoek ons leert -

Aromatische moleculen zijn, zoals de naam al zegt, moleculen met een uitgesproken geur. De chemische definitie van aromatische moleculen beschrijft moleculen, die een ring van atomen bevatten en die, door de wijze waarop de electronen zijn verdeeld, chemisch zeer stabiel zijn. Het eenvoudigste en meest bekende aromatische molecuul is benzeen, een veel gebruikt oplosmiddel, dat bestaat uit een ring van 6 koolstof atomen, waaraan zich 6 waterstof atomen bevinden. Aromatische moleculen zijn vaak terug te vinden als onderdeel van veel grotere systemen in ontelbare toepassingen, bijvoorbeeld in geneesmiddelen en brandstoffen. Er wordt dan ook zeer veel onderzoek gedaan naar deze groep moleculen. Dat kan leiden tot de ontdekking van nieuwe toepassingen, zoals het gebruik van geleidende polyaromatische moleculen in oplaadbare batterijen of in LED's (light emitting diodes = licht gevende diodes). Maar ook op fundamenteel niveau is nog veel te leren over deze groep moleculen. Zo bestaan, ondanks het vele onderzoek, zelfs over een relatief eenvoudig molecuul als benzeen nog steeds veel onduidelijkheden.

In dit proefschrift worden metingen beschreven aan een aantal kleine aromatische moleculen, waarvan het grootste systeem bestaat uit 30 atomen en gevormd wordt door twee benzoëzuur moleculen. De moleculen zijn bestudeerd met behulp van spectroscopische technieken, waarbij gebruik gemaakt is van een supersone moleculaire bundel in combinatie met één of meerdere lasersystemen. Wanneer de moleculaire bundel gekruist wordt met een laserbundel, kunnen de moleculen, wanneer het laserlicht de juiste golflengte heeft, energie hiervan absorberen om zo een energetisch aangeslagen toestand te bereiken. De golflengtes die worden geabsorbeerd zijn karakteristiek voor het molecuul en bevatten informatie over de structuur en dynamica van dat molecuul in de aangeslagen toestand en in de toestand waarin het molecuul zich bevond voor de absorptie, de grondtoestand. Om te bepalen welke golflengtes door een molecuul geabsorbeerd worden, kunnen verschillende detectiemethoden worden toegepast.

De eerste methode, die bij de experimenten in dit proefschrift is toegepast, is laser geïnduceerde fluorescentie (LIF). Een molecuul zal zich, na absorptie van laserlicht, slechts een beperkte tijd in de aangeslagen toestand bevinden. Het molecuul komt terecht in een lager energetische toestand, wat gepaard gaat met energieverlies. Wanneer de levensduur van het aangeslagen niveau

zeer kort is en het molecuul zijn energie verliest in de vorm van licht, kan een spectrum verkregen worden door deze fluorescentie te detecteren als functie van de laser golflengte. Een tweede methode om dit soort informatie te verkrijgen is resonante ionisatie van de moleculen. Nadat de moleculen energie van één laserbundel (de excitatie laser) hebben geabsorbeerd, wordt de moleculaire bundel gekruist met een tweede laserbundel (de ionisatie laser), waaruit de moleculen vervolgens voldoende energie kunnen absorberen om een electron los te maken. Door de ionen die zo ontstaan te detecteren als functie van de golflengte van de excitatie laser wordt een spectrum verkregen.

De moleculaire bundel wordt gevormd door de moleculen te mengen in een draaggas en dit mengsel door een zeer kleine opening te expanderen in vacuüm. Tijdens deze expansie wordt een deel van de interne energie van de moleculen omgezet in translatie energie; de moleculen worden dus zeer snel maar rotateren of vibreren nauwelijks meer. Het aantal bezette niveau's in de grondtoestand neemt hierdoor sterk af, wat een aanzienlijke vereenvoudiging van de gemeten spectra tot gevolg heeft. Daarnaast kunnen onder deze omstandigheden zwak gebonden clusters van moleculen ontstaan, zodat ook deze bestudeerd kunnen worden.

De moleculen beschreven in de hoofdstukken 2 t/m 4 zijn bestudeerd met behulp van laser geïnduceerde fluorescentie. Hierbij is gebruik gemaakt van een zeer smalbandige, continue UV laser, waarmee de moleculen elektronisch geëxciteerd worden. De laser is zo smalbandig dat hiermee rotatieniveau's van de moleculen bestudeerd kunnen worden. Het gemeten rotatiespectrum wordt voornamelijk bepaald door de structuur van de moleculen in zowel de grondtoestand als de aangeslagen toestand. Daarnaast bevat het ook informatie over de verandering van de elektronenverdeling ten gevolge van de excitatie en over de levensduur van de aangeslagen toestand.

Hoofdstuk 2 gaat over de moleculen 3- en 5-methylindole. Deze moleculen vertonen een zeer grote gelijkenis met het aminozuur tryptofaan. Naast de algehele rotatie is in de spectra van deze moleculen ook de rotatie zichtbaar van de methyl groep ten opzichte van het starre indole frame. Uit de spectra blijkt dat deze interne rotatie toe neemt wanneer de moleculen geëxciteerd worden. De interne rotatie in 5-methylindole is sterker dan in 3-methylindole, wat verband houdt met de elektronen verdeling in de buurt van de methyl groep.

In hoofdstuk 3 wordt *ortho*-fluorofenol besproken. Er bestaan 2 isomeren van dit molecuul, die verschillen in de richting van de OH groep ten opzichte van het fluor atoom. Van 2 sterke elektronische overgangen zijn de rotatiespectra gemeten. Allereerst is geverifieerd dat beide overgangen toebehoren aan hetzelfde isomeer. Uit de gemeten rotatiespectra blijkt vervolgens dat dit isomeer in de grondtoestand vlak is, maar dat dit niet meer het geval is in de aangeslagen toestand. Hierdoor wordt in de aangeslagen toestand een vibratie geactiveerd, waarbij enkele atomen een beweging loodrecht op het vlak van de aromatisch ring uitvoeren. De tweede sterke overgang kan worden toegeschreven aan de activering van deze vibratie.

Twee benzoëzuur moleculen kunnen een cluster vormen, waarbij twee waterstofbruggen de verbindingen vormen tussen de twee moleculen. Dit dimeer is het onderwerp van hoofdstuk 4. De waterstofkernen in de verbindingen kunnen zich tussen de twee moleculen heen en weer bewegen. Deze bewegingen zijn zichtbaar in het gemeten rotatiespectrum en leiden tot een verdubbeling van het aantal rotatielijnen. Hierdoor, en door de grootte van het dimeer, bevat het spectrum zoveel lijnen dat er veel overlap van de individuele rotatielijnen is.

Het laatste hoofdstuk beschrijft metingen aan pyrazine. In tegenstelling tot de hierboven beschreven experimenten, die te doen hebben met singlet toestanden, is hier een triplet toestand

onderzocht. De interesse voor dit molecuul komt voort uit een koppeling die plaats vindt tussen de onderzochte triplet toestand en een nabij gelegen singlet toestand. Hoewel aan dit molecuul zeer veel metingen zijn verricht, is over deze triplet toestand nog niet veel bekend. Een triplet toestand (ook wel donkere toestand genoemd) heeft een lange levensduur en fluoresceert niet, zodat in dit geval gebruik gemaakt is van de resonante ionisatie techniek. Daarnaast is meer laservermogen nodig om deze toestand vanuit de (singlet) grondtoestand te exciteren. Daarom zijn voor dit experiment gepulste UV lasers gebruikt, waarmee de triplet toestand is geëxciteerd en vervolgens geïoniseerd. Met behulp van een infrarode laser zijn vervolgens ook de vibraties in deze aangeslagen toestand bestudeerd, welke vergeleken zijn met berekeningen.

Curriculum Vitae

Op 18 augustus 1970 ben ik geboren in Tilburg. In deze stad heb ik gewoond tot ik in 1988 het Gymnasium B diploma aan het Theresialyceum te Tilburg in ontvangst mocht nemen. Daarna ben ik verhuisd naar Nijmegen (met een korte tussenstop in Beuningen) om aan de Katholieke Universiteit Nijmegen (KUN) Natuurkunde te gaan studeren. In 1990 was ik (mede-)mentor voor een groepje eerstejaars fysicastudenten tijdens de algemene introductie voor eerstejaars studenten aan de KUN. In 1991, 1992 en 1993 ben ik begeleider geweest tijdens de herfst/lentecursus voor VWO-studenten (een 3-daagse oriëntatiecursus) aan de KUN. Tijdens mijn studie ben ik ook werkzaam geweest als student-assistent bij het practicum Natuurkunde voor scheikunde studenten. Mijn afstudeerstage heb ik gedaan op de afdeling Molecuul- en Laserfysica, onder leiding van Giel Berden en Leo Meerts. Op 17 augustus 1993 ben ik moeder geworden van Marit. Na deze onderbreking heb ik in augustus 1994 mijn doctoraal diploma Natuurkunde gehaald. Vier maanden later ben ik in dienst gekomen van de KUN om, onder leiding van Leo Meerts, Dave Parker en later Gerard Meijer, promotie onderzoek te verrichten op de afdeling Molecuul- en Laserfysica. Na twee maanden, in maart 1995, werd mijn positie overgenomen door de stichting voor Fundamenteel Onderzoek der Materie (FOM) en ben ik als onderzoeker in opleiding (OIO) onderzoek gaan verrichten aan aromatische moleculen m.b.v. hoge-resolutie spectroscopie. De resultaten hiervan staan beschreven in dit proefschrift. Tijdens mijn promotietijd ben ik werkcollege-coördinator geweest bij het college Electrostatica en assistent bij het practicum Natuurkunde. Last but not least ben ik op 26 juni 1999 in het huwelijk getreden met Eric Vrijenhoek.

Publications

- *Internal rotation effects in the rotationally resolved $S_1(^1L_b) \leftarrow S_0$ origin bands of 3-methylindole and 5-methylindole*
K. Remmers, E. Jalviste, I. Mistrík, G. Berden and W. L. Meerts,
Journal of Chemical Physics **108**: 8436-8445 (1998).
- *Gas-phase infrared spectroscopy on the lowest triplet state of the pyrazine-argon complex*
K. Remmers, R. G. Satink, G. von Helden, H. Piest, G. Meijer and W. L. Meerts,
Chemical Physics Letters **317/3-5**: 197-202 (2000).
- *Structural information on the S_0 and S_1 state of *o*-fluorophenol by hole burning and high resolution UV spectroscopy*
K. Remmers, A. Zehnacker-Rentien, K. Le Barbu, F. Lahmani and W. L. Meerts,
Journal of Chemical Physics **112**: 6237-6244 (2000).
- *Proton tunneling in the benzoic acid dimer studied by high resolution UV spectroscopy*
K. Remmers, I. Ozier and W. L. Meerts,
Scheduled for publication in the Journal of Chemical Physics (June 22. 2000).

